DEVELOPMENT OF CARBON NANOTUBE EMBEDDED POLYACRILONITRILE/POLYPYRROLE ELECTROSPUN NANOFIBROUS SCAFFOLDS

A Thesis Submitted to
the Graduate School of Engineering and Sciences of
İzmir Institute of Technology
in Partial Fulfillment of the Requirements for the Degree of

DOCTOR OF PHILOSOPHY

in Materials Science and Engineering

by
Atike İNCE YARDIMCI

December 2017

We approve the thesis of **Atike İNCE YARDIMCI**

Examining committee members:

_____
Prof. Dr. Selahattin YILMAZ
Chemical Engineering Department, İzmir Institute of Technology

_____
Prof. Dr. Serdar ÖZÇELİK
Chemistry Department, İzmir Institute of Technology

_____
Prof. Dr. Erdal ÇELİK
Committee Member

_____
Assoc Prof. Dr. Pınar KARA KADAYIFÇILAR
Committee Member

_____
Assist. Prof. Dr. Gülistan MEŞE ÖZÇİVİCİ
Molecular Biology and Genetics Department, İzmir Institute of Technology

27 December 2017

_____
Prof. Dr. Selahattin YILMAZ
Supervisor, Chemical
Engineering Department
İzmir Institute of Technology

_____
Prof. Dr. Metin TANOĞLU
Co-Supervisor, Mechanical
Engineering Department
İzmir Institute of Technology

_____
Prof. Dr. Mustafa M. DEMİR
Head of the Department of Materials
Science and Engineering

_____
Prof. Dr. Aysun SOFUOĞLU
Dean of the Graduate School of
Engineering and Sciences

ACKNOWLEDGEMENTS

First of all, I would like to deeply thank to my advisor Prof. Selahattin Yilmaz for his encouragement and guidance during my studies and this thesis work. Working with him was an honour and a great experience for me.

I would like to commemorate my former advisor Assoc. Prof. Yusuf Selamet and thank him for his contributions and unique assistance. He will never be forgotten, rest in peace.

I would like to thank to my co-advisor Prof. Metin Tanoglu for his support and help during my studies.

Besides my advisors, I would like to thank other members of my thesis committee Prof. Serdar Ozcelik and Prof. Erdal Celik for their helpful comments and suggestions. I would like to thank to Assist. Prof. Gulistan Mese Ozcivici and Assoc. Prof. Engin Ozcivici for invaluable collaborations during tissue studies. I also would like to thank to Assoc. Prof. Pinar Kara Kadayifcilar for CV and EIS studies and Prof Mustafa M. Demir for electrospinning support.

I want to thank to IYTE Material Research Center and Biotechnology and Bioengineering Research and Application Center staff.

Thanks to each of my friends at Izmir Institute of Technology for providing a great atmosphere and a wonderful workplace. Especially, my best friends Nesli Yagmurcukardes, Duygu Ozaydın and Evrim Yakut Evecen and my office mates Yasemin Demirhan and Hasan Aydın.

Last, but most importantly, I would like to thank my precious family: my husband Cagri Yardimci, my son Atlas Yardimci, my daughters Alin Yardimci and Aden Yardimci and my mother Zehra Ince and my father Kaya Ince for their ceaseless support, motivation and love in all my life and believing in me. I need them always by my side.

ABSTRACT

DEVELOPMENT OF CARBON NANOTUBE EMBEDDED POLYACRILONITRILE/POLYPYRROLE ELECTROSPUN NANOFIBROUS SCAFFOLDS

In this study, electrospun polyacrilonitrile (PAN)/ polypyrrole (PPy) nanofibers containing different PPy content (10, 25, and 50 wt%) were prepared. Different carbon nanotube (CNT) amounts (1, 2, 3, and 4 wt%) were embedded into PAN/PPy nanofibers to improve their mechanical and electrical properties. CNT functionalization was carried out to solve agglomeration problem and functional CNTs effects on PAN/PPy nanofiber morphology was examined. Alignment of nanofibers was studied to improve mechanical properties of nanofibers. Obtained PAN/PPy and PAN/PPy/CNT nanofibers were utilized as kerotinocytes scaffold. PAN/PPy/CNT and aligned and randomly oriented PAN/PPy nanofibers were examined for bone marrow osteogenic differentiation of mesenchymal stem cells (MSCs).

10 wt% PPy content was optimum in terms of mechanical properties and usage with CNTs. Higher strain was observed for 10 wt% PPy content which was 23.3 %. When as-grown MWCNTs were added into PAN/PPy, disordered nanofibers were formed. To improve interficial properties of these composites, as-grown CNTs were functionalized with H_2SO_4/HNO_3/HCl solution. Upon functionalization, formation of hydroxylic and carboxylic groups were detected on the CNT surfaces. TEM examination of the nanofibers obtained with these CNTs showed decrease in beads formation. The functionalized CNTs were well dispersed within the electrospun nanofibers and aligned along the direction of nanofibers. The electroactivity of the fibers indicated that these nanofibers could be used as electrochemical actuator in acidic solutions.

PAN/PPy and PAN/PPy/CNT nanofibers supported the attachment and proliferation of keratinocytes and osteogenic differentiation of MSCs. It was found that these nanofibers could be utilized as scaffolds for both cell types.

ÖZET

ELEKTROEĞİRME YÖNTEMİ İLE KARBON NANOTÜP İLAVE EDİLMİŞ POLİAKRİLONİTRİL/POLİPİROL NANOLİFLİ YAPI İSKELELERİNİN GELİŞTİRİLMESİ

Bu tez çalışmasında, farklı oranlarda polipirol (PPy) içeren (%10, 25 ve 50) poliakrilonitril (PAN)/PPy nanofiberler elektroeğirme yöntemiyle sentezlenmiştir. Mekanik ve elektriksel özellikleri iyileştirmek için farklı karbon nanotüp (KNT) oranları (% 1, 2, 3 ve 4) PAN/PPy nanofiberler içine eklenmiştir. Karbon nanotüplerin topaklanma problemini çözmek için, KNTler fonksiyonel hale getirilmiştir ve fonksiyonel KNTlerin PAN/PPy nanofiberlerin morfolojisi üzerindeki etkileri incelenmiştir. Nanofiberlerin mekanik özelliklerinin iyileştirilmesi için nanofiberlerin yönlendirilmesi de çalışılmıştır. Elde edilen PAN/PPy ve KNT eklenmiş PAN/PPy nanofiberler keratin yapı iskelesi olarak kullanılmıştır. Yönlendirilmiş ve rastgele yönlenmiş PAN/PPy nanofiberler kemik iliği kaynaklı mezenkimal kök hücrelerin osteojenik diferansiasyonu için incelenmiştir.

Mekanik özellikler ve KNT ile birlikte kullanım açısından % 10 PPy içeriği optimum olarak bulunmuştur. %23.3 değerindeki daha yüksek gerinme değeri %10 PPy içeriği için gözlenmiştir. %1 ve 4 oranlarında çok duvarlı KNT PAN/PPy içerisine eklendiğinde, düzensiz nanofiberler meydana gelmiştir. Bu kompozitlerin interfaz özelliklerini iyileştirmek için KNT ler $H_2SO_4/HNO_3/HCl$ solusyonuyla fonksiyonel hale getirişmiştir. Fonksiyonelleştirme sonucu, KNT yüzeylerinde hidroksilik ve karboksilik gruplar saptanmıştır. Bu KNTlerle elde edilen nanofiberlerin TEM analizleri damlacık oluşumunda azalma ve nanofiberlerle aynı yönde yönlenme göstermiştir. Bu fonksiyonel KNTlerin PAN/PPy karışımı içerisindeki dağılımının iyileştiğini göstermektedir. Fiberlerin elektroaktiviteleri göstermiştir ki bu nanofiberler asidik solusyonlar içerisinde elektrokimyasal aktuatör olarak kullanılabilirler.

PAN/PPy ve KNT eklenmiş PAN/PPy nanofiberler keratinlerin tutunmasını ve çoğalmasını ve mezenkimal kök hücrelerin osteojenik diferansiasyonunu sağlamışlardır. Bu nanofiberlerin her iki hücre tipi için de yapı iskelesi olarak kullanılabileceğini gösterilmiştir.

TABLE OF CONTENTS

LIST OF FIGURES…….…….....ix

LIST OF TABLES…….…..……xiii

CHAPTER.1

INTRODUCTION……...……...….1

CHAPTER. 2 CONDUCTING POLYMERS.....3

2.1 Conducting Polymers.....3

2.2 Molecular Structure of Conducting Polymers……4

2.2.1 Electronic Structure of Intrinsic Conjugated Polymers……..….5

2.2.2 Doping Structures of Conducting Polymers……..……..….6

2.3 Synthesis of Conducting Polymers……..……..……..8

2.4 Properties of Conducting polymers……..……..……9

2.5 Applications of Conducting Polymers.....12

2.6 Literature Studies on Electrospun Conducting Polymer Nanofibers…14

2.6.1 Effects of CNTs on Conducting Polymers…..……..…..19

CHAPTER.3 ELECTROSPUN NANOFIBERS FOR TISSUE ENGINEERING SCAFFOLDS.....25

3.1 Tissue Engineering Scaffolds……...…..25

3.2 Nanofibrous Scaffolds and Their Fabrication Methods…….....…....26

3.2.1 Molecular Self-Assembly……..……26

3.2.2 Thermally Induced Phase Separation……..……...27

3.2.3 Electrospinning……..……27

3.2.3.1 Electrospinning Theory……..……..…….28

3.2.3.2 Electrospinning Parameters……..……..……...29

3.2.3.3 Cell-Electrospun Nanofibrous Scaffold Interactions…..…...31

3.2.3.4 Literature Studies on Use of Electrospun Nanofibers in Tissue Engineering……...……....32

CHAPTER. 4 EXPERIMENTAL STUDY……..……...44

4.1 Materials.....44

4.2 CNT Growth, Purification, Functionalization, and Characterization ..45
4.3 PAN/PPy and PAN/PPy/CNT Solutions Preparation and Electrospinning 45
4.4 Cell Culture and Seeding…….....……48
4.4.1 Keratinocytes Growth on PAN/PPy and PAN/PPy/CNT Nanofibrous Scaffolds…….....……48
4.4.2 Osteogenic Differentiation of Mesenchymal Stem Cells on PAN/PPy and PAN/PPy/CNT Nanofibrous Scaffold.....48
4.5 Nanofibers Characterization.....48
4.5.1 Scanning Electron Microscopy (SEM)……...……48
4.5.2 Transmission Electron Microscopy (TEM)……..……...49
4.5.3 X-Ray Diffraction (XRD)……..……49
4.5.4 Raman Spectroscopy……...……...……49
4.5.5 Thermogravimetric Analysis (TGA) ……..……49
4.5.6 Differential Scanning Calorimetry (DSC)……....……..49
4.5.7 Tensile Test……..……...50
4.5.8 Water Contact Angle Test ……50
4.5.9 Rheometer……..…..……..50
4.5.10 Fourier Transform Infrared Spectroscopy (FT-IR)……...50
4.5.11 Cyclic Voltammetry (CV)……..……..…....51
4.5.12 Electrochemical Impedance Spectroscopy (EIS)……..51
4.6 Cell Characterization.....52
4.6.1 Cell Morphology Study by SEM 52
4.6.2 Immunostaining of Keratinocytes……..……52
4.6.3 MTT Assay……...…….....52
4.6.4 Alizarin Red Staining……...……..53

CHAPTER. 5 RESULTS AND DISCUSSIONS.....54
5.1 CNT Characterization.....54
5.2 Electrospun PAN/PPy and CNT Embedded PAN/PPy (PAN/PPy/CNT) Nanofibers.....59
5.2.1 PAN/PPy Bicomponent Nanofibers.....59
5.2.2 Aligned and Random PAN/PPy Bicomponent Nanofibers…..….67

5.2.3 Electrospun PAN/PPy Nanofibers Containing Different Amount of CNTs.....69
5.3 CNT Embedded PAN/PPy Nanofibers as Keratinocytes Scaffold…...81
5.4 Random and Aligned CNT Embedded PAN/PPy Nanofibers for Osteogenic Differentiation of Mesenchymal Stem Cells…..…….89

CHAPTER.6 CONCLUSIONS.....98

REFERENCES.....100

LIST OF FIGURES

Figure **Page**

Figure 2.1 The backbone structure of PA containing conjugated double bonds……4

Figure 2.2 Main chain structure of common conducting polymers…….....….5

Figure 2.3 Structure of p-doped PPy, A^- represents counteranions such as Cl^-, NO_3^-…...6

Figure 2.4 Electronic bands and chemical structures illustrating a) undoped, b) polaron, c) bipolaron, d) fully doped states of PPy…….....…….…..…8

Figure 2.5. Schematic diagram of the electrochemical actuation of PPy. A voltage potential is applied between working and counter electrodes, here it causes expansion with diffusion of anions……...11

Figure 2.6 DSC graphss of PAN/PPy bicomponent nanofibers with different PPy contents in PAN (a) 0 wt%, (b) 5 wt%, (c) 10 wt%, (d) 15 wt%, (e) 30 wt%, (f) 50 wt% and (g) 100 wt% (pure PPy cannot be electrospun)…….……...15

Figure 2.7 A schematic representation of linear actuation of Cs/PPy microfiber.……..16

Figure 2.8 Cyclic voltammograms of chitosan/PANi fibers in aqueous HCl solutions with different pH……...…….……..….18

Figure 2.9 Electrical conductivity of PPy/PEO nanofibers as a function of their polypyrrole content. Solutions of PPy with 2.5 wt% PEO (●), and 1.5 wt% PEO (■) as carrier were used…….……....18

Figure 2.10 The stress–strain curves of PANi–CNT composite fibers with different CNT contents, before doping (thick lines) and after doping for 24 h in MSA (thin lines): (a,a') neat polyaniline, (b,b') PANi–CNT 0.5% (w/w) (c,c') PANi–CNT 1% (w/w) (d, d') PANi–CNT 2% (w/w), before and after doping…….22

Figure 2.11 Cyclic voltammograms of ACNF (PAN), ACNF/CNT (PAN/CNT), PPy/ACNF (PPy coated PAN), and PPy/ACNF/CNT (PPy coated PAN/CNT) nanofiber……....24

Figure 3.1 Schematic of a typical electrospinning system……..…….....…..29

Figure 3.2 SEM micrographs of (a) smooth muscle cells (b) endothelial cell seeded on electrospun P(LLA-CL) copolymer scaffolds after 7 days of culture……33

Figure 3.3 Schematic of PPy/PLGA nanofibers for in vitro cell culture and electrical stimulation studies……...……..…….…..…35

Figure 3.4 Immunostaining of PC12 cells cultured on (a) random PLGA, (b) aligned PLGA, (c) random PPy/PLGA (d) aligned PPy/PLGA nanofibers. Arrows indicate major directions of the aligned nanofibers……..…..36
Figure 3.5 Morphology of keratinocytes when grown on (a) random, (b) aligned nanofibers. The red arrows indicate the intercellular connections between the keratinocytes. Images were taken using 20-times magnification……..37
Figure 3.6 Young's modulus of random (grown at 300 rpm rotation speed of collector) and aligned (grown at 1500 rpm rotation speed of collector) nanofibers. Scaffolds were tested along the parallel and perpendicular directions of the fibers……..39
Figure 3.7 SEM images of myoblasts seeded on electrospun (a) aligned, (b) random PLGA scaffolds. Myoblasts were fixed and viewed after 7 days in culture ……..….39
Figure 3.8 SEM images of (a) murine Schwann cells , (b) murine osteoblast-like cells , (c) human keratinocytes, (d) human fibroblasts on chitosan electrospun nanofibers after 5 days of culture……..……....41
Figure 3.9 Proliferation of murine osteoblast-like cells on TCPS, chitosan (CS) film and CS nanofibers……..……...42
Figure 4.1 (a) Electrospinning set-up, (b) collectors…….…….……...…….…..46
Figure 5.1 (a) SEM picture (b) Raman spectrum (c) TGA graph of the CNT sample.....55
Figure 5.2 SEM micrographs of (a) as-grown (b) purified (c) functional CNTs……..…56
Figure 5.3 FT-IR spectra of CNTs..……..…….....……..57
Figure 5.4 Raman spectra of CNTs…….....……....58
Figure 5.5 SEM images of (a) PP1 (b) PP3 (c) PP4. Solutions were prepared at room temperature.....60
Figure 5.6 SEM micrographs of electrospun PAN/PPy nanofibers (a) PP1, (b) PP3 prepared at solution temperature of 60 ^{o}C at 2μm scale, (c) TEM micrograph of electrospun PAN/PPy nanofibers containing 10 wt% PPy at 0.1 μm.....61
Figure 5.7 XRD scans of the PAN/PPy electrospun nanofibers……..……63
Figure 5.8 Raman spectra of the PAN/PPy electrospun nanofibers……..…64
Figure 5.9 TGA graphs of the PAN/PPy electrospun nanofibers containing different amounts of PPy.....65

Figure 5.10 DSC graphs of electrospun PAN/PPy nanofibers containing different amount of PPy.....66
Figure 5.11 SEM images of aligned nanofibers PP2 at 5 μm scale.....67
Figure 5.12 Polarized FT-IR spectra (parallel (0^o) and perpendicular (90^o) polarized IR spectra of PP1 and PP2……..……..……...69
Figure 5.13 SEM micrographs of CNT embedded electrospun PAN/PPy nanofibers containing 25 wt% PPy (a) PPC1 (b) PPC2……70
Figure 5.14 SEM micrographs of CNT embedded electrospun PAN/PPy nanofibers containing 10 wt% PPy and (a) PPC3 (b) PPC4 (c) PPC5 (d) PPC6 at 2μm scale.....71
Figure 5.15 TEM images of beads on nanofibers caused by (a) CNT agglomeration (b) not embedded CNTs.....72
Figure 5.16 TGA thermograms of CNT embedded electrospun PAN/PPy nanofibers.....73
Figure 5.17 SEM micrographs of PAN/PPy/CNT electrospun nanofibers incorporated with 1 wt% and 4 wt% as-grown and functional CNTs, (a) PPC3 (b) PPC7 (c) PPC6 (d) PPC8.....74
Figure 5.18 Raman spectra of PAN/PPy/CNT nanofibers containing 1 wt% as-grown and functionalized CNTs……..……75
Figure 5.19 Raman spectra of PAN/PPy/CNT nanofibers containing 4 wt% as-grown and functionalized CNTs……...……..76
Figure 5.20 TEM images of PAN/PPy nanofibers containing 10 wt% PPy 1 wt% of functionalized CNT (PPC7).....77
Figure 5.21 FT-IR spectra of PAN/PPy and CNT embedded PAN/PPy nanofibers.....78
Fig. 5.22 Cyclic voltammograms of PAN/PPy nanofibers with different PPy and CNT contents in 0.1 M HCl solution…….…….…….79
Fig. 5.23 Electrochemical impedance plots of PAN/PPy nanofibers with different PPy and CNT contents…….....……...80
Figure 5.24 SEM images of skin cells seeded on electrospun PAN/PPy nanofibers (10 wt% PPy) after a) 1 day, b) 3 days, and c) 7 days of culture, scale bars 50 μm. …….....82
Figure 5.25 Fluorescence microscopy images of skin cells seeded on PP1 nanofibers after a) 1 day, c) 3 days, e) 7 days of culture and their glass control after b) 1 day d) 3 days f) 7 days of culture, scale bars 20 μm……..…….83

Figure 5.26 SEM images of electrospun nanofibers PP3 after keeping in cell culture for a) 1 day, b) 3 days, c) 7 days, scale bars 50 μm…….……84
Figure 5.27 Phase-contrast microscopy images of skin cells seeded on PP3 after a) 1 day, b) 3 days, c) 7 days of culture, scale bars 20 μm…….……85
Figure 5.28 SEM images of electrospun nanofibers containing 10 wt% PPy and 1 wt% CNT after keeping in cell culture for a) 1 day, b) 3 days, c) 7 days. Scale bars 50 μm…….86
Figure 5.29 Fluorescence microscopy images of keratinocytes seeded on PPC3 electrospun nanofibers after a) 1 day, c) 3 days, e) 7 days of culture and their glass control after b) 1 day, d) 3 days, f) 7 days of culture, scale bars 20 μm…….……88
Figure 5.30 MTT assay of keratinocytes seeded on PAN/PPy nanofibers containing 10 wt% PPy (PP1), 25 wt% PPy (PP3) and 10 wt% PPy and 1 wt% CNT (PPC3) nanofibers after 1, 3 and 7 days of culture……..……89
Figure 5.31 SEM images of mesenchymal stem cells after culturing in growth medium (a) 7, (c)14, (e) 21 days, after culturing in osteogenic medium for (b) 7, (d) 14, (f) 21 days on PP1.....91
Figure 5.32 SEM images of mesenchymal stem cells after culturing in growth medium (a) 7, (c)14, (e) 21 days, after cultiring in osteogenic medium for (b) 7, (d) 14, (f) 21 days on aligned nanofibers (1000 rpm).....92
Figure 5.33 SEM images of mesenchymal stem cells after culturing in growth medium (a) 7, (c)14, (e) 21 days, after cultiring in osteogenic medium for (b) 7, (d) 14, (f) 21 days on glass control coverslips.....93
Figure 5.34 SEM images of PP1 kept in (a) growth (b) osteogenic medium, and PP2 kept in (c) growth, (d) osteogenic medium after 21 days.....94
Figure 5.35 MTT assay of mesenchymal stem cells (gc) and osteoblasts (oc) seeded on glass coverslips and random PAN/PPy nanofibers after 1, 7, 14 and 21 days of culture……..……..….95
Figure 5.36 MTT assay of mesenchymal stem cells (gc) and osteoblasts (oc) seeded on glass coverslips and aligned PAN/PPy nanofibers after 1, 7, 14 and 21 days of culture……..……..……..…...….96
Figure 5.37 Alizarin red staining on (a) PP1, (c) PP2, (e) glass control at growth conditions, (b) PP1, (d) PP2, (f) glass control at osteogenic conditions…..97z

LIST OF TABLES

Table **Page**

Table 2.1 Conductivity values of common conducting polymers ……..…..10

Table 2.2 Properties of mammalian skeletal muscle.....14

Table 2.3 Properties of CNTs……..…….20

Table 2.4 The composition and properties of PPy.TFSI and PPy.TFSI/CNT laminates..21

Table 2.5 Tensile properties and electrical conductivity of (a) PVDF, (b) PVDF–MWCNTs, (c) PPy coated PVDF, and (d) PPy coated PVDF/MWCNTs nanofibers……..24

Table 3.1 Fiber Diameter, Contact Angle, and Mechanical Properties of Electrospun PPy/PCL/gelatin nanofibers with different PPy amount…….....34

Table 4.1. List of the chemicals used……..……..44

Table 4.2. The labels of the electrospun nanofibers prepared…….…….47

Table 5.1 Elemental composition of as-grown, purified and functional CNTs.....59

Table. 5.2 Viscosity values of the solutions containing different amounts of PPy at shear rate of 400 s^{-1}…….…….62

Table 5.3 Average diameter and tensile properties of PAN/PPy nanofibers containing 10 and 25 wt% PPy……...…….…….67

Table 5.4 Average diameter, tensile properties and contact angles of random and aligned PAN/PPy nanofibers containing 10 wt% PPy…….…..…..68

Table 5.5 Impedance values of PAN/PPy nanofibers with different PPy and CNT contents…….…81

Table 5.6 Contact angle values of PAN/ PPy nanofibers with different composition…….……...……81

CHAPTER 1

INTRODUCTION

Electrospun nanofibers utilization for biomedical applications has been widely investigated in last years and they also found use in tissue engineering scaffolds due to their scalability, adaptability, and ability to form fibers in the range of nano to micro scale (Sill and von Recum 2008). They offer a connected and porous tissue engineering scaffolds mimicking the extracellular matrix (ECM) of many types of tissues. Electrospun scaffolds must show appropriate biological properties to provide cell adhesion, proliferation and differentiation. Besides, nanofibers physical properties such as hydrophilicity, Young modulus and strength also should be coherent with physical properties of ECM.

There are many tissue engineering scaffolds reported in literature made from natural or synthetic polymers. Natural polymer have better biocompatibility and low immunogenicity (Liang, Hsiao, and Chu 2007). Four main class of natural polymers are proteins, polysaccharides, DNAs, and lipids and they can all electrospun. However, advantage of synthetic polymers over natural polymers is to exhibit specific function for specific needs (Gibas and Janik 2010). Moreover, they are cheaper and more reliable source of raw materials. In order to insert specific properties to the scaffolds, copolymer system usage can be improved significantly the performance of scaffolds. Biocompatible and biodegradable synthetic and natural polymer can also be utilized together. Besides, useful inorganic particles such as silver particles (Son et al. 2004), calcium carbonate (Fujihara, Kotaki, and Ramakrishna 2005), calcium phosphate (Fan et al. 2005) can be incorporated into the synthetic polymers and electrospun to prepare effective scaffolds.

Conducting polymers are organic polymers conducted electricity due to their unique conjugated backbone structure. Their biocompatible property make them an appropriate tissue engineering scaffold for cell types responding to electrical stimuli including nerve, bone, muscle, and cardiac cells. They can significantly improve cell adhesion and proliferation of cells via electrical stimulations (Schmidt et al. 1997).

Carbon nanotubes (CNTs) have attracted considerable attention in recent years because of their excellent electrical and mechanical properties (Popov 2004). They can

be incorporated into polymer matrix and find use in biomedical scaffold applications (Kim et al. 2015). CNTs enhance the electrical conductivity of scaffolds and therefore they can conduct an electrical stimulus in tissue healing. By incorporating CNTs to conducting polymers, its electrical, mechanical and electrochemical properties can be improved (Spinks et al. 2006).

In addition to polymer composition, diameter, morphology of scaffolds are also very important to obtain a scaffold with desirable functions and properties. Different innovative electrospinning techniques allow to design different three dimensional scaffold structures such as aligned scaffolds, dual-porosity scaffolds, core-shell nanofibers, multilayer electrospinning, mixing electrospinning (Liang, Hsiao, and Chu 2007). Among them, oriented electrospun scaffolds are very important to control the cell growth and obtain an anisotropic proliferation (Xu et al. 2004).

Under the view of above discussions, in this study, it was aimed to prepare PAN/PPy and CNT embedded PAN/PPy electrospun nanofibers. Effects of PPy content, CNT addition and CNT content on morphology of nanofibers were investigated. In addition, CNTs were functionalized and functional CNTs were examined to improve the quality of nanofibers. Nanofiber alignment was also studied.

Moreover, utilization of these nanofibers as scaffolds for keratinocytes and bone marrow mesenchymal stem cell osteogenic differentiation was studied. Scaffolds containing different content of PPy were tested for keratinocytes growth and CNT embedded PAN/PPy nanofibers were utilized in order to observe CNT influence on keratinocytes. Viability and morphology of keratinocytes were compared for different scaffolds. Moreover, effects of diameter of nanofibers were investigated on keratinocytes.

For osteogenic differentiation of bone marrow mesenchymal stem cells, nanofibrous scaffolds prepared at different orientations were tested. The effects of CNT addition of PAN/PPy nanofibers were also studied on morphology of mesenchymal stem cells and osteoblasts and their cytotoxicity.

CHAPTER 2

CONDUCTING POLYMERS

2.1 Conducting Polymers

Conducting polymers are organic polymers which have unique conjugated backbone structures that facilitate the delocalization of electrons along those chains. They possess alternating single (σ) and double (π) bonds, and these conjugated systems lend their inherent optical, electrochemical, and electrical properties. They are typically semiconducting, but become conducting when they are doped with donor or acceptor ions (Skotheim 1997). Doping can be done chemically or electrochemically. The first publication about a conducting polymer, electrical conductivity in doped polyacetylene (PA), was published in 1977 (Chiang et al. 1977). It was doped with electron-withdrawing AsF_5 and its conductivity increased nine fold, reached the order of 10^3 S/cm. It was an organic conducting polymer with the repeating unit $(C_2H_2)_n$. Discovery of new conducting polymer followed the invention of PA. Polypyrrole (PPy), polyaniline (PANi), and polythiophene (PTh) were reported at the end of 1970s. Electrical conductivity of these polymers led to deep interest especially in microelectronic applications. In 1990, electroluminescent property of poly(p-phenylene vinylene) (PPV) was investigated (Burroughes et al. 1990) and semiconducting intrinsic conjugated polymers have begun to utilize as the active light-emitting layer for polymer light-emitting diodes. In 1995, a conjugated polymer poly[2-methoxy-5-(2-ethylhexyloxy)-1,4-phenylenevinylene] (MEH-PPV) as donor was used in bulk-heterojunction polymer solar cells with a fullurene derivative [6,6]-Phenyl C71 butyric acid methyl ester (PCBM) as acceptor (Yu et al. 1995). After this report, conjugated polymer usage in optoelectronic materials and devices have been placed in hot research topics. In 2000, Heeger, MacDiarmid, and Shirakawa won Nobel Prize in Chemistry with their contributions to the discovery and developments of conducting polymers.

2.2 Molecular Structure of Conducting Polymers

Conducting polymers have a conjugated molecular structure where the π-electrons delocalize over the whole polymer chain. In order to become conducting, conjugated polymers should be doped. The most common conducting polymers are PA, PPy, PANi, PTh, PPV, poly(p-phenylene) (PPP), and polyfluorene (PF). Among these conjugated polymers, PA has the simplest main chain structure. Conjugation is possible with the existence of alternating single and double bonds. As observed in Fig. 2.1, PA consists of an alternate single bond and double bond carbon chain. Both single and double bonds contain a localized σ-bond forming a strong chemical bond and in addition, double bond also contains a localized π-bond which is weaker than σ-bond.

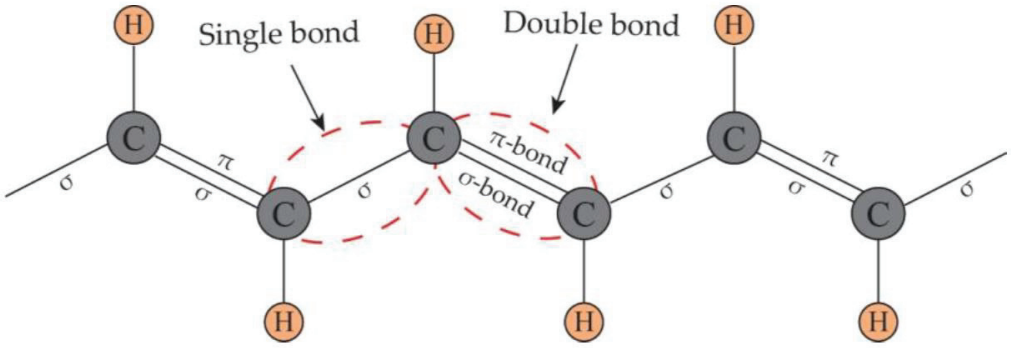

Figure 2.1 The backbone structure of PA containing conjugated double bonds (Source: Le, Kim, and Yon 2017).

There are two structure types of PA: cis-polyacetylene and trans-polyacetylene. Trans-polyacetylene consists of two hydrogen atoms on opposite sides of the double bond carbons while two hydrogen atoms are on the same in cis-polyacetylene. Trans-polyacetylene shows an equivalent structure after exchanging its single and double bond, it is a degenerate conjugated polymer. However, cis-polyacetylene is nondegenerate, its structure is not equivalent after exchanging its single and double bonds and other conjugated polymers also are nondegenerate similar to cis-polyacetylene. Among conjugated polymers, PANi has a complicated main chain structure. It has three different structure, these are leucoemeraldine (x=1), emeraldine base (x=0.5), pernigraniline (x=0). Generally, emeraldine base structure is significant for conducting PANi because

conducting PANi takes place with proton-acid doping of emeraldine base structure (Li 2015). Main chain structures of common conducting polymers are given in Fig. 2.2.

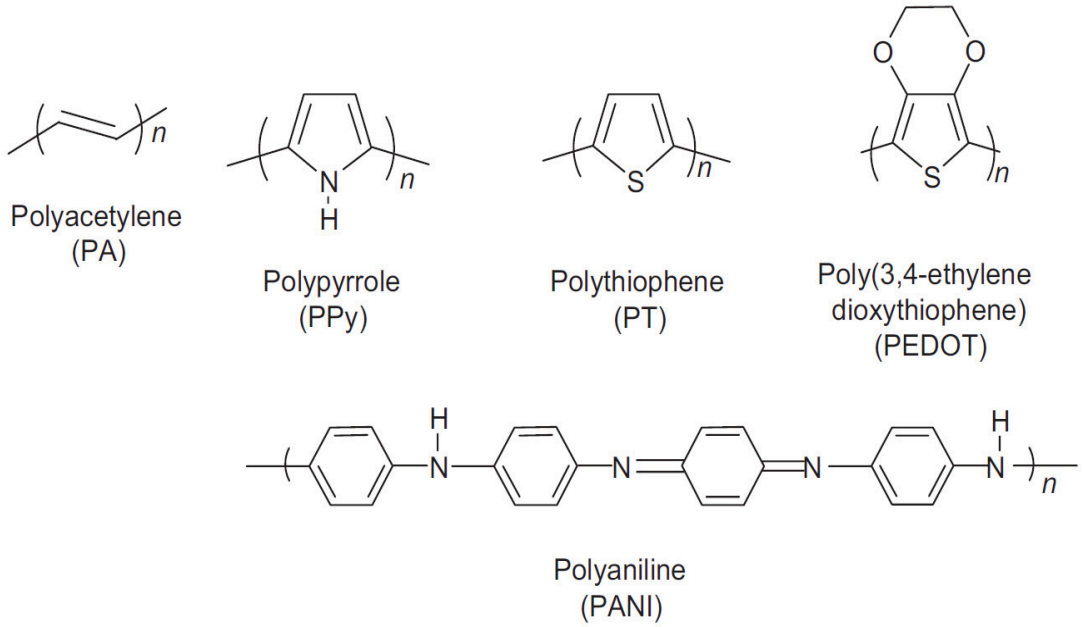

Figure 2.2 Main chain structure of common conducting polymers.

2.2.1 Electronic Structure of Intrinsic Conjugated Polymers

All valance bands are filled with electrons and conduction bands are empty in the basic state of the intrinsic conjugated polymers. Band gap (E_g) of the conjugated polymers defines as the energy level between the highest occupied molecular orbital (HOMO) or conduction band and the lowest unoccupied molecular orbital (LUMO) or valence band. Generally, conjugated polymers have an E_g value between 1.5-3 eV, so they are organic semiconductors in their intrinsic form. E_g value of conducting polymers can be calculated using the equation (2.1) below (adsorption edge wavelength λ_{edge} is taken from absorption spectra of the conducting polymer film):

$$\mathrm{Eg(eV)} = \frac{1240}{\lambda\mathrm{edge(nm)}} \qquad \text{(Eq.2.1)}$$

There are different factors affecting the electronic structure and E_g values of the conjugated polymers. For PPy, PTh, and poly(p-phenylene) (PPP), conjugated polymers which have single bonds between the aromatic rings, the deviation of the conjugated main

chain from planar structure between the two neighboring aromatic rings increases E_g value. The angle between two aromatic rings also influences the E_g value. Large angle causes small overlap between the molecular orbitals and therefore high E_g values. Another factor is the substituents on the main chain. Electron donating substituents up-shift LUMO and HOMO energy levels, HOMO is up-shifted more than LUMO. Electron-withdrawing substituents down-shift LUMO and HOMO energy levels, LUMO is down-shifted more than HOMO. Therefore, both electron donating and electron withdrawing substituents reduce the E_g value. When the electron donating and accepting units copolimerise, conjugated copolimers have lower E_g. Existence of quinone structure in main chain is also a factor decreasing the E_g values. Agglomerations of the polymer main chains also affect the energy levels of conjugated polymers. Lastly, for degenerate trans-polyacetylene, decrease in difference between the alternating single bond length and double bond length results in decrease in E_g values.

2.2.2 Doping Structures of Conducting Polymers

Doping of conduction polymers can be carried out chemically or electrochemically by oxidation or reduction of the conjugated polymers. In the p-type doping state of conducting polymers, main chain is oxidized with counteranion doping and conducting polymer become p-type with the existence of holes in the main chain. In the n-type doping state of conducting polymers, main chain is reduced with countercation doping and conducting polymer become n-type with the existence of electrons in the main chain. P-type doped PPy structure with positive charge on polymer main chain is shown in Fig. 2.3.

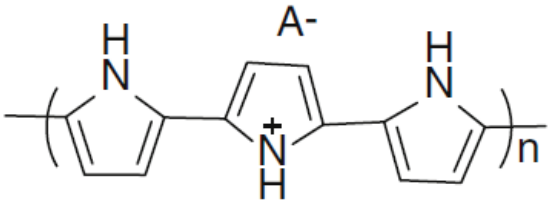

Figure 2.3 Structure of p-doped PPy, A^- represents counteranions such as Cl^-, NO_3^-.

Doping degree of a conducting polymer is the number of counteranions per monomer unit. Main chain structure of the polymer determines maximum doping degree. Doping degree for p-type PPy is usually 0.25-0.35 and in its conjugated main chain, 3-4 pyrrole units can be doped with 1 counteranion.

In inorganic semiconductors with crystalline structure, for example Si, doping takes place by adding impurities to intrinsic semiconductors. Some Si atoms are changed with outer shell electrons one more or one less than Si for n-type doping or p-type doping. In conducting polymers with amorphous structure, doping occurs with oxidation or reduction of main chain. Charge neutrality is provided with counterions doping. Doping degree of conducting polymers is very high than that of inorganic polymers. Besides, counterion doping causes volume change (actuation) in conducting polymers.

There are different charge carriers for conducting polymers. Charge carriers for transpolyacetylene at degenerate basic state, charge carriers are solitons and polarons. Charge carriers for cis-PA, PPy, PTh, PANi, etc. are polarons and bipolarons (Bredas and Street 1985). Soliton is unpaired π-electron delocalized on a long trans-polyacetylene main chain. When a neutral soliton is oxidized, it loses an electron and a positive soliton forms. When it reduces, it gains an electron and a negative soliton forms. Major charge-carriers in basic state degenerate trans-polyacetylene and non-degenerate conducting polymers are polarons. Positive polaron generates with oxidation and negative polaron generates with reduction of the main chain. Bipolaron is a charge carrier coupling of two positive and two negative polarons on the main chain and has double charges. Bipolaron formation can occur as a result of high polaron concentration in polymer main chains. Positive bipolaron correspond to the hole pair and negative bipolaron corresponds to the electron pair. While spin of negative polaron and positive polaron is 1/2, bipolaron has no spin.

The conductivity of PPy is provided with p-type doping. PPy chain shows four different electronic band structures with different doping levels. PPy is an insulator in its undoped state and its band gap is approximately 3.16 eV. During oxidation process, an electron is removed from the neutral PPy chain, and a polaron forms with a local deformation from the benzenoid structure to a guinoid structure (Bredas and Street 1985) and subsequently two localized electronic levels occur within the band gap while the unpaired electron occupies the bonding state as observed in Fig. 2.4.b. With further oxidation a second electron is removed from the PPy chain and a double charged bipolaron forms. Benzenoid to guinoid deformation is stronger in the bipolaron than

polaron. After bipolaron formation, if the polymer is further oxidized, an overlap between bipolarons takes place and results with the formation of two narrow bipolaronic bands (Fig. 2.4.d) and the energy gap decreases 1.4 eV.

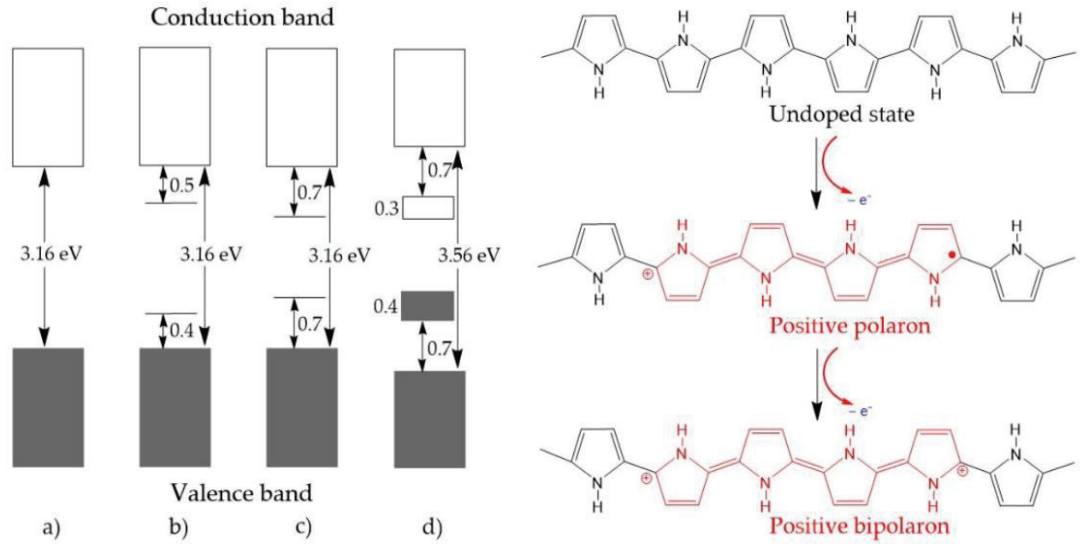

Figure 2.4 Electronic bands and chemical structures illustrating a) undoped, b) polaron, c) bipolaron, d) fully doped states of PPy (Source: Le, Kim, and Yoon 2017).

2.3 Synthesis of Conducting Polymers

Most common synthesis methods for conducting polymers are chemical or electrochemical oxidation polymerization methods. The other methods are photochemical method, methathesis method, concentrated emulsion method, inclusion method, solid state method, plasma polymerization and pyrolysis method (Awuzie 2017).

Electrochemical synthesis of conducting polymers is carried out through oxidative polymerization of their monomers by constant current (current controlled method), constant potential, or cyclic voltammetry (potential controlled method) in a potential range. An electrolyte solution containing solvent, electrolyte salt and the monomer is required for electrochemical polymerization. Solvent, electrolyte salts, concentration of the monomer, pH of the solution, polymerization potential, current, temperature, etc. all affect the electropolymerization process. However, the most important parameter influencing the process is the polymerization potential. Low oxidation polymerization potential allows the polymerization takes place easier. With 0.7 V polymerization potential of pyrrole and 0.8 V polymerization potential of aniline, electropolimerization

of polypyrrole and polyaniline occur easier than the other conducting polymers and can be take place in aqueous solutions.

Conducting polymers are synthesized by chemical oxidation method through the oxidation or reduction of monomers and polymerization of its monomer. It is performed in solution by using oxidants such as $FeCl_3$ and $(NH_4)S_2O_8$, etc. and this method is appropriate for enlargement the production scale, therefore mass production and low cost are the main advantages of this method. PPy and PANi can be synthesized chemically. Stability after conjugation is required during chemical polymerization. Oligomers and low molecular weight polymers should be enough reactive and soluble to polymerize for a successful chemical polymerization.

2.4 Properties of Conducting polymers

Generally, common conducting polymers show conductivity between 10^{-3} and 10^{3} S/cm after doping, whereas conductivity of conjugated polymers is between 10^{-9} and 10^{-6} S/cm in their intrinsic state (Li 2015). Charge transport mechanism is different in conducting polymers from crystalline conducting materials. While charge carriers can move freely in energy bands in crystalline conducting materials, they are found in the local doping energy levels in limited length of conjugated polymer chain. Charge carriers can move readily on the main chain, however, they must hop for charge transport between the conjugated polymer chains and activation energy for hopping is higher that the activation energy of the charge transport on the main chain. Conductivity values of some conducting polymers with their type of doping are given in Table 2.1.

Table 2.1 Conductivity values of common conducting polymers
(Source: Guimard, Gomez, and Schmidt 2007).

Conducting Polymer	**Maximum Conductivity (S/cm)**	**Type of Doping**
Polyacethylene (PA)	200-1000	n,p
Polyparaphenylene (PPP)	500	n,p
Polyparaphenylene sulfide (PPS)	3-300	p
Polyparavinylene (PPv)	1-1000	p
Polypyrrole (PPy)	40-200	p
Polytiophene (PTh)	10-100	p
Polyisothionaphthene (PITN)	1-50	p
Polyaniline (PANi)	5	n,p

Besides high electrical conductivity that they exhibit, good optical and magnetic properties, flexible mechanics, effective microwave absorption and their light weight are the main advantages of conducting polymers (Awuzie 2017). A special property of conducting polymer is the electrochemical redox activity. Besides, they show muscle-like properties such as high power to mass ratio, inherent compliance, and direct drive-capability. These conducting polymers use dimensional changes resulting from electrochemical ion insertation and deinsertation. A voltage potential is applied between the conducting polymer film and a non-reactive counter electrode. Depending upon the conducting polymer/electrolyte system used and the rate of applied voltage, electron insertion into one electrode results with a volume increase if cations are inserted or with a volume decrease if anions are removed. Expansion is observed perpendicular to the polymer chain orientation for oriented polymers, suggesting that ions and accompanying solvent are slotted between chains. The conducting polymer actuation mechanism is depicted in figure 2.5.

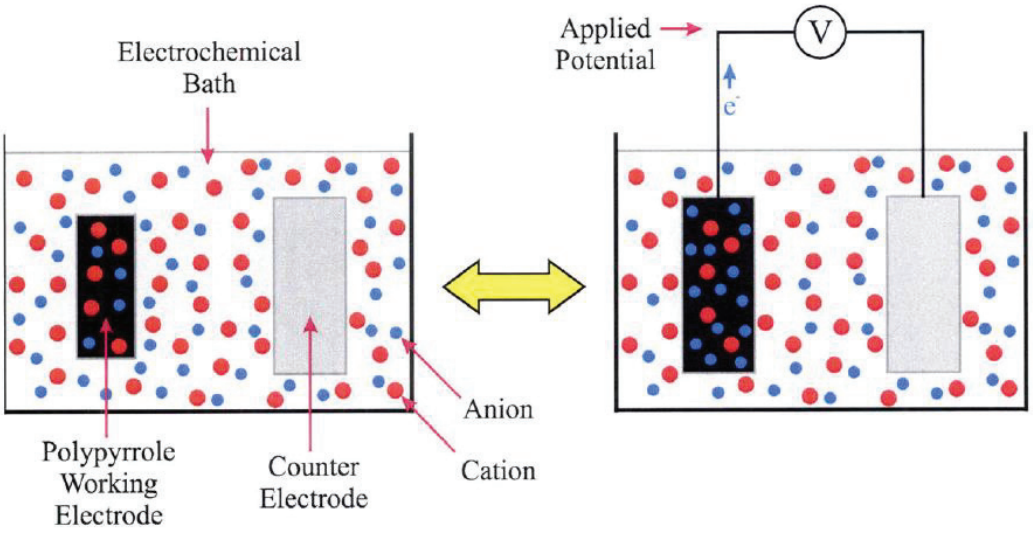

Figure 2.5. Schematic diagram of the electrochemical actuation of PPy. A voltage potential is applied between working and counter electrodes, here it causes expansion with diffusion of anions (Source: Fofonoff 2008).

Dimensional change under application of voltage potential results with utilization of conducting polymers as actuators. There are two common types of conducting polymer actuators. These are layered actuators and linear actuators. In a layered polymer actuator one or two active layers are made to contract and expand with respect to a passive layer or an opposing active layer. These actuators can be used in an electrolyte bath or in air by using a central ionically conducting gel layer (Madden et al. 1999). Layered actuators generally produce one single bending motion , and it is difficult to configurate and attach a layered actuator. A basic conducting polymer linear actuator consists of a polymer film ribbon connected at its two ends. One or both of these connections also act as electrical connections used to charge and discharge the film with respect to a counter electrode, thus causing an expansion or contraction. Linear polymer actuators have some advantages compared to layered actuators. Linear actuators are generally able to produce greater forces than layered actuators and they are more easily preloaded and attached. Another advantage of linear actuators is that they can be scaled more easily and linear actuators fundamental behaviour does not change when its dimensions are changed.

Besides their advantages, disadvantage of conducting polymers is insolubility which does not allow large scale applications of conducting polymers. In order to solve this problem attaching suitable subtituents is an effective method. However, substituents to enhance solubility is not appropriate for doped conducting polymers. A substituent on the conducting polymer main chain causes distortion of the conjugated main chain and

decreases the conjugation degree therefore it causes decrease in conductivity. Cao et al. reported a method utilizing counteranion induction to improve the solubility of doped PANi by using proton acid and acid containing anions with flexible side chain (Cao, Smith, and Heeger 1993). They obtained a conductivity value for PANi film (10^2 S/cm) higher than obtained with the other methods.

2.5 Applications of Conducting Polymers

Because of their good electrical and optical properties and ease of synthesis and processing, conducting polymers find use in a wide range of applications such as battery technology, photovoltaic devices, light emitting diodes, and electrochromic displays (Gurunathan et al. 1999). Besides their use in electronics, conducting polymers are used as artificial muscles owing to their actuation property. Baughman et al. reported usage of conducting polymers as actuator firstly in 1996 (Baughman 1996). The key advantages of conducting polymers over other actuator materials are the low operating voltage comparatively large strokes and ability to operate against high mechanical loads. Their operating voltage is about 2 V, however, in order to increase actuation rate higher voltages of up to 10 V are sometimes used. Generally strains are 2-10% and actuator strokes can reach 40% (Madden et al. 2004, Mazzoldi, Della Santa, and De Rossi 2000, Smela and Gadegaard 1999, Hara et al. 2004a). High-quality electrochemically grown conducting polymer films and solution-spun conducting polymer fibers have tensile strengths on the order of 100 MPa or higher (The tensile strength of a material is the maximum amount of tensile stress that it can take before failure, such as breaking or permanent deformation). Strains smaller than 0.2% are obtained at loads of 100 MPa (Spinks et al. 2006), with operating stresses about 1-34 MPa. Work densities (Spinks and Truong 2005) approach 100 MJ/m3.

Among conducting polymers, PANi and PPy show the largest active stress and active strain. Although PANi is more processable than PPy (Herod and Schlenoff 1993, Dufour, Rannou, Djurado, Zagorska, et al. 2003, Dufour, Rannou, Djurado, Bee, et al. 2003), it requires an acidic bath for actuation (Smela, Lu, and Mattes 2005, Smela and Mattes 2005) whereas PPy actuates in a variety of environments, such as in aqueous solutions (Smela and Gadegaard 1999, 2001). PPy films actuation ability also was examined (Han and Shi 2006). Film was synthesized by direct oxidation of pyrrole. The

conductivity of the as-grown PPy film was measured to be about 15 S cm^{-1}, it has a tensile strength of 36±5 MPa and an elongation at break of 4.5±0.5%. The PPy film was subjected to multiple potential steps of reduction at −0.8V and oxidation at 0.8V at 0.5 Hz. After 20,000 cycles, the film still can bend to 90º at a potential of 0.8V. However, its movement rate was decreased from 40 to 3º s−1. The high performance of this actuator is mainly due to the PPy film has a high conductivity. In an other study PPy films were synthesized by electrodeposition method (Madden et al. 2007). Although the maximum tensile strength was 120MPa, creep behavior suggested that sustained loads of over 20 MPa were not practical if position control was to be maintained. The creep was much faster at the higher temperature. PPy films passively cycled at a peak-to-peak amplitude of 8 MPa under an average load of 10MPa for 10^6 cycles showed no apparent fatigue. The strain amplitude decreased from 2% to 1% after 7000 cycles and an increased rate of creep was also observed during actuation. When the potential range was reduced such that the initial strain amplitude is 1.5% the strain drops to 1% after 32,000 cycles. The actuation of PAN gel fibers also was observed (Choe and Kim 2006). The diameter and length of the PAN fiber in a basic solution environment (1M LiOH) were observed to be 40 and 350 μm, respectively. In an acidic solution environment (1M HCl), the diameter and length of the PAN fiber were observed as 14 and 120 μm, respectively. The amount of H+ present affected the shrinking of the fibers and the response time.

After discovery of biocompatibility of conducting polymers in 1980s, conducting polymers were began to be utilized in biological applications and they have been used in many biomedical applications such as tissue engineering scaffolds, drug delivery, bisensors, bioactuators, and neural probes (Guimard, Gomez, and Schmidt 2007). Conducting polymers can support many cellular activities including cell adhesion and migration, DNA synthesis, and protein secretion via electrical stimulation (Wong, Langer, and Ingber 1994, Umana and Waller 1986, Foulds and Lowe 1986). Cells responding to electrical impulses are nerve, bone, muscle, and cardiac cells. Therefore, conducting polymers in their oxidized state with the presence of electrical stimulilation significantly enhance cell adhesion and proliferation for these types of cells (Schmidt et al. 1997). Electrochemical actuation and coherent mechanical properties with mammalian skeletal muscles, make conducting polymers a good candidate for artifial muscles studies. Natural muscles are biological organs which transform chemical energy into mechanical energy and heat. For their actuation it requires an aqueous media, an electric pulse arriving from the brain to the muscle, liberation of calcium ions inside the sarcomere,

chemical reactions, conformational changes along natural polymeric chains with change of the sarcomere volume and water exchange. Artificial muscles are materials or devices which have structural or functional properties like natural muscles. They must include, at least, electric pulses, polymeric chains, aqueous solutions, volume variations and strain and stress changes. Mechanical properties of mammalian skeletal muscles are given in Table 2.2.

Table 2.2 Properties of mammalian skeletal muscle
(Source: Mirfakhrai, Madden, and Baughman 2007).

Property	**Typical Value**	**Maximum Value**
Strain (%)	20	>40
Stress (MPa)	0.1 (sustainable)	0.35
Work density (kj/m^3)	8	-
Density (kg/m^3)	1037	-
Power to mass (W/kg)	50	200
Efficiency (%)	-	40
Cycle life	-	10^9
Young Modulus (MPa)	10-60	-

2.6 Literature Studies on Electrospun Conducting Polymer Nanofibers

Electrospun PAN/PPy **c**arbon nanofibers were synthesized using 15, 30, and 50 wt% PPy and a carbonization process at 700 ◦C followed by electrospinning (Ji et al. 2010). SEM images of nanofibers showed that all nanofibers had regular and straight morphology and with the increase of PPy content, beads were observed on nanofibers. Thermal properties of electrospun PAN/PPy bicomponent nanofibers were explored using differential scanning calorimetry (DSC). DSC graphs of nanofibers are given in Fig. 2.6. PAN nanofibers showed a large and sharp exothermic peak at about 290 ◦C, which was due to the complex and multiple chemical reactions such as dehydrogenation,

instantaneous cyclization, and crosslinking of PAN during the process of thermal treatment via the free radical mechanism. This peak was also observed for PAN/PPy bicomponent nanofibers, but its intensity decreased with the increase of PPy content. With the addition of PPy a new exothermic peak was observed at around 250 ◦C. With the increase of PPy content, the intensity of this peak increased and the peak position shifted to higher temperatures. The addition of PPy into PAN could affect the complex chemical reaction mechanism of PAN due to the inter-molecular interaction between the protonated PPy and nitrile groups of PAN. The 250 ◦C peak was wider than the peak at 290 ◦C and the total reaction was smaller because the propagation through the ionic mechanism was slower than that via the free radical mechanism. The DSC results indicated that pure PPy gave only an endothermic peak at about 143 ◦C.

These PAN/PPy carbon nanofibers were used as anodes for rechargeable lithium-ion batteries without adding any polymer binder or conductive material and they displayed high reversible capacity, improved cycle performance, relatively good rate capability, and clear fibrous morphology even after 50 charge/discharge cycles.

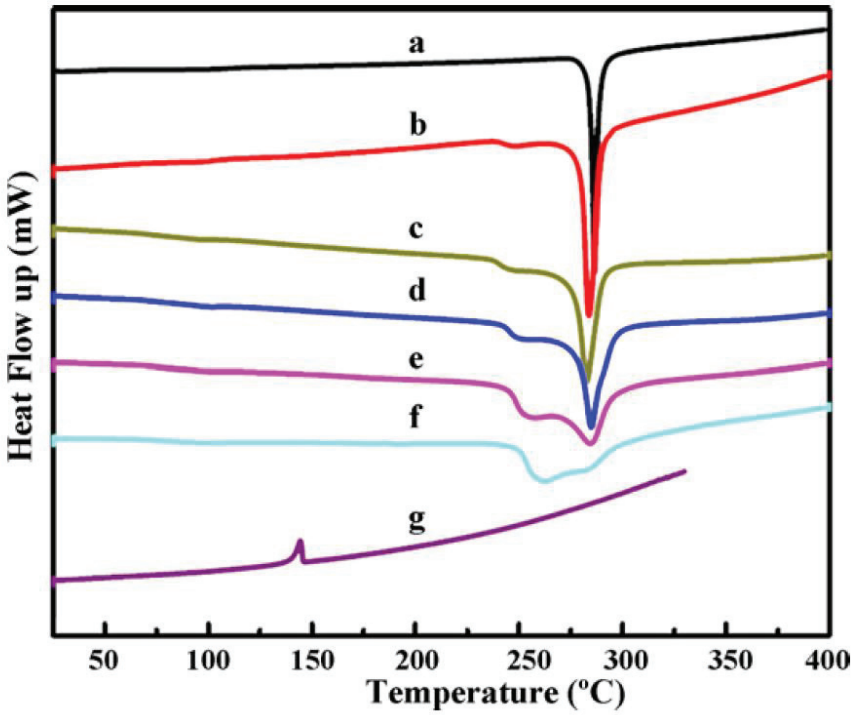

Figure 2.6 DSC graphss of PAN/PPy bicomponent nanofibers with different PPy contents in PAN (a) 0 wt%, (b) 5 wt%, (c) 10 wt%, (d) 15 wt%, (e) 30 wt%, (f) 50 wt% and (g) 100 wt% (pure PPy cannot be electrospun) (Source: Ji et al. 2010).

Hybrid chitosan (Cs)/polypyrrole microfibers were fabricated from a chitosan solution through wet spinning technique followed by in situ chemical polymerization of pyrrole in 2011 (Ismail et al. 2011). The schematic representation of linear actuation mechanism of Cs/PPy microfibers is given in Fig. 2.7. Linear actuation behavior of Cs/PPy microfibers were tested with a muscle lever arm. PPy concentration of microfiber was higher at the external part of fibers than the internal part, therefore the external part of fibers provided greater actuation than the internal part. Cs/PPy microfibers showed an average linear actuation strain of 0.54% upon cycling the potential.

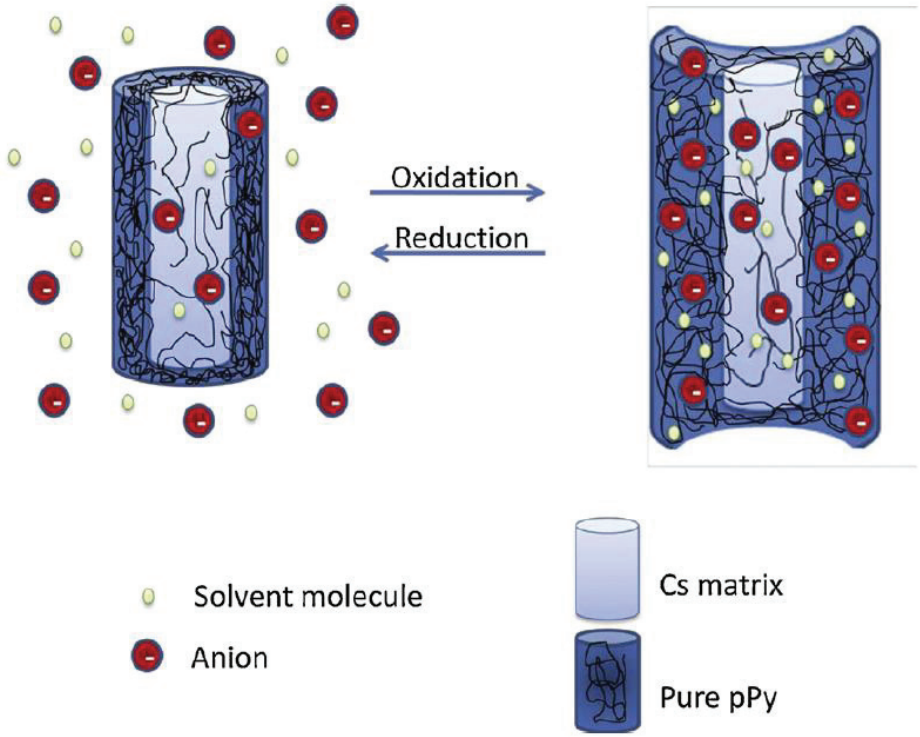

Figure 2.7 A schematic representation of linear actuation of Cs/PPy microfiber (Source: Ismail et al. 2011).

The Young modulus of Cs/PPy microfibers and PPy film were obtained by submitting the samples to a steady stretching force (F). Young modulus is given by the equation 2.2:

(Eq .2.2)

$$Young\ Modulus = \frac{F/S}{\Delta L/Lo}$$

where L_o is the initial length of PPy/Cs microfiber or PPy film, ΔL is the length change after application of the force F, and S is the transversal area of the sample with the unit of m^2. The obtained Young's modulus of Cs/PPy microfiber (5250 MPa) was 3 times higher than that of pure PPy film (1706 MPa) in their study. Their study also indicated that the Cs/PPy microfiber can act as a current sensor, a linear temperature sensor and a concentration sensor. Cs was tried also with PANi (Ismail et al. 2008). Cs fibers were prepared using a wet spinning method and Cs/PANi microfibers were fabricated through an in situ chemical polymerization of aniline. The obtained fibers showed high electrical conductivity of 2.856×10^{-2} S/cm (measured with 2-point method) and the chemical actuation resulted in a high strain ratio of 6.73 %. Cs/PANi fibers expanded in length at higher pH values, and contracted at low pH values. For Cs/PANi fibers it is observed that there was a dual actuation, electrochemical actuation is highly dependent on both the conductivity and the pH of the electrolyte. Fig. 2.8 shows the cyclic voltammograms of the fibers at three different pH values. Cyclic voltammograms of Cs/PANi fibers were similar to that of neat PANi, so electroactive behavior of Cs/PANi fibers originated from PANi. PANi oxidation peaks were observed at 0.25 V (leucoemeraldine to emeraldine salt conversion) and at 0.65 V (the emeraldine salt to pernigraniline conversion). For Cs/PPy fibers a middle peak was observed around 0.4-0.5 V corresponding to over oxidation or the presence of benzoquinone.

Conductive electrospun polypyrrole nanofibers with diameters in the range of about 70–300 nm and thickness of about 10-20 μm were prepared by Chronakis et al (Chronakis, Grapenson, and Jakob 2006). The average diameter increased with increasing PPy concentration. The electrical conductivity of PEO/PPy nanofibers were measured with two-point method. As shown in Fig. 2.9 the conductivity depended on the diameter of nanofiber and so PPy content in nanofibers. The thickness of the electrospun PEO/PPy nanofibers increased by two orders of magnitude from the lowest to the highest concentration of PPy and increased from $4.9\text{x}10^{-8}$ to $1.2\text{x}10^{-5}$ S/cm. For the highest PPy content of the PPy/PEO nanofibers, the highest electrical conductivity was obtained because contacts between conducting polymer regions (PPy regions) remained less isolated from non-conducting regions and increased electrical conductivity.

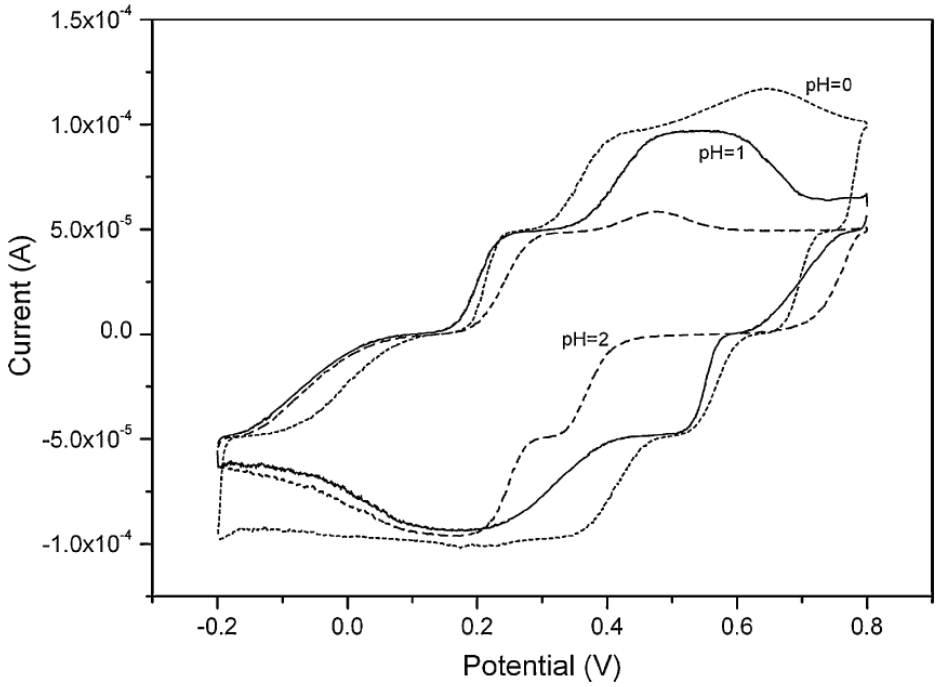

Figure 2.8 Cyclic voltammograms of chitosan/PANi fibers in aqueous HCl solutions with different pH (Source: Ismail et al. 2008).

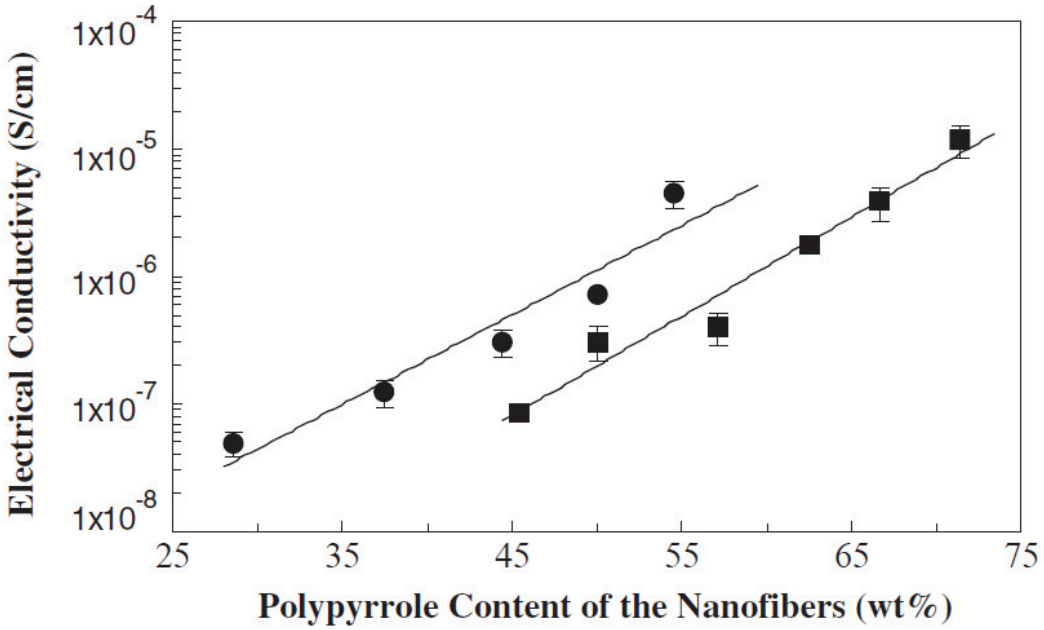

Figure 2.9 Electrical conductivity of PPy/PEO nanofibers as a function of their polypyrrole content. Solutions of PPy with 2.5 wt% PEO (●), and 1.5 wt% PEO (■) as carrier were used (Source: Chronakis, Grapenson, and Jakob 2006).

Tavakkol et al. (Tavakkol et al. 2017) reported the production of PPy/Poly(vinyl pyrrolidone) (PVP) nanofibers via the electrospinning of pyrrole solution and subsequent oxidation. The low solubility and low viscosity of PPy was enhanced with PVP and made electrospinning of PPy possible. It was found that increasing the viscosity of pyrrole by adding poly(vinyl pyrrolidone) (PVP) (9% w/w), made its electrospinning possible. Average diameter of prepared PPy/PVP nanofibers was 440 nm. Their electrical conductivity was measured with 4- point probe technique. The highest electrical conductivity was recorded for the anthraquinone-2-sulfonic acid sodium salt doped PPy-PVP nanofibers with an average diameter of around 830 nm and it was 5.22×10^{-1} S/cm.

2.6.1 Effects of CNTs on Conducting Polymers

A single-wall carbon nanotube (SWCNT) is defined by a graphene sheet rolled into a cylindrical shape with a diameter of about 0.4-10 nm and lengths extending up to several microns. If we ignore two ends of carbon nanotube and focus on the large aspect ratio of the tube, carbon nanotubes can be considered as one-dimensional nanostructures with axial symmetry and they have excellent properties because of this symmetric structure (Baddour and Briens 2005). Multi-walled carbon nanotube (MWCNT) consists of tubes made of more than one concentric graphene cylinders coaxially arranged around a central hollow with a constant interlayer spacing which is nearly equal to 0.34 nm (Jorio et al. 2001). MWCNTs consist in 2 to 30 concentric graphene, diameters of which range from 2.5 to 100 nm. There is a great research and industrial interest to use carbon nanotubes (CNTs) as nano-fillers to obtain polymer composites with improved mechanical, electrical and thermal properties (Zhou et al. 2008, Guo et al. 2012, Wang, Bradford, et al. 2011, Arash, Wang, and Varadan 2014, Yardimci, Tanoglu, and Selamet 2013). Because of their superior mechanical properties such as modulus, strength and thermal and electrical conductivity with their low weight (Miyagawa et al. 2004, Fidelus et al. 2005, Rajoria and Jalili 2005), they have been attractive candidate for composite systems. Properties of CNTs are given in Table 2.3. The main problem in using CNTs as filler materials is their dispersion in matrix. Dispersion and alignment of CNTs influences directly the mechanical properties of final composite. Agglomerated CNTs cause defect sites, porous regions, and crack initiation points, etc. which reduce the mechanical properties of composite. There are several techniques to achieve a good dispersion of

CNTs in a polymer matrix such as, high speed mixing (Sandler et al. 1999), in situ polymerization (Jia et al. 1999), chemical functionalization (Xie, Mai, and Zhou 2005, Zhu et al. 2003, Dyke and Tour 2004) and high shear mixing (Thostenson, Karandikar, and Chou 2005). Surface functionalization of CNTs has been found be an effective method to obtain a good CNT dispersion and enhance the bonding between the CNTs and polymer matrix.

Table 2.3 Properties of CNTs
(Source: Ong et al. 2010).

Properties	**SWCNTs**	**MWCNTs**
Specific Gravity	0.8 g/cm^3	1.8 g/cm^3
Elastic Modulus	~1 TPa	~0.3 – 1 TPa
Strength	50 – 500GPa	10 – 60 GPa
Resistivity	5 – 50 μΩ cm	5 – 50 μΩ cm
Thermal Conductivity	3000 W m^{-1} K^{-1}	3000 W m^{-1} K^{-1}
Thermal Stability	>700 °C (in air) 2800°C (in vacuum)	>700 °C (in air) 2800°C (in vacuum)
Specific Surface Area	~400-900m^2/g	~200 – 400m^2/g

In addition to their high electrical conductivity and good mechanical properties (Spinks et al. 2006), CNTs show electromechanical actuation behavior. This electromechanical behavior makes CNTs a good candidate for application such as sensors and actuators (Li, Thostenson, and Chou 2008). By incorporating 0.5 and 1 volume % CNTs into P(VDF-TrFE-CFE) terpolymer, actuation response of the polymer is significantly improved and actuation occurs at lower voltages as compared to those of without CNTs. At E =54 Vμm^{-1}, the composite with 0.5 wt% CNTs exhibited a strain of -2 % in comparison with -1.1 % for the neat terpolymer. At E =72 Vμm^{-1}, the composite with 1wt% CNTs changes its thickness by -2.5 %, whereas the thickness change is only -1.8 % for the original terpolymer (Zhang, Zhang, et al. 2005). It was also revealed that

CNTs added into conducting polymers may increase actuation strain and conductivity, therefore, electrochemical efficiency in the actuation is provided (Tahhan et al. 2003). Courty et al. (Courty et al. 2003) reported substantial dielectric anisotropy by aligning CNTs in the polymer. The actuation response was due to the large anisotropy in nanotube polarizability. Zheng et al. (Zheng et al. 2011) fabricated polypyrrole (PPy)/CNT laminates by electrochemically polymerizing PPy on a glassy carbon substrate. Incorporation of the CNT sheets resulted in an increase of strength for both transverse and longitudinal directions and enabled actuation at much higher loads, as compared to those for electrolyte-contacting neat PPy. Electrical conductivity was improved with the CNTs content as observed in Table 2.4.

Table 2.4 The composition and properties of PPy · TFSI and PPy · TFSI/CNT laminates (Source: Zheng et al. 2011).

Wt% CNTs	**No. of PPy layer**	**Young's Modulus [GPa]**		**Tensile Strength [MPa]**		**Electrical Conductivity [S cm^{-1}]**	
		longitudinal	Transverse	longitudinal	Transverse	longitudinal	Transverse
0	1	0.4	0.4	21	21	163	163
0.9	4	1.2	0.8	46	38	191	181
1.8	7	1.7	1.1	53	48	224	207
3.5	14	2.1	1.7	79	35	257	221

Park et al. (Park et al. 2012) added flouro group bonded functional CNTs slurry to the PAN solution. Reduction of thermal damage on the surface of PAN during the stabilization process was noticed. The DSC results indicated that the cyclization enthalpy of F-Ph-CNT/PAN composite (688 J/g) were much lower than those for homo PAN (1601J/g). The cyclization temperature also decreased with fluoro group addition from 191 ^{o}C to 265 ^{o}C. The integration of SWCNTs into polyaniline fibers (PANi) was investigated using wet spinning by Mottaghitalab et al. (Mottaghitalab et al. 2006). The addition of CNT in N,N'-Dimethyl propylene urea (DMPU) to PANi was found to limit aggregation of CNTs. The influence of CNTs on mechanical properties of the PANi fibers

was investigated and their stress-strain curves are given in Fig. 2.10. Addition of 2 wt% CNTs to PANi increased its yield stress by 100% (from 120 MPa to 250 MPa), tensile stress by 50% (from 168 MPa to 260 MPa), and Young's Modulus by >200% (from 7GPa to 17 GPa) and decreased its elongation break by 30% (from 3.1 % to 2.2%).

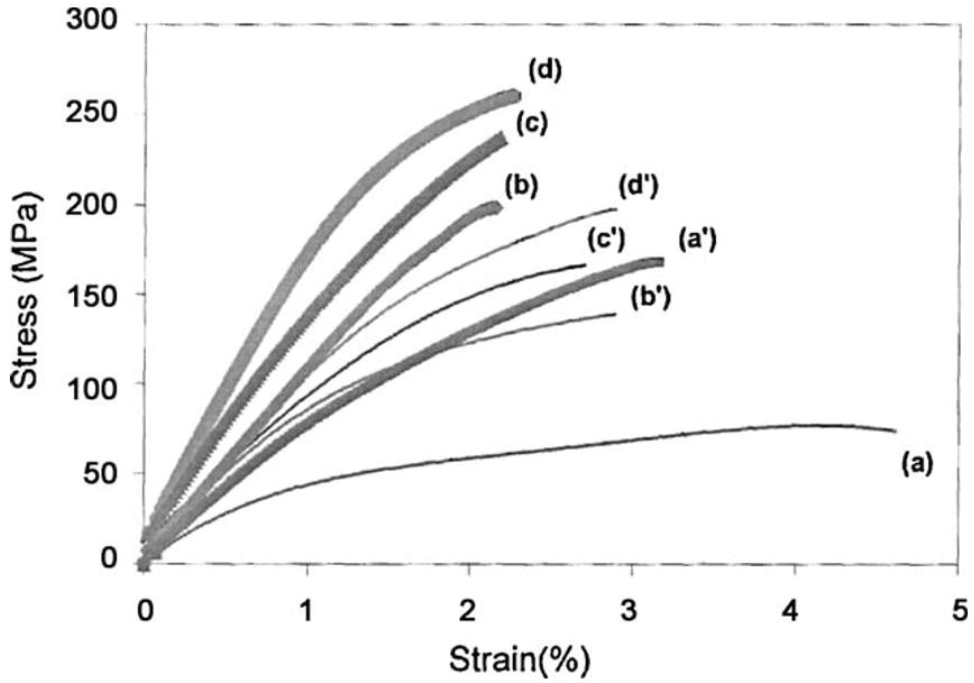

Figure 2.10 The stress–strain curves of PANi–CNT composite fibers with different CNT contents, before doping (thick lines) and after doping for 24 h in MSA (thin lines): (a,a') neat polyaniline, (b,b') PANi–CNT 0.5% (w/w) (c,c') PANi–CNT 1% (w/w) (d, d') PANi–CNT 2% (w/w), before and after doping (Source: Park et al. 2012).

Chitosan/PANi/SWCNT fibers were fabricated by wet spinning method by Spinks et al. (Spinks et al. 2007). The conductivity of the synthesized material (10^{-4} S/cm) was 3 to 4 order of magnitude higher than those of the PANi/chitosan composite film. The mechanical properties were improved and the actuation strains (0.3%) were reduced due to the stiffening effect of the nanotubes. Tensile strength of chitosan/PANi/SWNT fibers was 95 MPA whereas that of pure chitosan was 42 MPa, and elongation at break were increased by 60%.

PPy is one of the commonly studied conducting polymers due to its low actuation voltage, high conductivity and good biocompatibility (Kai et al. 2011, Lee et al. 2009). Its actuation voltage is lower than 2 V, reach up to 30 MPa active stress and 39%

maximum strain (Madden et al. 2004, Bay et al. 2003, Hara et al. 2004b). It reaches to the largest stroke value among all the conducting polymers for an electrochemical actuation (Chen, Wang, and Chen 2010). PPy actuators have been synthesized by a variety of methods. Electrodeposition (Madden et al. 2007), drop casting (Zheng et al. 2011) and electrospinning (Chronakis, Grapenson, and Jakob 2006) are the most common methods. Electrospinning method provides extremely rapid formation of the nanofiber structure, huge material elongation rate and a cross-sectional area reduction (Doshi and Reneker 1993). Because of its poor solubility, pure PPy cannot be electrospun, therefore PPy is used generally with a co-polymer such as poly ethylene oxide (PEO) (Nair, Natarajan, and Kim 2005), PAN (Li et al. 2008), polyvinylidene difluoride (PVDF) (Ketpang and Park 2010) and poly strene (PS) (Bai et al. 2009). In general, PPy based coatings containing nanofibers were investigated to obtain linear actuators. Ketpang et al. (Ketpang and Park 2010) synthesized PVDF/CNT electrospun nanofibers using 1 wt% CNT, then they coated those nanofibers by vapor-phase polymerization of PPy. Tensile tests were carried out to analyse nanofibers mechanical properties. Table 2.5 shows tensile properties and electrical conductivities of the PVDF/PPy/CNT nanofiber composites. After PPy coating the Young modulus increased two fold for PVDF nanofibers, however, the tensile strength was lower because of the brittle mechanical property of PPy. According to electrical conductivity measurements, PPy coated PVDF/CNT nanofibers showed the highest conductivity of 0.388 S/cm. Samples containing 1 wt% MWCNTs.

Ju et al. (Ju et al. 2008) synthesized PAN/CNT electrospun nanofibers and coated with PPy by in situ chemical polymerization to improve electrochemical performance. The average dimeter of PAN nanofibers was 330 nm, while after CNT addition the average diameter decreased to 230 nm with rough surface due to higher solution conductivity of CNT added polymer solution. The specific surface area of PAN nanofibers and PAN/CNT nanofibers were 984 m^2/g and 1170 m^2/g, respectively. Fig.2.11 shows the cyclic voltammograms of nanofibers. Rectangular and symmetric shape of PAN and PAN/CNT nanofibers voltammograms indicated their capacitance behavior. Current increased with CNT addition in PAN nanofibers. For PPy coated nanofibers they did not observe any redox peaks and they also showed a rectangular shape. However, PPy coating provided increase in electrical conductivity for both PAN and PAN/CNT nanofibers.

Table 2.5 Tensile properties and electrical conductivity of (a) PVDF, (b) PVDF–MWCNTs, (c) PPy coated PVDF, and (d) PPy coated PVDF/MWCNTs nanofibers (Source: Ketpang and Park 2010).

Sample	Young Modulus (MPa)	Tensile Strength (MPa)	Tensile Strain (%)	Electrical Conductivity (S/cm)
a	20.28	2.23	86.29	2.50E−12
b	39.06	2.61	41.12	2.88E−8
c	40.94	2.15	18.58	4.02E−2
d	41.02	4.31	67.27	3.88E−1

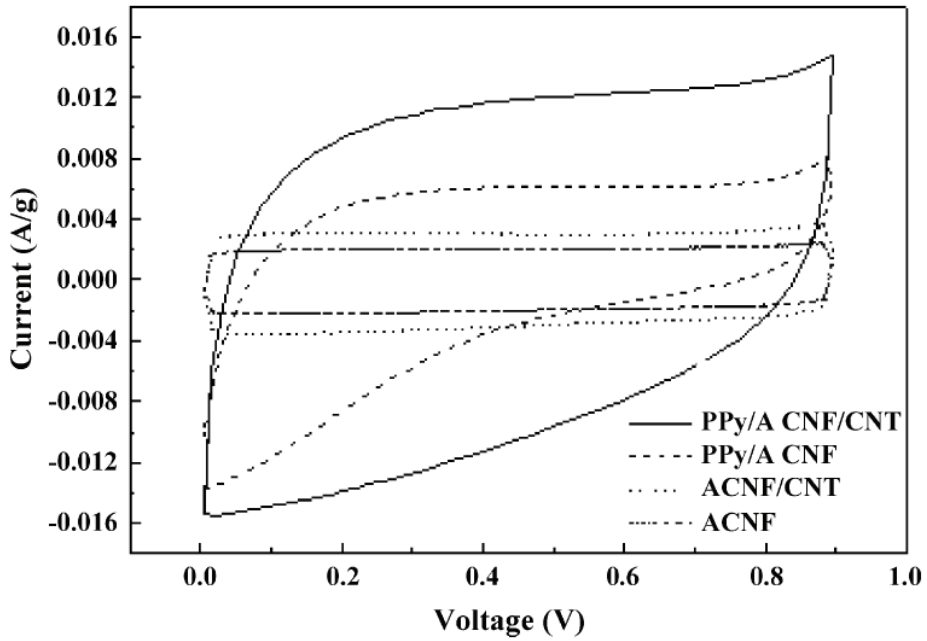

Figure 2.11 Cyclic voltammograms of ACNF (PAN), ACNF/CNT (PAN/CNT), PPy/ACNF (PPy coated PAN), and PPy/ACNF/CNT (PPy coated PAN/CNT) nanofibers (Source: Ju et al. 2008).

In this thesis study, PPy was utilized as a conducting polymer because of its advantages explained above and PAN was used as a co-polymer to enhance spinnability and brittle property of PPy. Preparation of CNT incorporated PAN/PPy electrospun nanofibers with different amount of PPy and CNT was reported. PAN/PPy nanofibers were prepared in both their random and aligned forms.

CHAPTER 3

ELECTROSPUN NANOFIBERS FOR TISSUE ENGINEERING SCAFFOLDS

3.1 Tissue Engineering Scaffolds

Tissue engineering is a fast growing scientific field which utilizes a combination of scaffolds, cells, and biologically active molecules to improve or replace biological functions (Ladd et al. 2011). Many diseases and injuries cause loss of organ or tissue functions and the aim of tissue engineering is to incorporate appropriate cells to a three dimensional (3D) scaffold and implant a cell-scaffold combination providing active and passive healing properties into a damaged tissue or whole organs. Overall, tissue engineering can be splitted into three subtitles (Subbiah et al. 2005) : (1) injection or transplantation of isolated cells to a defect site or an injured tissue, (2) delivery of tissue-inducing biomolecules to a targeted tissue, (3) growth and differentiation of specific cell types in 3D scaffolds. Among them, scaffold based tissue engineering is the most popular because of its potential to incorporate chemical, physical, and biological stimuli at different scales that can direct cell activity.

Scaffolds are generally made from polymers and there are various methods to synthesize them including solvent casting and particulate leaching, melt molding, rapid prototyping, phase separation, and electrospinning (Yang et al. 2001). Tissue engineering scaffolds should provide an environment that resembles their natural extracellular matrix (ECM) for cells. The ECM is different for each tissue type and scaffolds can mimic structural, mechanical and chemical properties of the ECM of the tissue. The composition of these protein molecules define its properties. Generally, ECM consists of connected protein molecules and forms an environment for cells to live, move and receive and transmit signals. Molecular composition of the ECM directly affects the structural properties of the tissue.

In many types of tissue, the ECM consists of protein networks such as collagen and elastin, and proteoglycans such as perlecan (Lodish 2008). These molecules provide an environment for cells to live, move, receive and transmit signals. Structural properties

of ECM are also significant for tissue. The ECM is generally at nano scale and fibrous and its orientation vary for different tissue types. While dermis has a randomly oriented structure to provide stretching in different directions, ligaments require a directional ECM to provide support in the direction of stress.

3.2 Nanofibrous Scaffolds and Their Fabrication Methods

Many ECM proteins show a fibrous structure with a fiber diameter from nanometer to micrometer scales. A successful scaffold supporting adhesion, proliferation and differentiation of cells should mimic both physical properties and chemical composition of the native ECM. Therefore, developing nanofibrous scaffold that mimic the natural fibrillar form of the ECM is a hot topic of tissue engineering. Molecular self-assembly, phase separation and electrospinning are the three main techniques to synthesize nanofibrous scaffolds (Chen et al. 2013).

3.2.1 Molecular Self-Assembly

Molecular self-assembly is a spontaneous process to manufacture ordered and stable nanostructured scaffolds (Goldberg, Langer, and Jia 2007) through some non-covalent interactions such as electrostatic, hydrophilic and van deer Waals interactions (Philp and Stoddart 1996). The main parameters affecting structural properties of the resulting materials in molecular self-assembly are kinetics, molecular chemistry, and assembly environment. Morphology of nanofibers can be controlled by changing process parameters. The most important thing in self-assembly is to develop small molecular building blocks having a well-defined pattern which shows the structural properties of biological systems (Smith, Liu, and Ma 2008). These blocks consist of small molecules, nucleic acids, and peptides and they can self-assemble into nanofibers. Among these building blocks peptide-amphiphile (PA) units which are significant because of the versatility in their design for biological applications are found.

Nanofibrous scaffolds obtained by molecular self-assembly technique have been investigated for different tissues including nerve (Guo et al. 2007), bone (Sargeant et al. 2008), and cartilage regeneration (Shah et al. 2010).

There are still some lack of this technique. Pore size and pore structure which are significant for cell proliferation and migration cannot be controlled and scaffolds obtained with this technique are generally mechanically weak and do not sustain and transfer mechanical loadings to the cells and surrounding tissues.

3.2.2 Thermally Induced Phase Separation

Thermally induced phase separation is another technique to synthesize nanofibrous scaffolds. In this technique, a homogeneous polymer solution is separated into a polymer rich phase and a polymer-poor phase under high temperature. Then, solvent is evaporated and a film is casted. Polymer-rich phase creates a 3D structure and polymer-poor phase forms a void space. Five main steps to synthesize a nanofibrous scaffold with this technique are raw material dissolution, gelation, solvent extraction, freezing, and drying (Ramakrishna 2005).

Thermally induced phase separation method can be combined with other techniques such as particulate leaching and solid free-form fabrication to develop nanofibrous scaffolds with well-defined pore shape and pore size (Holzwarth and Ma 2011) and therefore, to provide increase in cell adhesion (Woo, Chen, and Ma 2003, Zhang, Hu, and Ma 2012). The pore morphology of the scaffolds can be changed by optimizing processing parameters (Zhang, Hu, and Ma 2012). While control of the final structure is possible in this technique, control of fiber orientation and diameter is different. Besides, synthesis time is very long and mechanical properties of the final product is weak like molecular self-assembly technique.

3.2.3 Electrospinning

Electrospinning is a simple and robust fiber synthesis method for the fabrication of long organic fibers by using a high voltage. It was firstly patented by Anton Formhals in 1934 (Bhattarai et al. 2004). Formhals firstly utilized electrospinning to synthesize cellulose acetate fibers. Electrospun nanofibers have an extremely high surface to volume ratio and so they have been used in many fields such as nanocatalysis, tissue engineering, protective clothing, filtration, biomedical, optical electronics, biotechnology, and environmental engineering (Luu et al. 2003). Some other advantages of electrospinning

are tunable porosity, fiber synthesis in a wide variety of sizes and shapes, and the ability to control fiber composition (Bhardwaj and Kundu 2010).

Electrospun nanofibers provides excellent interconnectivity (Pham, Sharma, and Mikos 2006) and porosity for the integration of cells into the scaffold if the pore size is large enough (Ju et al. 2010). Therefore, there has been an important interest to utilize the electrospinning for tissue engineering. Electrospun nanofibrous scaffolds closely mimic the ECM and in order to add specific features of tissues, by changing electrospinning process parameters, specific features of tissues can be supported by electrospun scaffold. For example, some tissues require anisotropic structure because aligned nanofibers significantly affect mechanical properties of scaffold and so cell behavior. Using some collecting devices, electrospun nanofibers can be aligned easily. These collecting devices can use three different forces (Liu, Thomopoulos, and Xia 2012); mechanical forces by using a rotating collector, electrostatic forces by using parallel electrodes, magnetic forces by using parallel magnets. In order to adjust the properties of specific tissue types, electrospinning is an appropriate technique by allowing to control process parameters. Electrospinning is a versatile scaffold fabrication technique with its usage for tissues ranging from bone to nerve.

3.2.3.1 Electrospinning Theory

In order to produce fibers in electrospinning technique, electrostatic forces ars utilized, a DC voltage supply is required which should have a capacity of tens of kilovolts. Electrospinning setup mainly consists of three parts; a high voltage supply, a spinneret (syringe pump), and a grounded collector. There are vertical and horizontal types of electrospinning setups (Dosunmu et al. 2006).

In electrospinning process, the high voltage is generated between a negatively charged polymer solution filled into a syringe and a grounded conducting collector (Fig. 3.1). When the polymer solution drop is subjected to the electric field, an electric charge is created onto the polymer solution drop. Then, electric field reaches to a sufficient value and the electrostatic charge becomes larger than the surface tension of the polymer solution at the capillary tip, a charged jet is created and the solvent evaporates. The drop stretches as a Taylor cone. A charged jet is ejected from the tip of the Taylor cone and it has a uniform shape for a few milimeters, and then this charged jet demonstrates an unstable and fast way till the collector. Finally, solvent of the polymer solution evaportes,

solid polymer fibers deposited on the collector (Deitzel et al. 2002). The size of electrospun fibers can be varied micro to nanometer scale in diameter (Prabaharan, Jayakumar, and Nair 2011).

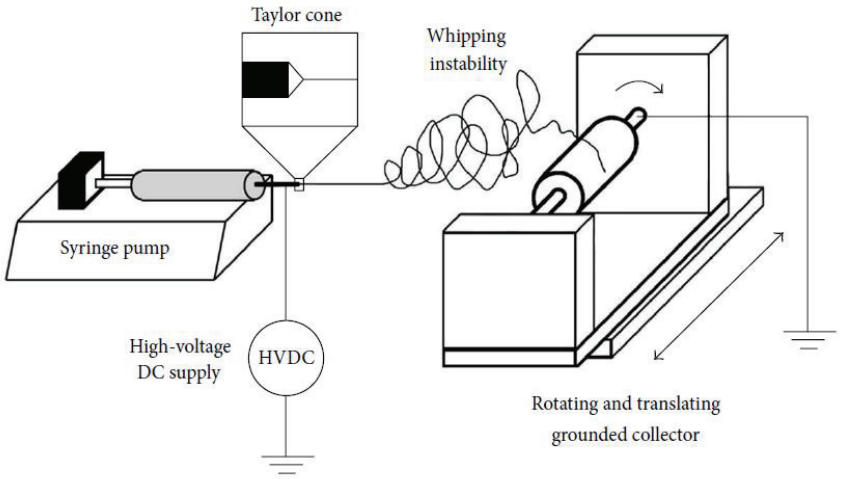

Figure 3.1 Schematic of a typical electrospinning system
(Source: Sill and von Recum 2008).

3.2.3.2 Electrospinning Parameters

There are many variables affecting the mechanics of the fiber formation in electrospinning process. Three main types of parameters is affected the fiber formation and structure (Sill and von Recum 2008). These are solution properties, process factors, and ambient conditions.

Solution properties including solution concentration, viscosity, conductivity, and surface tension. Polymer concentration has an important effect on electrospinning process, it influences surface tension besides fiber morphology. Finding optimum polymer concentration is significant for fiber formation as the polymer strands must have sufficient chain overlap in order to physically link and form fibers. At very low concentrations fiber formation does not occur and low concentrations causes beads on the fibers (Bhardwaj and Kundu 2010). Bead formation is because of the capillary breakup of the jet by the surface tension. Increasing polymer concentrations generally results with increasing fiber diameter and at high polymer concentrations, continuous flow of the solution through the spinneret is disabled, therefore continuous fiber formation does not

occur (Patel 2012). Molecular weight of the polymer defines the number of entanglements of the polymer chains. Therefore, it affects morphology of the fibers. Using polymers with high molecular weight provides fiber formation and good spinnability (Haghi and Akbari 2007). Another solution parameter is viscosity. If the viscosity is too high, electrostatic forces cannot overcome the surface tension and will prevent to form continuous fibers. Low viscosity causes shorter stress relaxation times and results in beads formation on fibers, so, an optimum viscosity value should be defined to obtain continuous and uniform fibers. Solution conductivity depends on polymer type, solvent, and the presence of ionizable salts in the solution. When a polymer solution with high electrical conductivity is utilized, an electrical force which elongates the polymer jet emerging from Taylor cone is created and it provides formation of uniform fibers with smaller diameter. However, if the solution is very conductive, it will be unstable in electrical field and causes significant bending of the polymer jet at Taylor cone and fiber diameter will become larger (Hayati, Bailey, and Tadros 1987). Radius of the polymer jet is inversely proportional with the cube root of the conductivity of the polymer solution (Baumgarten 1971).

Second one is process factors consisting of applied voltage, distance between the syringe and the collector, emitting electrode polarity, and solution flow rate. Applied voltage is a significant parameter for fiber formation and fiber morphology. Optimum voltage changes for different polymer/solvent systems (Sill and von Recum 2008). Deitzel et al. indicated that for poly(ethylene oxide) (PEO) and water solution, increasing voltage causes a recession of the Taylor cone and so formation of beads on the fibers (Deitzel et al. 2001). Another study showed that voltage does not significantly influence diameter of PEO fibers (Reneker and Chun 1996). There are many studies reporting that with increasing voltage, dimeter of fibers also increases while several studies suggested increasing voltage provides thinner fibers. For example; for poly(vinyl alcohol) PVA/water solution increasing voltage caused thick fibers formation (Zhang, Yuan, et al. 2005) and for polysulfone (PSA)/ dimethylacetemide (DMAC)/ water solution, increasing voltage narrows the diameter of fibers (Yuan et al. 2004). Applied voltage value also directly influence beading on the fibers. As a conclusion, voltage has a significant effect on fibers, however response of polymers to changing voltage vary for different polymer systems. Another important electrospinning parameter is solution flow rate. In literature, generally it is indicated that lower flow rate value is more suitable to get higher quality smooth fibers. At lower flow rates solution has enough time for

polarization while at higher flow rates solution cannot evaporate until it reaches to the collector and it causes bead formation and thick fibers (Megelski et al. 2002, Buchko et al. 1999). The distance between the tip of syringe and the collector also influences morphology and diameter of the fiber (Ki et al. 2005). If the jet length is too short for solvent evaporation before reaching to the collector, this condition increases fiber diameter and also bead formation (Yuan et al. 2004, Megelski et al. 2002). Using different types of collector the geometry of the electrospun mat can be controlled. Flat mats can be obtained by utilizing a flat collector while tubular patterned mats can be obtained by a rotating cylindrical collector. Using a rotating collector can also provide formation of aligned fibers to utilize for some special tissues. Generally Al foils is utilized as a collector, however transfer of the fiber from Al foil to other substrates is very difficult, thus, diverse collectors are designed. Some of these diverse collectors include wire mesh (Yeow, Liu, and Li 2005), pin (Deshmukh and Li 1998), grids, parallel bar (Jansen, Macchione, and Drioli 2005), rotating rod (Jansen, Macchione, and Drioli 2005) , liquid bath (Bhardwaj and Kundu 2010), etc.

Ambient conditions is the third type of parameter for electrospinning process. Temperature, humidity and velocity of the air in the spinning chamber also influence fiber formation. Temperature changes the viscosity of the polymer jet, so it can affect diameter of the fibers (Pham, Sharma, and Mikos 2006). Humidity affects the surface morphologies of the fibers (Casper et al. 2004), especially aqueous solutions. Low humidity causes fast solvent evaporation and high humidity neutralizes the charges on the jet decreases the stretching forces and causes thicker fiber diameter.

3.2.3.3 Cell-Electrospun Nanofibrous Scaffold Interactions

Pore size, surface topography, structural size, and porosity of the scaffold influence attachment, proliferation, and differentiation of cells (Bhardwaj and Kundu 2010). Yang et al. suggested that optimum pore size for cell attachment, proliferation, and migration was between 5 to 500 μm (Yang et al. 2001). For osteoblasts, fibroblasts, and chondrocytes having a mean size of 10 μm, cell infiltration and attachment decreased with smaller pore size (Eichhorn and Sampson 2005). The main challenge in use of electrospun nanofibers as scaffolds is the non-precise fiber diameter and scaffold porosity (Bhardwaj and Kundu 2010). It causes non-uniform cell distribution and therefore poor cell

infiltration. Smaller fiber diameter provides an increase in contacts between fibers and so decrease in the pore size (Eichhorn and Sampson 2005). Small pore size does not allow cells having large size to migrate interior of the scaffold and these cells cannot proliferate inside of the scaffold. The main advantage of electrospun nanofibrous scaffolds is their three dimensional structure which provides high surface area for cell infiltration and attachment. There are several methods to promote cell infiltration in nanofibrous scaffolds. First method Heprasil, a thiol-modified hyaluronic acid with thiol-modified heparin, co-deposition with polymer solution. Heprasil is a successful solution for three dimensional cell culture (Bhardwaj and Kundu 2010). Enzymatic degradable matrix pockets are formed in electrospun fibers with heprasil co-deposition, thus, scaffold depth increases and cells move easily in scaffold, cell infiltration improves (Prestwich 2007). In order to add specific properties to the scaffolds , the most common and easiest way is to manipulate solution and process parameters. Cells remodel their structure throughout tissue development. Electrospinning technique allows to develop biomimetric scaffolds with controllable structure and chemical properties and electrospun nanofibers can mimic in a wide range of tissues. Scaffolds should have different mechanical properties for different type of tissues such as linearity, anisotropy, viscoelasticity, and poroelasticity. Mechanical properties of skeletal muscle, cartilage, and vasculature are anisotropic and therefore, these tissues show high elasticity in the direction of fiber alignment (Kennedy, Bhaw-Luximon, and Jhurry 2016). When cells are seeded on anisotropic electrospun nanofibers, they proliferate along the direction of fiber alignment (Nerurkar, Elliott, and Mauck 2007).

3.2.3.4 Literature Studies on Use of Electrospun Nanofibers in Tissue Engineering

Electrospun fibrous scaffolds are appropriate substrates for tissue engineering with their morphologic properties resembling to ECM (Liu et al. 2013). They provide cell adhesion (Flemming et al. 1999), facilitate migration, proliferation and differentiation (Sheridan et al. 2001) with their high surface area. Furthermore, electrospun nanofibers can be optimized in mechanical, chemical and degradative properties that can greatly influence their interaction with cells (Nur-E-Kamal et al. 2005). In literature many electrospun polymer nanofibers have been studied as scaffolds for different cell types. By varying solution and process parameters properties of nanofibrous scaffolds can be

optimized for each individual application and after formation of nanofibrous scaffolds, its surface can be modified with a high density of bioactive molecules to obtain relatively high surface area. Thus, electrospun polymer nanofibers are important components of a large number of applications in tissue engineering (Huang et al. 2003, Thavasi, Singh, and Ramakrishna 2008, Fang et al. 2008, Pham, Sharma, and Mikos 2006) and drug delivery (Oliveira et al. 2015, Potrč et al. 2015, Wang et al. 2015, Aytac et al. 2015). Some tissue types studied with these fibers are vascular, neural, bone, cartilage, and tendon/ligament (Liu et al. 2013).

Mo et al. synthesized poly(l-lactide-co-e-caprolactone) [P(LLA-CL)] with l-lactide to e-caprolactone ratio of 75 to 25 electrospun nanofibers. These nanofibers biocompatibility was investigated for smooth muscle cell and endothelial cell. Cell morphology on nanofibers were observed by SEM for 7 days. SEM images of smooth muscle cell and endothelial cells grown on P(LLA-CL) electrospun nanofiber on day 7 after seeding are given in fig. 3.2. It was observed that both type of cells adhered and spread on the surface of nanofibers. At day 7 the cell number significantly increased and almost reached confluency on the nanofibrous scaffold, especially for smooth muscle cells. These nanofibers were found as a suitable scaffold for both type of cells (Mo et al. 2004).

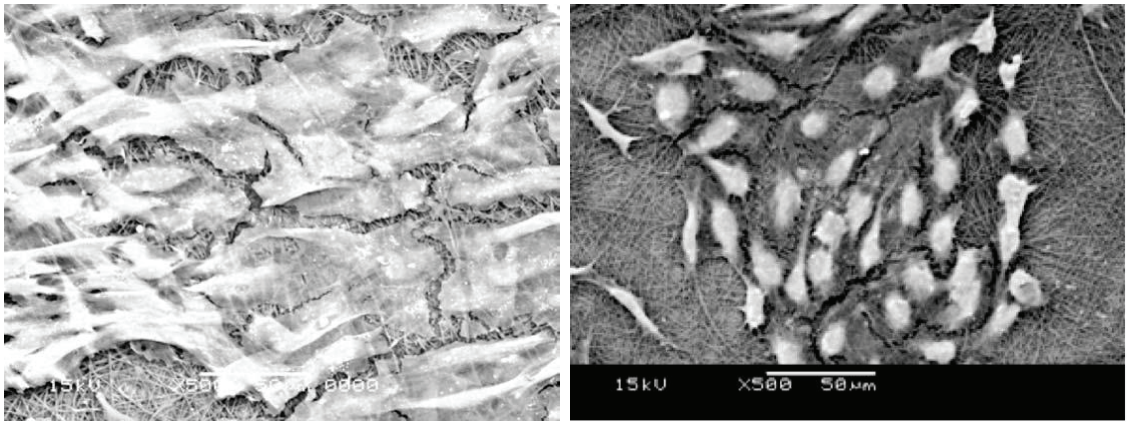

(a) (b)

Figure 3.2 SEM micrographs of (a) smooth muscle cells (b) endothelial cell seeded on electrospun P(LLA-CL) copolymer scaffolds after 7 days of culture cells (Source: Mo et al. 2004).

Conductive PPy/PCL/gelatin electrospun nanofibrous scaffolds were studied for cardiac tissue engineering (Kai et al. 2011). Different kind of biomaterial scaffolds were

analysed for cardiac tissue engineering, but few supported biocompatible environments for cardiac cell adhesion and growth. The utilization of conducting polymers with their ability to transmit electrical signals offers an easy alternative. Nanofibers containing different amount of PPy were synthesized and their properties are given in Table 3.1. With increasing amount of PPy average fiber diameter decreased and contact angle results showed the hydrophilicity of nanofibers, however incorporation of PPy increased hydrophobicity of nanofibers because of hydrophobic behavior. Young modulus of the nanofibers increased with PPy amount, at the same time, the maximum elongation decreased dramatically. Electrical measurements of nanofibers demonstrated that addition of PPy was an effective method for preparation of a conductive scaffold a high amount of PPy resulted with higher electrical conductivity. Nanofibers containing 15% PPy showed the most balanced mechanical, electrical and biodegradable properties for regeneration of cardiac tissue. The cell proliferation assay exhibited that sample containing 15% PPy promoted cell attachment, proliferation, interaction, and expression of cardiac-specific proteins better.

Table 3.1 Fiber Diameter, Contact Angle, and Mechanical Properties of Electrospun PPy/PCL/gelatin nanofibers with different PPy amount (Source: Kai et al. 2011).

PPy amount	Fiber Diameter (nm)	Contact Angle (^{o})	Young Modulus (MPa)	Elongation (%)	Conductivity (mS/cm)
0/100	239±37	24.3±1.8	7.9±1.6	61.1±17.3	0
15/85	216±36	46.9±2.0	16.8±1.9	13.6±3.2	0.013
30/70	191±45	63.5±2.8	50.3±3.3	3.7±1.4	0.37

PPy/PLGA fibers were investigated as scaffolds for neural cells with their electrical stimulation and topographical guidance (Lee et al. 2009). To synthesize electroconducting nanofibers, firstly PLGA electrospun nanofibers were synthesized in random and aligned forms, then PPy deposition was performed on nanofibers. Electrical stimulation was studied to test these nanofibers for neuronal tissue engineering scaffolds. PC12 cells were inoculated on random and aligned PPy/PLGA scaffolds and after 24 h in

cell culture, a constant 10 mV/cm and 100 mV/cm electrical potential was applied across two electrodes for 2 h in the incubator as shown in fig. 3.3.

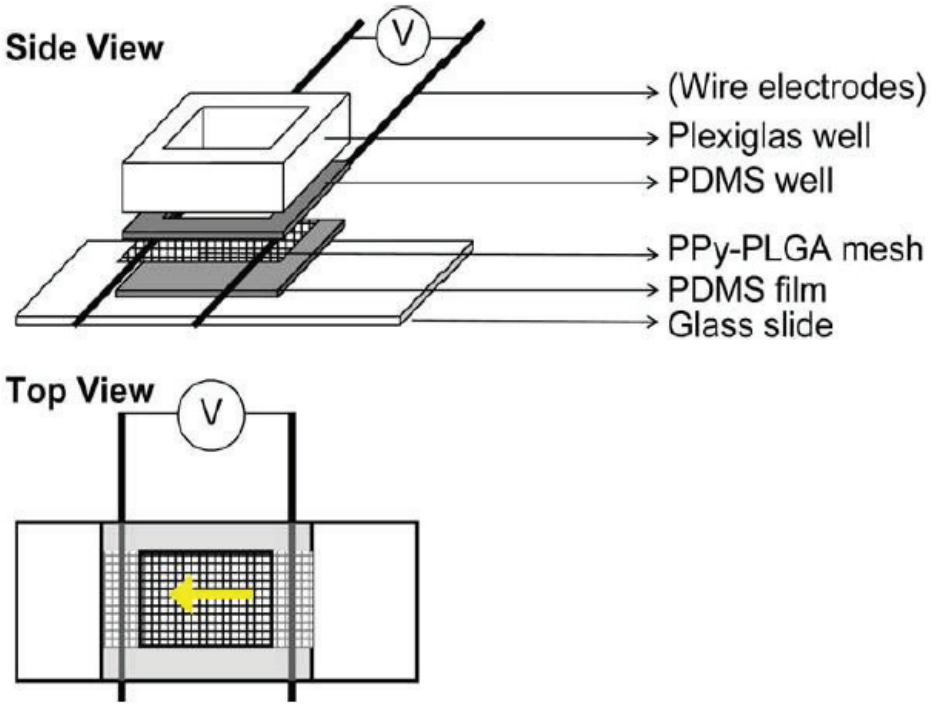

Figure 3.3 Schematic of PPy/PLGA nanofibers for in vitro cell culture and electrical stimulation studies (Source: Lee et al. 2009).

PC12 cells were stained with Alexa 488-labeled phalloidin for actin filaments and 4',6-diamidino-2-phenylindole dilactate for nuclear stain. Fluorescence images of PC12 cells stained for actin filament exhibited that cells formed neurites on all substrates (Fig. 3.4). Longer neurites formed on the aligned fibers than formed on random fibers regardless of PPy deposition. PC12 cells were electrically stimulated on random and aligned and neurite lengths, neurite-bearing cells, and numbers of neurites per cell were examined. More neurite-bearing PC12 cells and longer neurites per cell were observed with electrical stimulation. As a result, PPy/PLGA nanofibers found to be an appropriate scaffold for neural tissue applications.

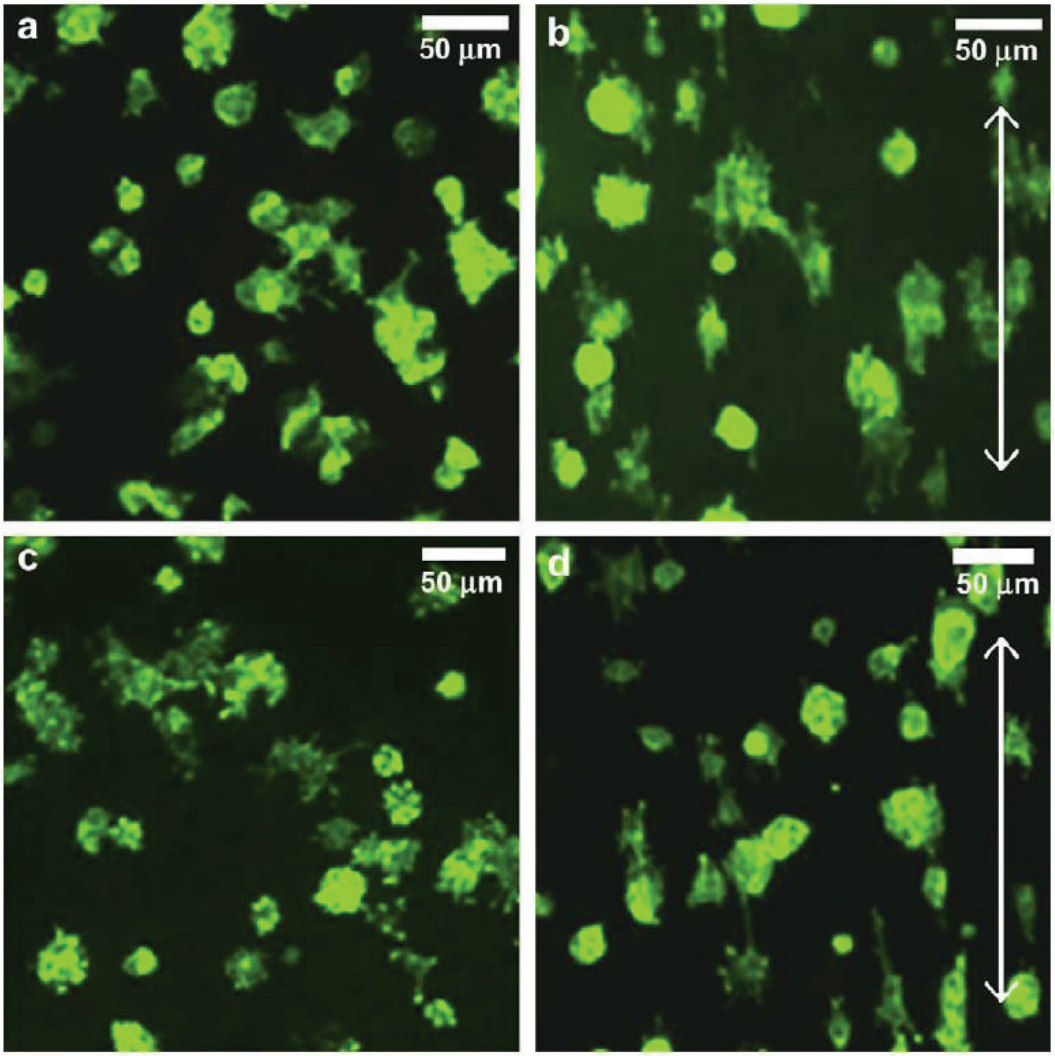

Figure 3.4 Immunostaining of PC12 cells cultured on (a) random PLGA, (b) aligned PLGA, (c) random PPy/PLGA (d) aligned PPy/PLGA nanofibers. Arrows indicate major directions of the aligned nanofibers (Source: Lee et al. 2009).

PPy films treated with different extracellular matrix components were found to support skeletal myoblast proliferation, adhesion and differentiation (Gilmore et al. 2009). PPy films and nanofibers were utilized in artificial muscle because its actuation voltage was lower than 2 V, its active stress reached up to 30 MPa and it had 39% maximum strain (Madden et al. 2004, Bay et al. 2003, Hara et al. 2004b).

Out of many potential electrospun nanofibers, poly (vinyl alcohol) (PVA) nanofibers were examined as potential scaffolds for human keratinocytes (Pelipenko et al. 2013). The results showed that using aligned PVA nanofibers supported linear cell orientation (Fig. 3.5), however, in such an environment, keratinocytes were entrapped between individual nanofibers and could not migrate. Therefore, randomly oriented PVA

nanofibrous scaffold delayed cell adhesion, they improved strength of cells, alter cellular morphology, increased metabolic activity of cells and limited the mobility. Aligned nanofibrous scaffolds are not appropriate for keratinocytes growth. Another electrospun scaffold promoted cell attachment and spreading of human keratinocytes and fibroblasts was chitin (Noh et al. 2006). Chitin nanofibers could be a potential scaffold for wound healing and regeneration of skin with extracellular matrix proteins such as type I collagen or alone.

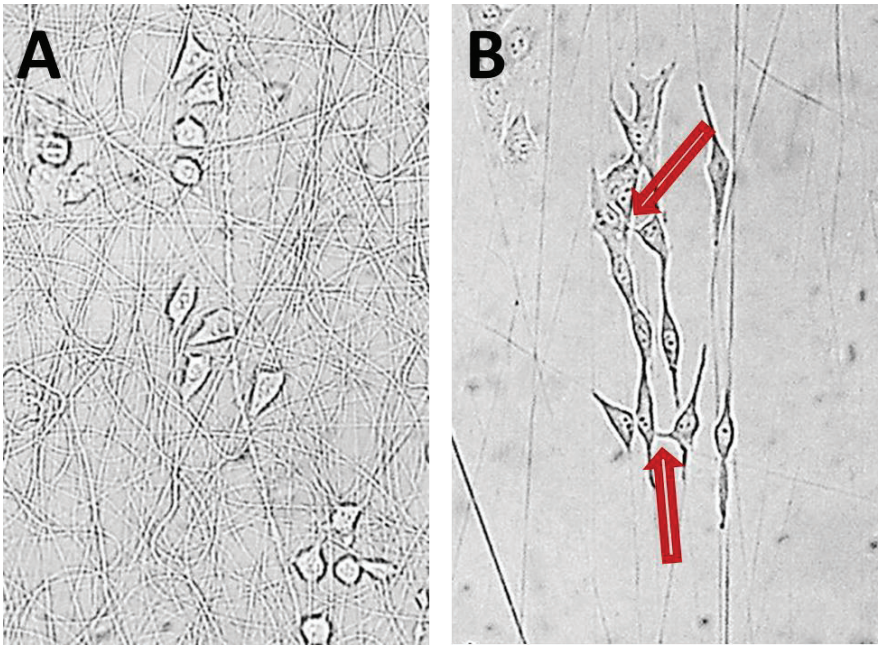

Figure 3.5 Morphology of keratinocytes when grown on (a) random, (b) aligned nanofibers. The red arrows indicate the intercellular connections between the keratinocytes. Images were taken using 20-times magnification (Source: Pelipenko et al. 2013).

As described before, nanofibrous scaffold orientation has a significant influence on cell proliferation and orientation. Sao et al. studied random and aligned PLA/MWCNT electrospun nanofibers and investigated the electrical conductivity, mechanical properties and in vitro degradation stability of these nanofibers and synergetic effect of topographic cues, electrical stimulation on bone tissue regeneration (Shao et al. 2011). MWCNTs with diameter range of 10-20 nm were used with 1, 2, 3, 4, and 5 wt% ratios. Average diameter of obtained electrospun nanofibers were 425 nm and 402 nm for random and aligned samples, respectively. After CNT addition average diameters of random samples were measured as 272, 248, 243, 247, 312 nm and and aligned samples average diameter were

251, 241, 232, 236, 281 for 1, 2, 3, 4, and 5 wt% CNT contents. After CNT addition diameters decreased dramatically because of the increase in solution conductivity, however for higher CNT content a small increase was observed because of the CNT agglomerations. Before electrical stimulation, proliferation was better on aligned nanofibrous scaffold, osteoblasts proliferated along the axis of aligned nanofibers. Electrical stimulation was applied by a direct current supply after 1 day of cell seeding and stimulated 4 h per day for 6 days. It enhanced elongation of osteoblasts obviously on random nanofibers, however, elongation on aligned nanofibers is enhanced only a bit. Smooth muscle tissue is made up of thin-elongated muscle fibers and cells, so this tissue type also requires an appropriate aligned nanofibrous scaffold.

Aligned and random PLGA/PCL electrospun nanofibers were examined for human vascular smooth muscle cells using PLGA/PCL film as control (Zhong et al. 2015). Almost all the cells proliferating on aligned scaffold exhibited spindle-shaped similar to the normal shape of human vascular smooth muscle cells. They did not change with time while film and random fibers of PLGA/PCL could change cell morphology. Therefore aligned nanofibers were found to be a promising scaffold for human vascular smooth muscle cells culture in vitro and cell regeneration in vivo. Poly(L-lactic acid) (PLLA)/trifluoroethanol (TFE) electrospun nanofibrous scaffolds with different orientations were tested for osteoblast-like MG63 cells proliferation and differentiation (Wang, Cai, et al. 2011). The results indicated that cells grown on randomly oriented scaffolds are in an irregular form, whereas cells grown on aligned scaffolds showed shuttle-like shapes and PLLA fiber orientation may be utilized to control osteoblast-like cell responses. Aligned PCL electrospun nanofibrous scaffolds exhibited directional mechanical property and facilitate the endothelial cell attachment on PCL nanofibers (Wu et al. 2010). Aligned PLGA electrospun nanofibers were investigated for myoblasts (C2C12) (Aviss, Gough, and Downes 2010). Mechanical tests results indicated that aligned nanofibers tested along the length of the directional axis were stiffer with a higher Young modulus than random nanofibers (Fig. 3.6) tested in the same direction and also when tested with perpendicular to the directional axis. There was no significant difference between Young's modulus of random and aligned samples in perpendicular and parallel tests. Young' modulus of aligned samples in parallel direction was significantly higher than the other samples. Elongation at break was calculated as 45% for aligned sample and 50% for random sample in parallel direction. Elongation values in perpendicular direction were much higher; 250% for aligned sample and 175% for random sample.

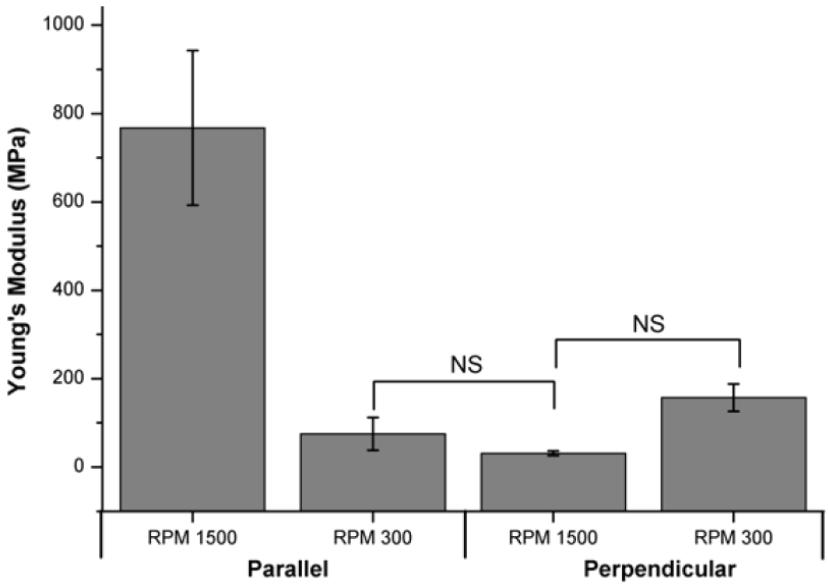

Figure 3.6 Young's modulus of random (grown at 300 rpm rotation speed of collector) and aligned (grown at 1500 rpm rotation speed of collector) nanofibers. Scaffolds were tested along the parallel and perpendicular directions of the fibers (Source: Aviss, Gough, and Downes 2010).

SEM images of myoblasts grown on random and aligned nanofibers, shown in Fig. 3.7, showed that the cells were aligned along the direction of nanofibers with an elongated morphology, and appeared more polygonal, less organized on random nanofibers. The results indicated that these nanofibers provide required topography and contact guidance for myoblasts (C2C12) elongation and alignment.

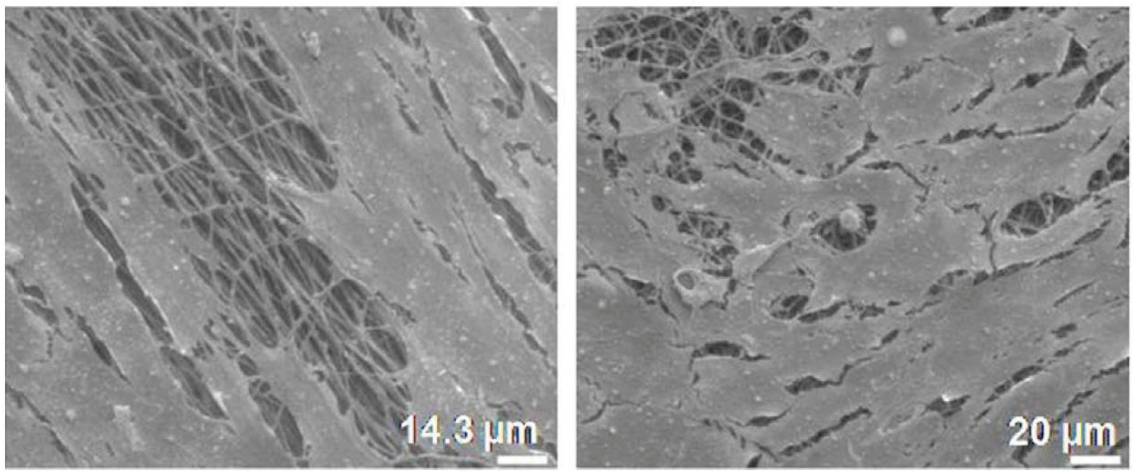

(a) (b)

Figure 3.7 SEM images of myoblasts seeded on electrospun (a) aligned, (b) random PLGA scaffolds. Myoblasts were fixed and viewed after 7 days in culture (Source:Aviss, Gough, and Downes 2010).

Bone tissue engineering is another branch depending on osteogenic cells growth on an appropriate scaffold which also provides the physiological requirements for bone development. Shao et al. synthesized graphene oxide/PLGA/tussah silk ultrafine hybrid electrospun nanofibers which have good mechanical properties, surface hydrophilicity, protein adsorptivity (protein adsorption), and hemocompatibility. The results indicated that graphene oxide and tussah silk improved the osteogenic potential of mesenchymal stem cells, cell attachment, proliferation, expression of marker gene expression, alkaline phosphatase activity, and osteocalcin content. They indicated that hydrophilicity and biocompatibility provide a gradual enhancement in osteogenesis (Shao et al. 2016).

With its biocompatibility, biodegrability, and non-toxicity, chitosan is one of the most appropriate naturel polymers for biomedical applications. Chitosan electrospun nanofibrous scaffolds were studied for different types of cells; schwann cells, osteoblast-like cells, keratinocytes, and fibroblasts (Sangsanoh et al. 2010). Figure 3.8 showed SEM images of Schwann cells, osteoblast-like cells, keratinocytes and fibroblasts seeded on electrospun chitosan nanofibers after culturing 5 days. For Schwann cells, cytoplasmic expansion of cells cultured on the nanofibrous scaffold and interconnection between the cells were noticeable. While the majority of observed osteoblast-like cells were in spindle morphology, the cells were expanded on nanofibrous scaffold relatively better compared to osteoblast-like cells grown on control chitosan film. Keratinoceytes seeded on chitosan nanofibers appeared to grow on top of one another and formed multilayers of a cellular construct. After 5 days of culture, substrate was well covered with keratinocytes. Human fibroblasts were also well expanded on nanofibrous scaffold and interconnection of adjacent cells was clear. Overall, chitosan nanofibers promoted attachment and proliferation for all these types of cells.

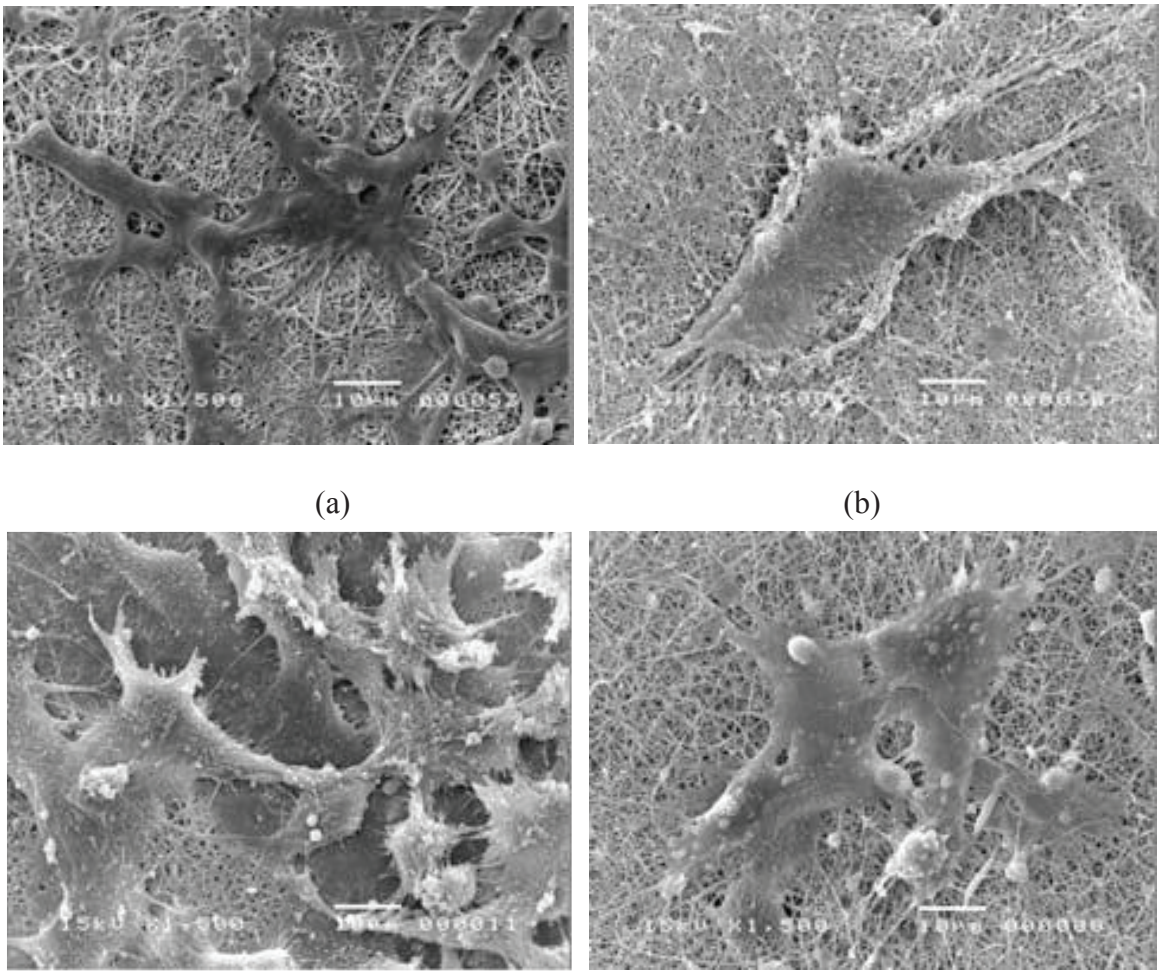

(a) (b)

(c) (d)

Figure 3.8 SEM images of (a) murine Schwann cells , (b) murine osteoblast-like cells , (c) human keratinocytes, (d) human fibroblasts on chitosan electrospun nanofibers after 5 days of culture (Source: Sangsanoh et al. 2010).

Figure 3.9 shows the viability of osteoblast-like cells seeded on different substrates for 1, 3, and 5 days. The largest increase in the viability of osteoblast-like cells was observed on tissue culture polystyrene plate (TCPS). The viability of the cells remained almost constant on chitosan film and chitosan nanofibers during 5 days. Therefore, chitosan was found to be cytostatic for osteoblast-like cells despite the good attachment of cells on the surface.

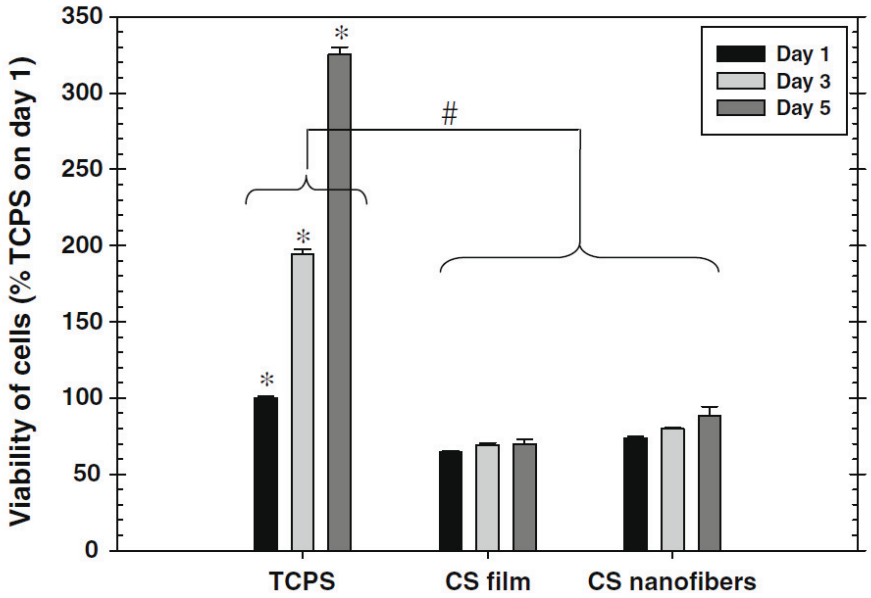

Figure 3.9 Proliferation of murine osteoblast-like cells on TCPS, chitosan (CS) film and CS nanofibers (Source: Sangsanoh et al. 2010).

PLLA/PCL/hydroxyapatite (HAP) electrospun nanofibers was another scaffold tested for the mouse calvaria-derived pre-osteoblastic cells (MC3T3-E1). This scaffold exhibited a good attachment and proliferation of osteoblasts and differentiation also was facilitated with this scaffold (Jaiswal et al. 2013, Qi et al. 2016). PVA thin layer was deposited on electrospun nylon 6 hybrid nanofibers by a hydrothermal process were found to be very effective for bone tissue regeneration (Abdal-hay, Hamdy, and Khalil 2015). Gelatin electrospun fibrous scaffolds also supported adhesion and proliferation of osteoblasts and osteo-differentiation of mesenchymal stem cell (Lin et al. 2016). Cross-linked boron-nitride reinforced gelatin electrospun scaffold was examined for human bone cells and showed nontoxic and biodegradable behavior (Nagarajan et al. 2017). It is confirmed that this material is suitable to use as a bone tissue engineering scaffold with its excellent mineralization ability. Generally, many polymeric materials including natural and synthetic polymers in their fiber form have been developed for bone tissue engineering. However, the crucial thing is to find a scaffolds supported the adhesion, proliferation and differentiation of mesenchymal stem cells for bone tissue engineering.

Overall, literature studies indicated that conducting polymer nanofibers with their high surface area and 3D structure are good candidates for development of scaffolds for different types of cells. Scaffold type is very important for cell growth. Biocompatibility is vital for a polymeric scaffold, however, its mechanical and electrical properties also directly influence the behavior of cells. There are many studies on literature on

electrospun nanofibers usage for tissue engineering. This dissertation study focused on the synthesis of PAN/PPy and CNT embedded PAN/PPy electrospun nanofibrous scaffolds with appropriate properties to support keratinocytes growth and osteogenic differentiation of mesenchymal stem cells. PAN/PPy/CNT nanofibers utilized as keratinocytes scaffold to investigate their biocompatibility. PAN/PPy nanofibers were investigated for attachment, proliferation and osteogenic differentiation of mesenchymal stem cells for both their random and aligned forms.

CHAPTER 4

EXPERIMENTAL STUDY

4.1 Materials

List of the chemicals used in this study are given in Table 4.1. CNTs were purified and fuctionalized using H_2SO_4, HNO_3 HCl and ammonium hydroxide. To fabricate nanofibers PAN (MW=150000), PPy (conductivity > 0.005 S/cm) and solvent N,N-dimethylformamide (DMF) were utilized. All these reagents were used without further purification.

Table 4.1. List of the chemicals used.

Chemical	**Purity**
H_2SO_4	Sigma Aldrich, 95-97%
HNO_3	Sigma Aldrich, >65%
HCl	Sigma Aldrich, 37%
ammonium hydroxide	Sigma Aldrich, >99.99%
Polyacrilonitrile	Aldrich
Polypyrrole	Aldrich, 5 wt% dispersion in H_2O
N,N-Dimethylformamide	Sigma Aldrich, 99%

4.2 CNT Growth, Purification, Functionalization, and Characterization

CNT growth were carried out on Co-Mo/MgO catalyst prepared by gel-combustion method as reported in our previous study (Yardimci, Yılmaz, and Selamet 2015). Growth was performed under atmospheric pressure at 1000 ºC. After reducting catalyst under 200 sccm H_2 flow for 1 hour at 850 ºC, CH_4-H_2 gas mixture flow was fed at 1000 ºC for 40 min for CNT growth. After growth process the system was left for cooling under H_2 ambient.

As-grown CNTs was put into 30 ml HNO_3 solution and was stirred at 60 ºC for 30 min to remove MgO and the other catalyst components. Then, CNTs was washed with distilled water until the solution pH became neutral and dried at 100 ºC. After purification of CNTs, for functionalization process, purified CNTs were sonicated in a mixture of H_2SO_4 and HNO_3 with volume ratio of 3:1 (30 ml/10 ml) for 2h. After 24 h, 20 ml HCl was added to the solution. Subsequently, the solution was neutralized with ammonium hydroxide and filtered. Functionalized CNTs were washed with deionized water until the solution pH was 5.5 (Osorio et al. 2008).

Obtained as-grown and functionalized CNT samples were characterized scanning electron microscopy (SEM), thermo-gravimetric analysis (TGA), Raman spectroscopy, and Fourier transformed infrared spectroscopy (FTIR).

4.3 PAN/PPy and PAN/PPy/CNT Solutions Preparation and Electrospinning

In order to synthesize nanofibers electrospinning method was utilized. Photo of the electrospinning setup is given in Fig. 4.1.a. Electrospinning setup consists of three major components. First part is a high voltage power supply (1) which can increase up to 40 kV. The second part is a spinneret (2). Polymer solution is filled into a syringe for electrospinning process and adjusted to a specific rate by this syringe pump. The third part is an electrically conductive collector (3). There are two different collector utilized in this study, see Fig. 4.1.b. First one is a flat collector to obtain random nanofibers and the second is a rotating drum collector with dimensions of 10 cm in diameter and 25 cm in length which allows to obtain aligned nanofibers. A piece of Al foil is covered on the collector and nanofibrous mat is collected on this foil.

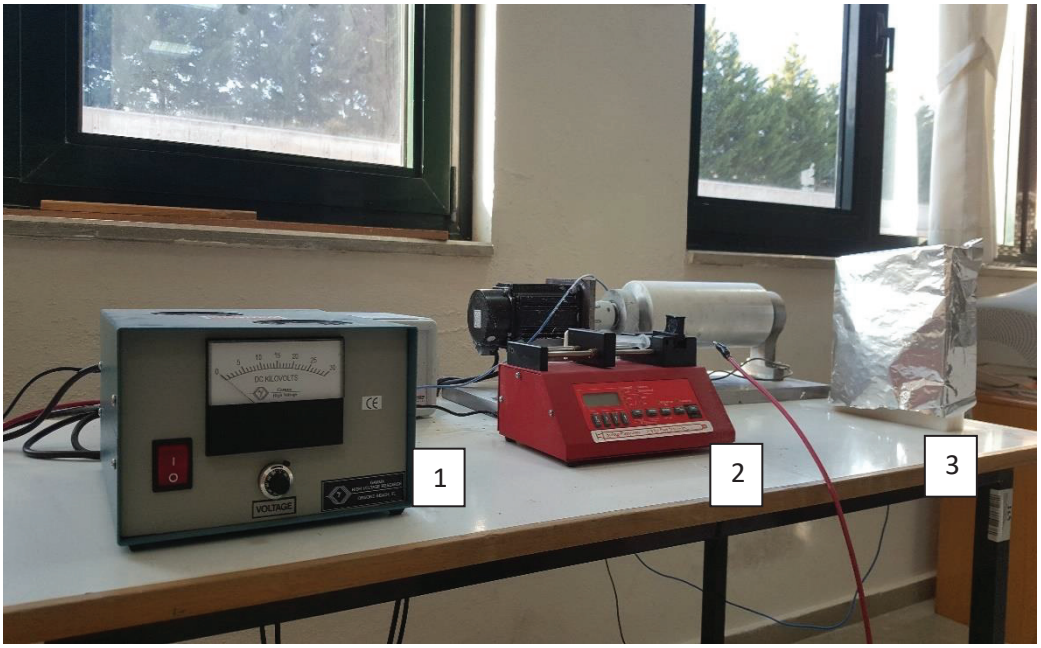

(a)

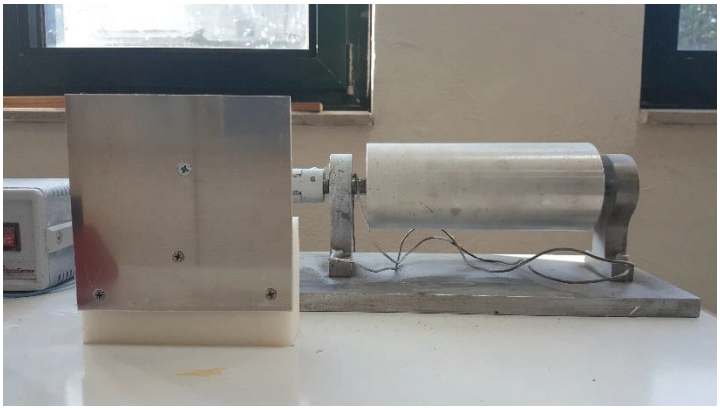

(b)

Figure 4.1 (a) Electrospinning set-up, (b) collectors.

PPy was used in this thesis study because of its high electrical conductivity and its biocompatibility. PAN was used as a co-polymer to enhance poor solubility and brittle property of PPy. In order to improve electrical and mechanical properties of PAN/PPy polymer composite, CNTs were incorporated into these polymers in different amounts using their as-grown and functionalized forms.

In order to prepare PAN nanofibers, 0.41 g (8 wt%) PAN was dissolved in 5 ml DMF until a clear solution was obtained by mechanical stirring. To obtain PAN/PPy nanofibers, DMF solution containing 8 wt% PAN was prepared with different amounts of PPy. Investigated PPy amounts corresponded to 10, 20 and 50 wt% of PAN mass. These PAN/PPy solutions were stirred for 3 days at 60 ^{o}C.

For PAN/PPy/CNT nanofiber synthesis, the mixture was prepared for four different amounts of CNTs corresponding to 1, 2, 3, and 4 wt% of the total polymer mass. CNTs were added in PAN/PPy solution and dispersed by using ultrasonic bath for 24 h.

The solutions prepared were filled into a 5 ml syringe connected to a high voltage for electrospinning process. For all samples 15 kV voltage was applied for 1 h and flow rate of solution was kept 1.5 ml/h. The distance between the syringe and collector was 30 cm and the fibers were collected on the Al foil. For samples used as scaffold for skin cells and mesenchymal stem cells, the fibers were collected on 10 mm diameter cover slips which are fixed on the Al foil.

To synthesize aligned nanofibers rotation speed of the drum collector was 1000 rpm.

Table 4.2. The labels of the electrospun nanofibers prepared.

Labels	PPy Content (wt%)	CNT content (wt%)
PAN	0	0
PP1	10	0
PP2	10 (aligned)	0
PP3	25	0
PP4	50	0
PPC1	25	1
PPC2	25	5
PPC3	10	1
PPC4	10	2
PPC5	10	3
PPC6	10	4
PPC7	10	1 (functionalized)
PPC8	10	4 (functionalized)

4.4 Cell Culture and Seeding

4.4.1 Keratinocytes Growth on PAN/PPy and PAN/PPy/CNT Nanofibrous Scaffolds

The cover slips with electrospun nanofibers were sterilized at 200 ^{o}C for 2h and were then placed in 12-well tissue culture plates where 25,000 HaCaT cells/well were plated on fibers for experiments.

4.4.2 Osteogenic Differentiation of Mesenchymal Stem Cells on PAN/PPy and PAN/PPy/CNT Nanofibrous Scaffold

The cover slips with electrospun nanofibers were placed in 24-well plates. Samples were sterilized at 200 ^{o}C for 3h. After sterilization, mesenchymal stem cells were split at 500 cells/well containing nanofibers. Morphological study of cells grown on PAN/PPy nanofibers was performed after 1, 7 and 14 days of cell culture by SEM. The viability of the cells growing on nanofibers was quantified with MTT assay.

For osteogenic differentiation, mesenchymal stem cells were seeded on PAN/PPy nanofibers in 24-well plates at the density of 500 cells/wells. Then, medium was changed with osteogenic medium supplemented with 10nM β-glycerolphosphate and 50μg/ml Ascorbic Acid. Cells were incubated in osteogenic medium for 14 days to induce osteogenesis.

4.5 Nanofibers Characterization

4.5.1 Scanning Electron Microscopy (SEM)

The morphology and diameter of CNTs and electrospun nanofibers were analysed by SEM. The SEM utilized throughout this thesis work was FEI QUANTA 250 FEG. SEM was used in secondary electron (SE) mode, at 5-7 kV and 3 spot size.

4.5.2 Transmission Electron Microscopy (TEM)

TEM was used to indicate the existance and alignment of CNTs in electrospun nanofibers and also to determine the wall numbers of CNTs. Used TEM was FEI-Tecnai G2 F30 in this study.

4.5.3 X-Ray Diffraction (XRD)

XRD studies using Philips X' Pert diffractometer with Cu Kα radiation source were utilized to understand the crystal phase of synthesized electrospun nanofibers. The scattering angle 2θ was varied from 5^o to 70^o and the step length is 0.02.

4.5.4 Raman Spectroscopy

Raman spectroscopy was used with 514 nm Ar laser excitation to characterize the graphitic nature of CNTs, pure PAN/PPy nanofibers and their CNT added forms.

4.5.5 Thermogravimetric Analysis (TGA)

In order to determine thermal properties of CNTs and electrospun nanofibers TGA is carried out from 25 to 800 ^oC with the ramp rate of 10 ^oC/min in air atmosphere. TGA used in this thesis study was Perkin Elmer Diomand TG/DTA.

4.5.6 Differential Scanning Calorimetry (DSC)

In order to determine thermal properties of electrospun nanofibers, another characterization technique was DSC. Nanofibers were heated from 25 to 400 ^oC with the ramp rate of 10 ^oC under nitrogen atmosphere. Utilized DSC was a TA instruments Q10.

4.5.7 Tensile Test

Tensile tests of nanofibers were performed by using a TA.XT plus texture analyser with a 5 kg load cell and 0,1 mm/s test speed. For tensile tests samples dimensions were kept as 8mmx60mm.

4.5.8 Water Contact Angle Test

The wettability of PAN/PPy electrospun nanofibers was analysed by water contact angle measurement test using a Attention-Theta analysis system. The droplet size was 3 μl and at least 5 readings were taken for each samples.

4.5.9 Rheometer

The viscosity of PAN/PPy solutions was measured using a TA AR 2000ex rheometer. All tests were conducted at room temperature and ambient air.

4.5.10 Fourier Transform Infrared Spectroscopy (FT-IR)

FT-IR characterizations of CNTs were carried out between 400 and 4000 cm-1 wavenumbers with Perkin Elmer FT-IR System Spectrum BX. CNT samples were prepared with KBr pellet method by pressing 2 mg CNT with 200 mg KBr. Electrospun nanofibers did not require any sample preparation for FT-IR, they were analysed with FTIR-ATR. The resolution of FT-IR was 4 cm^{-1}.

To examine the changes in the molecular orientation, random and aligned PAN/PPy nanofibers were analysed with FT-IR polarizor (FT-IR with a wire grid polarizor). The resolution of FT-IR was 4 cm^{-1}. The number of scans collected was 128. In parallel polarization, the direction of ossilating electric field of the IR beam was parallel to the alignment direction of nanofibers and in perpendicular polarization, it was perpendicular to the nanofibers alignment direction.

Reflective FT-IR spectra of PAN/PPy and PAN/PPy/CNT nanofibers were recorded with ATR technology. Nanofibers were directly mounted on a diamond crystal platform of the spectrophotometer and the IR beam was focused to a small area of the

nanofibrous mat to record the FT-IR spectra. The resolution of FT-IR was 4 cm^{-1}. The number of scan collected was 32.

4.5.11 Cyclic Voltammetry (CV)

Electrochemical measurements of the nanofibers were performed with CV technique. CV is an electrochemical technique performed by cycling the potential of a working electrode, and measuring the resulting current.

A three-electrode electrochemical cell is used in this technique. The electrochemical potential of the reference electrode is usually fixed, therefore the measured cell potential can be interpreted in terms of an equilibrium half-cell reaction involving an analyte species in contact with the working electrode.

For CV study, working electrode was graphite electrode covered with our nanofibers during electrospinning process, reference electrode was Ag/AgCl and counter electrode was a Pt wire. Autolab CV was utilized between the voltage range of 0.2 V and 1 V and the electrolyte solution was 0.1 M HCl solution.

4.5.12 Electrochemical Impedance Spectroscopy (EIS)

Impedance is the frequency-dependant resistance to current flow of a circuit element such as resistor, capacitor, inductor. Impedance (Z_ω) assumes an AC current of a specific frequency in Hertz and it is calculated by the equation 4.1:

$$Z_\omega = E_\omega / I_\omega \qquad \text{(Eq. 4.1)}$$

where E_ω is frequency-dependant potential and I_ω is frequency-dependant current. The fundamental approach of EIS is to apply a small amplitude sinusoidal excitation signal to the system and measure the response (current or voltage). Impedance of a system is a complex quantity with a magnitude and a phase shift depending on the frequency of the signal. By varying the frequency of the applied signal, impedance of the system can be taken as a function of frequency.

For impedance measurements the same three-electrode electrochemical cell was used with CV. The solution for EIS was Fe[CN6]3-/4- and measurements were carried out between 0.01 Hz and 100 kHz.

4.6 Cell Characterization

4.6.1 Cell Morphology Study by SEM

For keratinocytes both keratinocytes and osteoblasts, morphology of cells were analyzed with SEM. Cells were washed with phosphate-buffered saline (PBS) and then fixed with paraformaldehyde for 3-4 h at room temperature. After PBS washes, cells were air dried. Dry cellular constructs were sputter coated with gold and observed under the SEM at an accelerating voltage of 5 kV. SEM analysis was carried out for keratinocytes after 1, 3 and 7 days of culture and for osteoblasts after 7,14 and 21 days of culture.

4.6.2 Immunostaining of Keratinocytes

Cellular morphology of HaCaT on PAN/PPy electrospun nanofibers was investigated by immunostaining of actin cytoskeleton with Alexa Fluor 488 Phalloidin. Cells were washed with 1X PBS and then fixed with 4% paraformaldehyde (PFA) for 20 minutes, permeabilized with 0.1% Triton-X 100 for 15 minutes and blocked with 5% bovine serum albumin (BSA) for 1 h at room temperature (RT). Then, cells were incubated with a 1:200 dilution of Alexa Fluor 488 Phalloidin (Invitrogen, Cat# A12379) and DAPI (1:200) (Sigma, Cat# D95242) for 45 minutes at RT in dark. After washing with PBS, coverslips were dipped in distilled water, dried and mounted on glass slides. Staining was verified under a fluorescence microscope (IX83, Olympus, Japan) with 40x objective and images were taken with a CCD digital camera.

4.6.3 MTT Assay

For osteoblasts growth 500 d1orl-uva cells, for keratinocytes growth 10,000 HaCaT cells were seeded onto electrospun nanofibrous scaffolds in 12-well tissue culture plates (n=4 per condition). Cells were incubated at 37 ^{o}C and 5% CO_2. Medium is removed and 600 µl 10% MTT solution was added onto cells. After 4 h of incubation, MTT mixture was removed and 600 µl of DMSO was added. After solubilization of MTT crystals, absorbance was measured at 570, 650 and 670 nm with Thermo Scientific

Multiskan Spectrum. MTT measurements were performed at day 1, 3 and 7 for keratinocytes and day 7, 14 and 21 for osteoblasts.

4.6.4 Alizarin Red Staining

Presence of calcified matrix on PAN/PPy electrospun nanofibers was detected with Alizarin Red assay. Firstly cells were washed with 1 ml of PBS 3 times and fixed with 500 μl of 10% neutral buffered formalin for 30 min. Afterwards, cells were washed again 2 times with 1 ml of deionized (DI) water and stained with 1 ml of alizarin red dye for 30 min. After again rinsing 2 times with DI water, cells were emained in PBS for 15 min to remove non-specific binding of dye. Micrographs of calcified matrix were taken through the light field of an inverted microscope (Olympus, IX-83) Incubation time for alizeriin red dye was 21 days.

CHAPTER 5

RESULTS AND DISCUSSIONS

5.1 CNT Characterization

SEM image of the CNT sample (Fig.5.1.a) displays that as-grown CNTs used in PAN/PPy nanofibers were straight and nontangled and their average dimeter was 8.9 nm. Raman spectra of the sample, given in Fig. 5.1.b, indicated low intensity of D-band (about 1300 cm^{-1}) relative to the G-band (1574 cm^{-1}). It showed low defect density and high crystallinity. Radial Breathing Mode (RBM) peaks (100-300 cm^{-1}) were also observed. Each point tried on the sample resulted in with RBM peaks which indicated that the CNT growth was mostly SWNTs.

TGA curve of the sample taken under O_2 atmosphere is given in Fig.5.1.c There was a significant weight loss between 500 and 800 ^oC, this temperature range is the oxidation temperature of SWNTs and MWNTs (Hata et al. 2004). The oxidation of amorphous carbon was observed between 200 ^oC and 450 ^oC. TGA curve indicated extremely low level of amorphous carbon presence, 2.8% in the CNT.

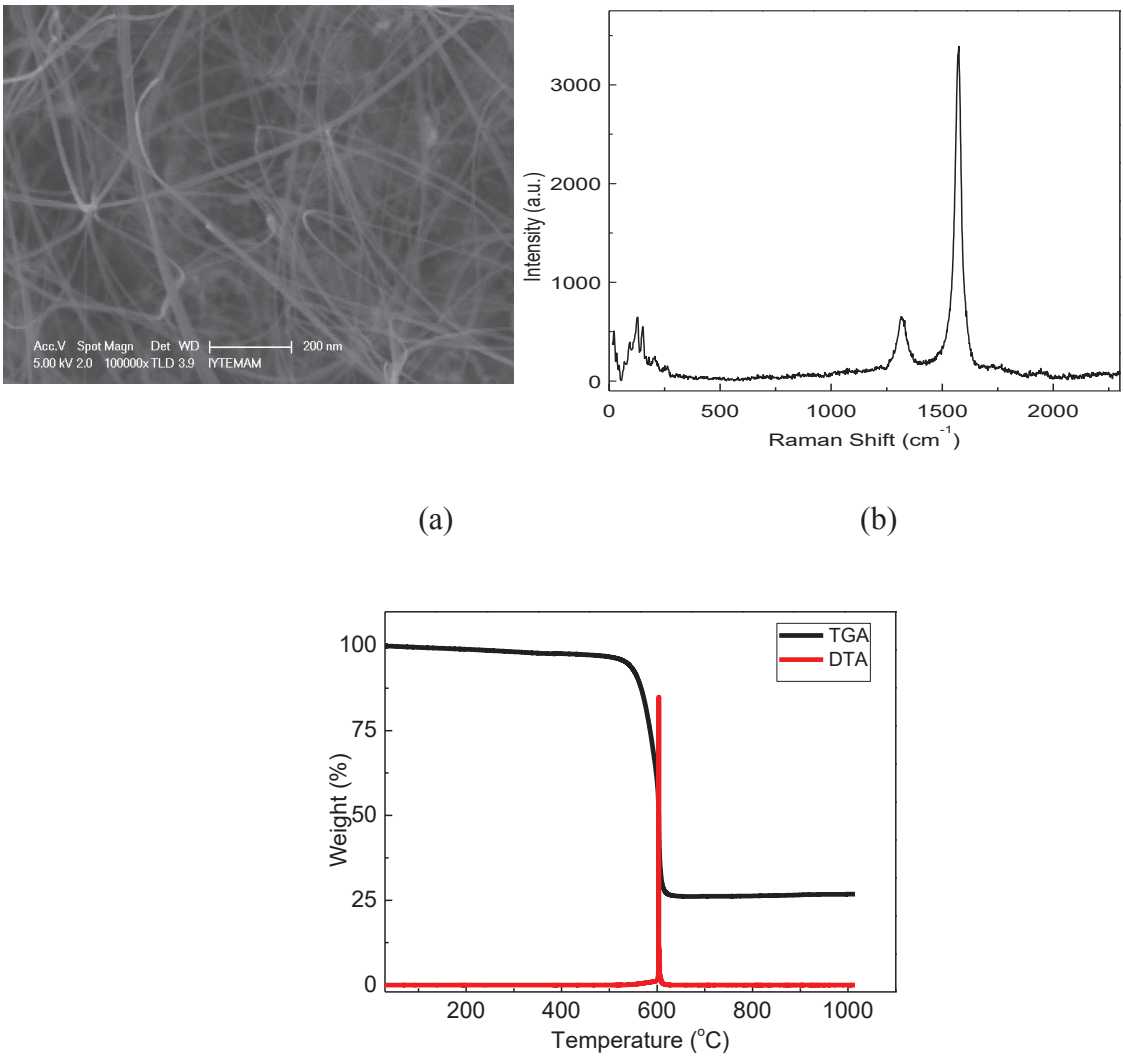

Figure 5.1 (a) SEM picture (b) Raman spectrum (c) TGA graph of the CNT sample (Source: Yardimci, Yılmaz, and Selamet 2015).

The main problem of polymer composites including CNTs is agglomeration of CNTs. In order to enhance CNT dispersion, functionalization of CNTs is the best way (Ma et al. 2010). SEM image of the CNT samples (Fig. 5.2) revealed that as-grown CNTs were straight, nontangled and individual. However, after treatment with acid for purification and functionalization, the length of CNTs decreased significantly and nanotubes diameter got thicker compared to as grown product. It was observed that functional CNTs were in CNT groups instead of individual CNTs.

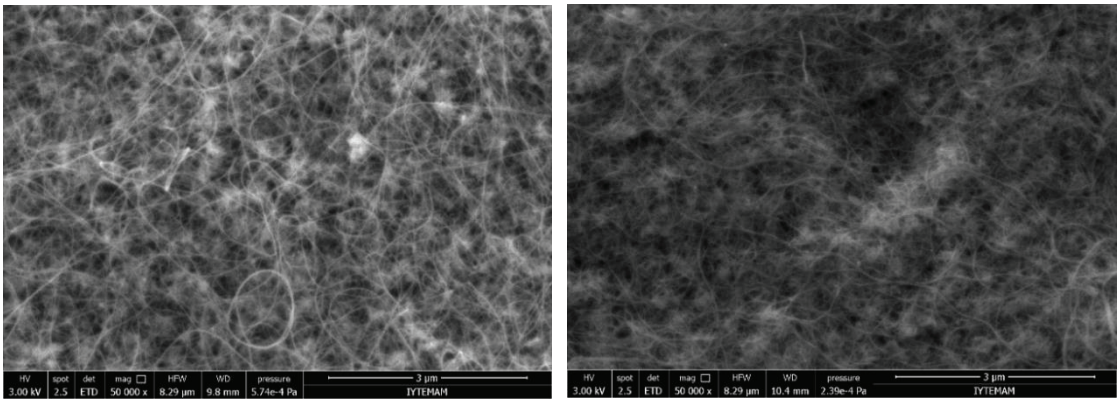

(a) (b)

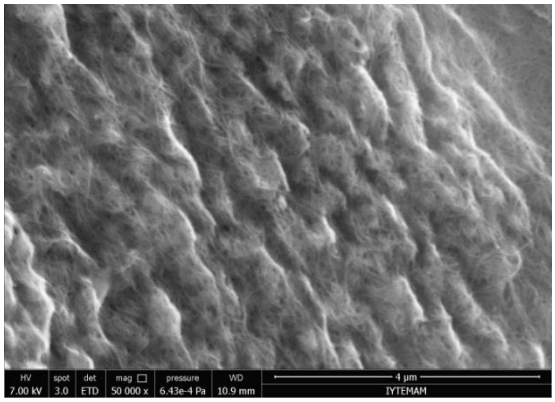

(c)

Figure 5.2 SEM micrographs of (a) as-grown (b) purified (c) functionalized CNTs.

The presence of functional groups after acid treatment was determined by FT-IR spectroscopy, Fig.5.3. The high symmetrical structure of pristine CNTs gave very weak infrared signals because charge state between carbon atoms do not show significant difference and this small difference of charge state causes very small induced electric dipole. The peak indicating C=C bonding presence at about 1600 cm^{-1} was not observed in the FT-IR spectrum of as-grown CNTs and this is explained with very low formation of electric dipoles. Peaks between 2800-3500 cm^{-1} were characteristic peaks of C-H and O-H bonds after purification and functionalization processes. These peaks could be related to carboxylic and hydroxylic groups (Osorio et al. 2008). The peak appearance after purification indicated that stretching OH was from carboxylic group after treatment with HNO_3. However, the peak appearence after functionalization indicated that streching OH was from hydroxylic group after treated with $H_2SO_4/HNO_3/HCl$. FT-IR spectra of both purified CNTs and functional CNTs gave a peak at about 1475 cm^{-1} which was related to the C-O strectching and indicating the presence of carboxylic groups due to

surface oxidation. As a result FT-IR spectra confirmed the presence of functional groups after acid treatment.

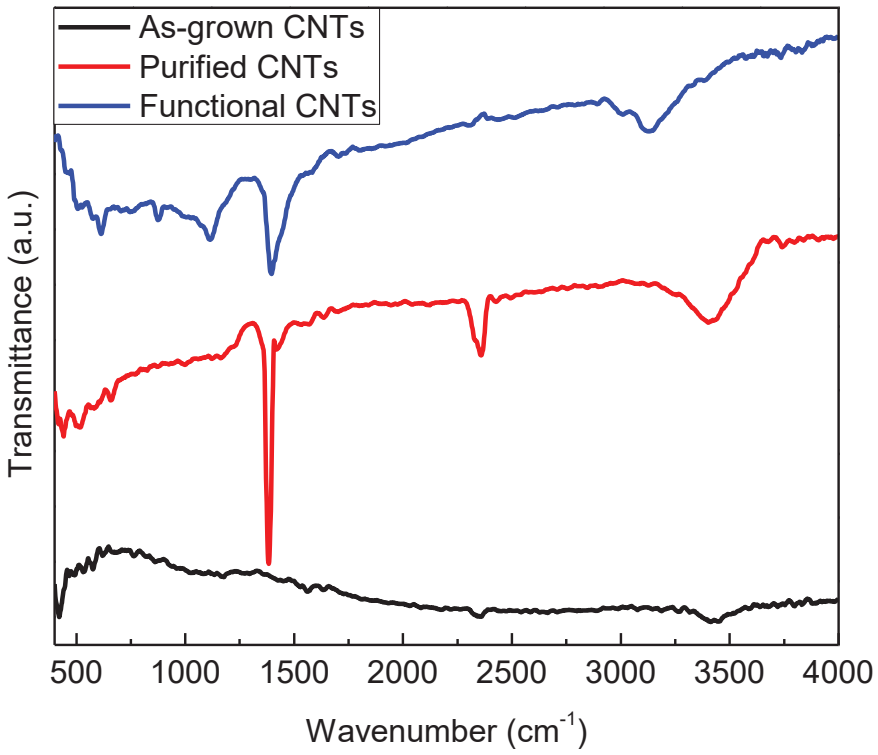

Figure 5.3 FT-IR spectra of CNTs.

Raman spectra of the CNT samples, given in Fig. 5.4, displayed the characteristics peaks of CNTs; defect-derived D-band (about 1300 cm^{-1}) and graphitization-derived G-band (1574 cm^{-1}). The high intensity of the G band with respect to D band of pristine CNTs indicated low defect density and high crystallinity. After acid treatment these characteristic peaks of CNTs could still be observed which exhibited that the structure of CNTs was not damaged by acid treatment. After purification process, I_D/I_G value decreased. Probably, treatment with HNO_3 removed MgO and other catalyst components and it enhanced the graphitization. However, after functionalization I_D/I_G ratio increased. The oxidation of CNTs broke some of its bonds and inserts chemical groups that could be interpreted as defects on the structure of nanotube.

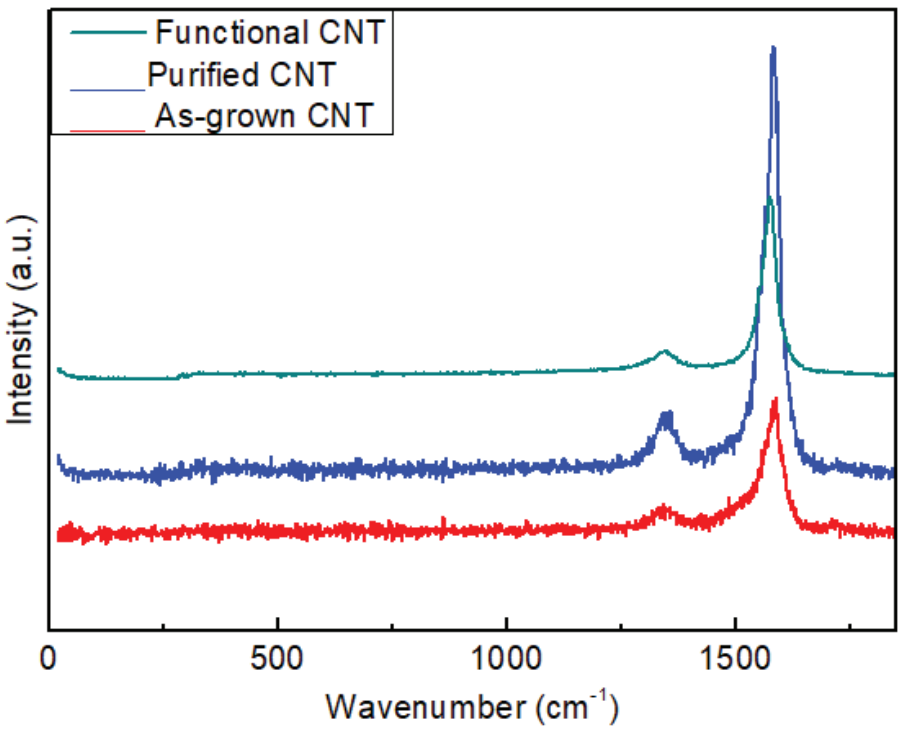

Figure 5.4 Raman spectra of CNTs.

Table 5.1 shows the EDX analysis of as-grown, purified and functional CNTs. EDX is an important characterization technique to define the extent of CNT oxidation and elemental composition. EDX results were consistent with Raman results. As-grown CNTs contained a large amount of catalyst components. After HNO_3 treatment the extent of graphitic C increased significantly and HNO_3 removed MgO, however Co and Mo could not be separated. For functionalization a mixture of three acid, HNO_3/H_2SO_4/HCl, was used and it was observed that the oxygen extent of CNTs after fuctionalization process increased by 18.08 wt% and simultaneously C extent decreased by 20.33 wt%.

Table 5.1 Elemental composition of as-grown, purified and functional CNTs.

Element (wt%)	As-grown CNTs	Purified CNTs	Functional CNTs
C	71.67	96.24	75.91
O	16.38	0	18.08
Mg	9.47	0.15	0.12
Co	1.10	2.04	1.75
Mo	1.38	1.57	4.14

5.2 Electrospun PAN/PPy and CNT Embedded PAN/PPy (PAN/PPy/CNT) Nanofibers

5.2.1 PAN/PPy Bicomponent Nanofibers

Fig. 5.5 displays SEM images of electrospun PAN/PPy bicomponent nanofibers with 10, 25 and 50 wt% PPy amounts referred to as PP1, PP3, PP4 respectively. Diameter of nanofibers decreased with the increase of PPy content (Zheng et al. 2006, Ji, Medford, and Zhang 2009a, Kai et al. 2011) and changed between 198 nm and 76 nm. This could be due to the increase in conductivity and decrease in viscosity of the PAN/PPy solution at high PPy content (Ji, Medford, and Zhang 2009a, b). Upon higher PPy addition, solution has higher conductivity, electrical force elongates the polymer jet and fibers with smaller diameter forms. At low PPy content, obtained fibers were more regular. Irregularities increased with increasing PPy content as observed from SEM pictures (Fig. 5.c). High solution conductivity causes instability in electrical field and therefore irregularities on the surface of nanofibers. In literature also it was reported that PAN improved the surface regularity of PPy fibers (Ji et al. 2010).

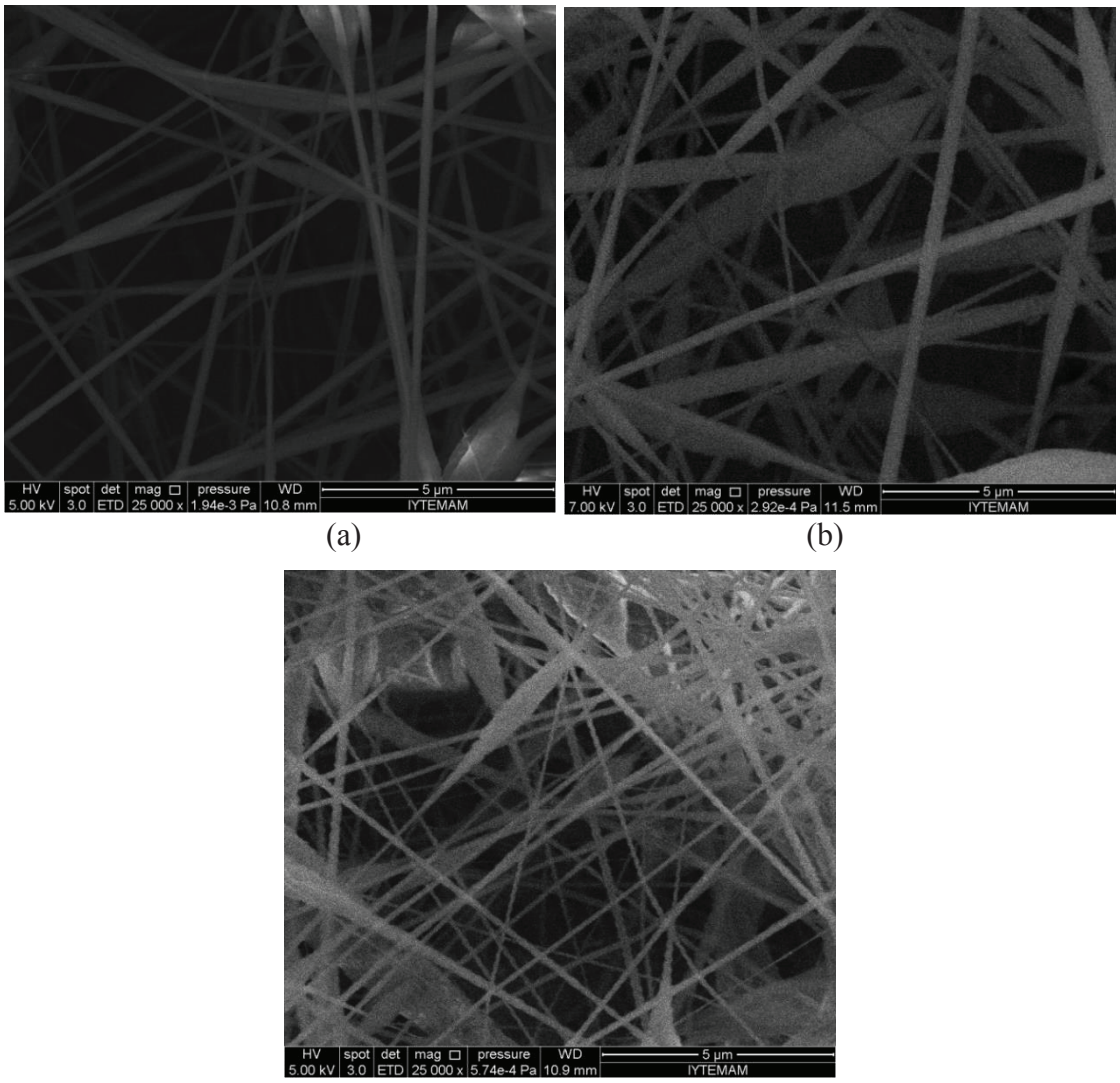

(a) (b)

(c)

Figure 5.5 SEM images of (a) PP1 (b) PP3 (c) PP4. Solutions were prepared at room temperature.

Fig. 5.6 displays SEM images of electrospun PAN/PPy bicomponent nanofibers with 10 and 25 wt% PPy amounts, when polymer solution was prepared at 60 ^{o}C. Beadless PAN/PPy nanofibers were obtained because high solution preparation temperature provides low solution viscosity and therefore ordered structure. At low PPy content, surface morphology of nanofibers were still more regular. More irregularities were observed at higher PPy content. PAN improved the poor solubility and therefore the surface regularity of PPy fibers. In literature, Ji et al. also indicated the irregularities on the surface morphology of PAN/PPy nanofibers with the increasing content of PPy (Ji et

al. 2010). TEM image of PAN/PPy nanofibers containing 10 wt% PPy indicated that actually surface of these nanofibers were not smooth as observed from SEM images.

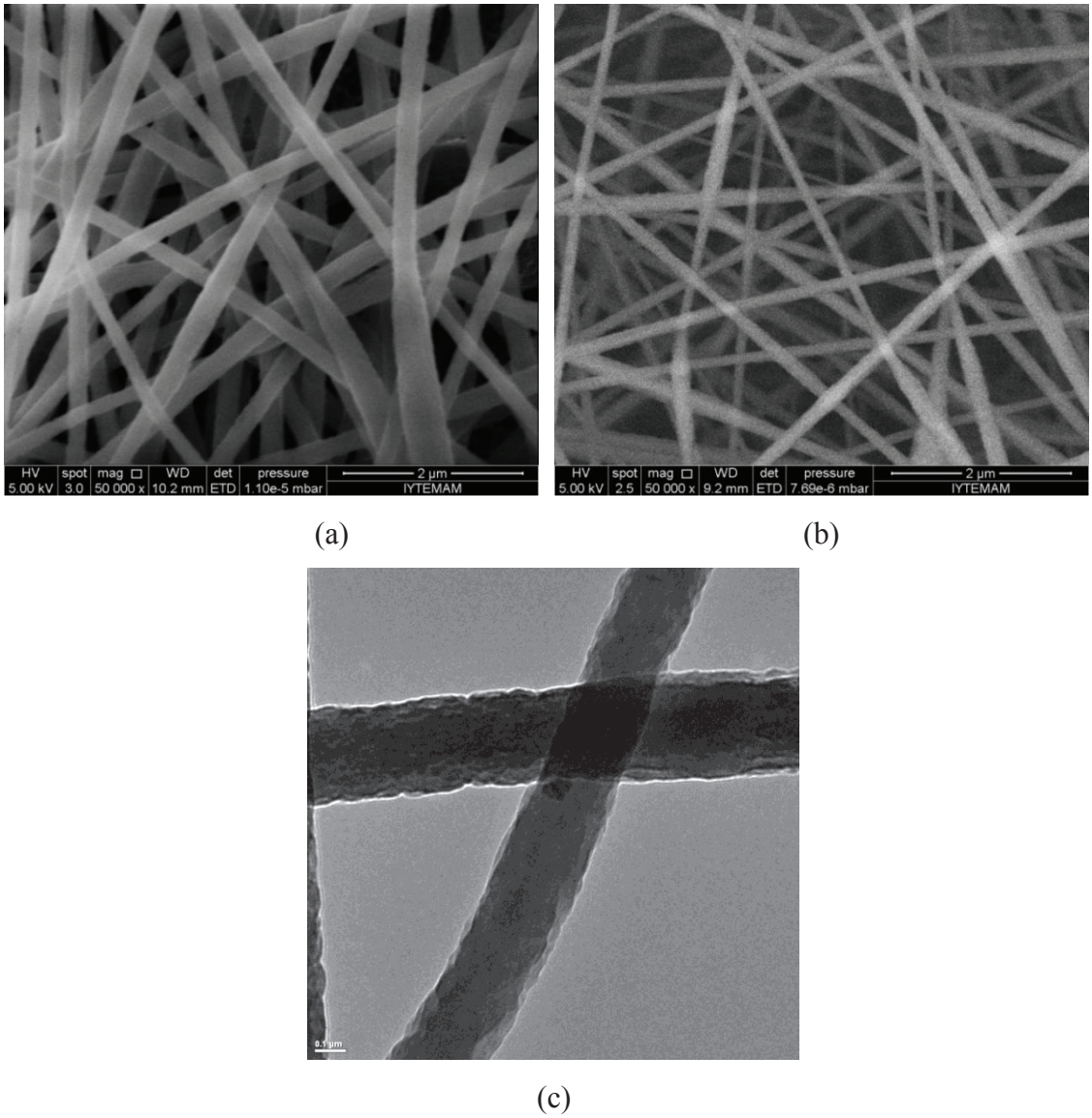

(a) (b)

(c)

Figure 5.6 SEM micrographs of electrospun PAN/PPy nanofibers (a) PP1, (b) PP3 prepared at solution temperature of 60 ^{o}C at 2µm scale, (c) TEM micrograph of electrospun PAN/PPy nanofibers containing 10 wt% PPy at 0.1 µm.

The polymer solution viscosity has a significant influence on obtaining uniform fibers and diameter of obtained fibers. The viscosity of the solutions are given in Table 5.2. The viscosity values of prepared solutions containing different amount of PPy were determined in the range of 11.59×10^{-2} and 1.16×10^{-2} Pa.s at 400 1/s shear rate. Viscosity of PAN was about 10 times higher than viscosity of PPy. Increasing PPy amount in solution decreased the solution viscosity and these results were consistent with SEM

results. Increasing solution viscosity resulted with thicker PAN/PPy nanofibers because it is more difficult to overcome surface tension for electrical forces at higher viscosity values and therefore high viscosity prevents continuous and ordered fibers formation.

Table. 5.2 Viscosity values of the solutions containing different amounts of PPy at shear rate of 400 s^{-1}.

PPy (wt%)	Viscosity (Pa.s) ($x10^{-2}$)
0	11.59
10	10.7
25	4.94
50	1.47
100	1.16
10 + 1 wt% CNT	5.49

XRD patterns of the PAN/PPy nanofibers are shown in Fig.5.7. It can be observed that there was a broad amorphous diffraction peak centered at around $2\Theta = 28°$, corresponding to the scattering from bare polymer chains at the interplanar spacing of protonated PPy (Seo, Pyo, and Cho 2002). For 50 % PPy content, this peak was resolved better as a result of improvement in PPy chain ordering. Other peaks belong to PAN (200) and (020) crystal plane peaks at 2Θ 17.19º and 29.95º, respectively. Intensity of (200) plane peak increased with increasing PPy content, whereas intensity of (020) plane peak decreased.

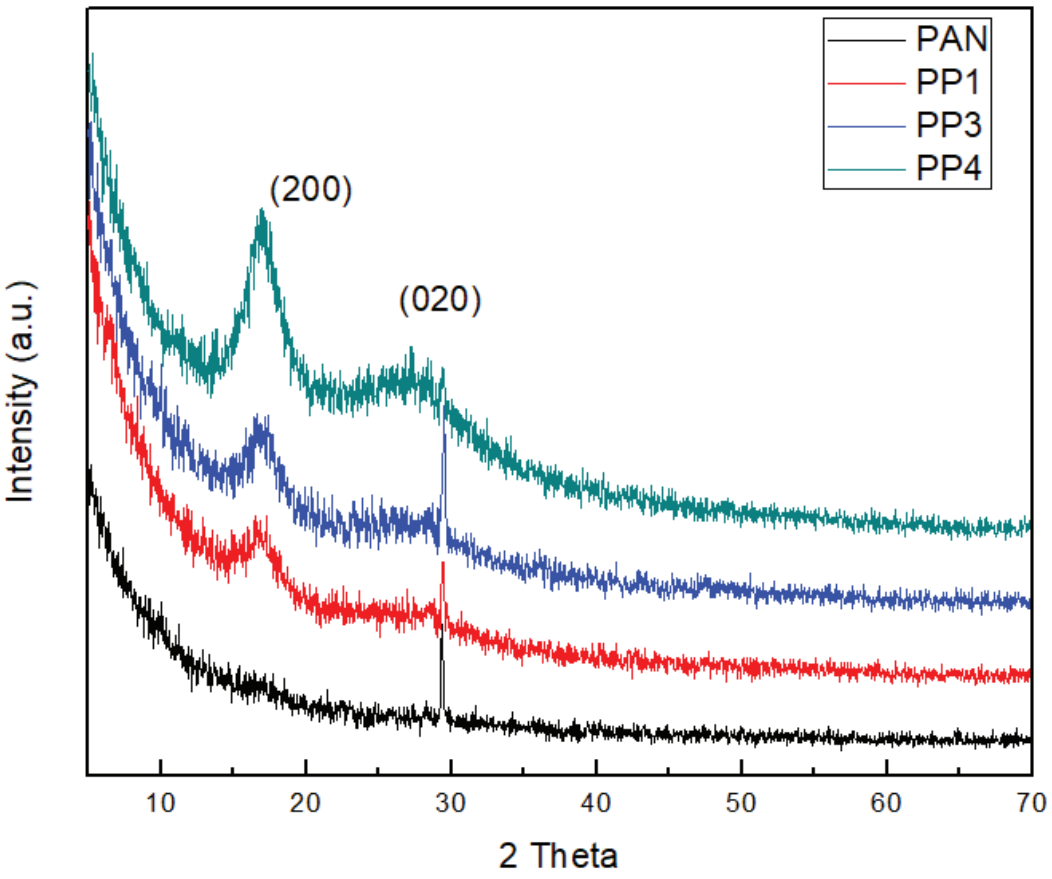

Figure 5.7 XRD scans of the PAN/PPy electrospun nanofibers.

Fig. 5.8 depicts the Raman spectroscopy of the PAN/PPy nanofibers. It showed well-known D-band and G-band. For these electrospun PAN/PPy nanofibers G peak was greater than D peak for 10 wt% and 25 wt% PPy contents, however for 50 wt% PPy content, D peak increased. This indicated that they contained significant amount of disorder and defects. In addition, the presence of PPy caused more defects in the resultant nanofibers, therefore D peak was stronger at higher PPy content (Ji et al. 2010). For PAN nanofibers, there was no D peak and G peak, only a peak about 2250 cm^{-1} observed corresponding to the existance of nitrile group of PAN, after addition of PPy this peak dissappeared.

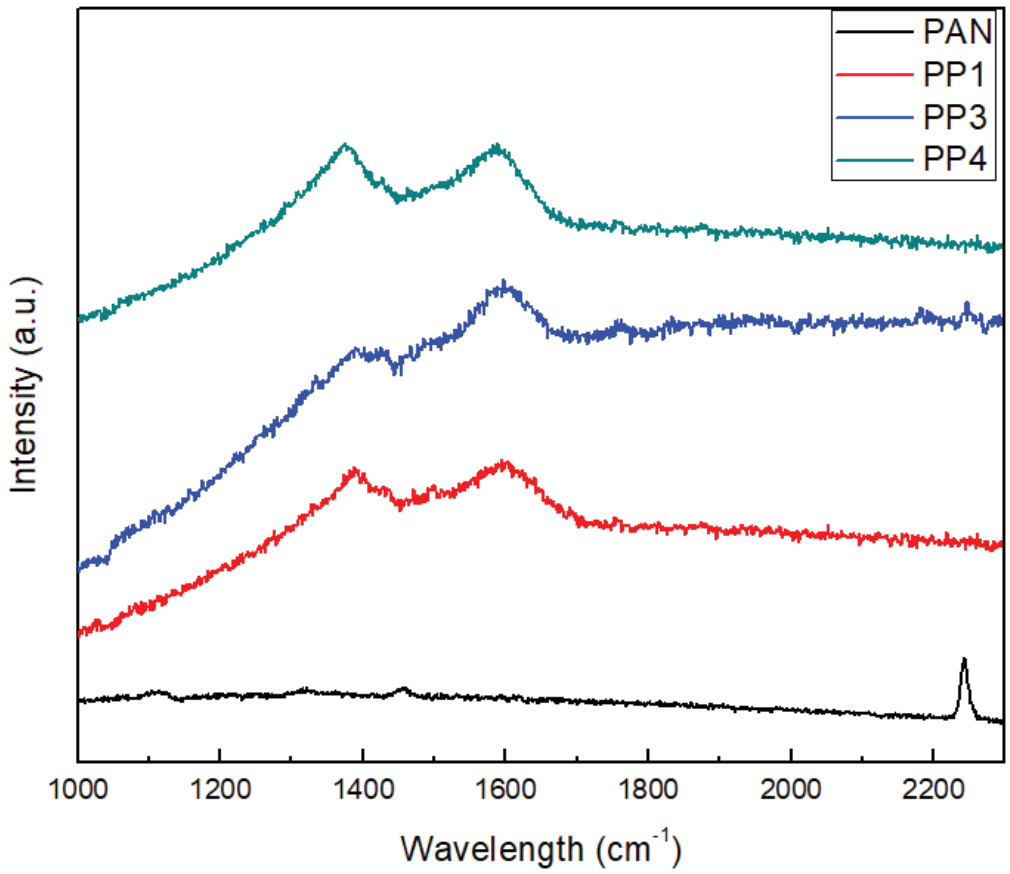

Figure 5.8 Raman spectra of the PAN/PPy electrospun nanofibers.

Thermal properties of the PAN/PPy electrospun nanofibers were analysed by TGA and DSC analysis. TGA results for different PPy amounts are given in Fig. 5.9. Main weigth loss for pure PAN nanofibers in air atmosphere are observed at about 310 and 500 ^{o}C, whereas pure PPy (pure PPy can not be electrospun) gave TGA peaks at about 210 and 410 ^{o}C (Ji et al. 2010). PAN/PPy nanofibers began to decompose between the decomposition temperature of two polymers. Decomposition temperature of low PPy content was higher than the sample contain high PPy content, because PPy phase degradation was easier than PAN phase in air environment.

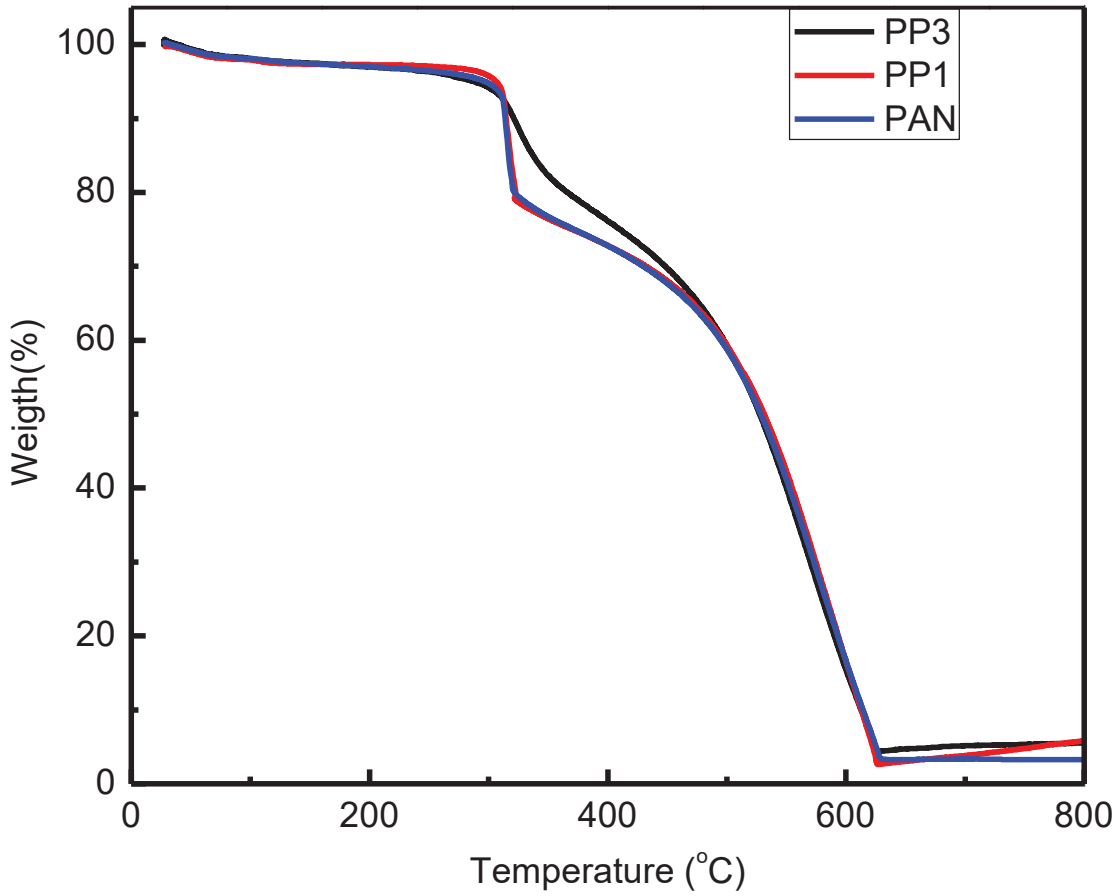

Figure 5.9 TGA graphs of the PAN/PPy electrospun nanofibers containing different amounts of PPy.

DSC graphs of the electrospun nanofibers containing different amout of PPy are depicted in Fig. 5.10. All of the samples showed a phase transition between 280 and 335 °C. Exothermic phase transition peak at 308 °C was observed the sharpest for the sample containing neat PAN. Intensity of this peak decreased slightly for samples containing PPy. This peak could be because of chemical reactions of PAN during the heating process via free radical mechanism (Kim et al. 2007).

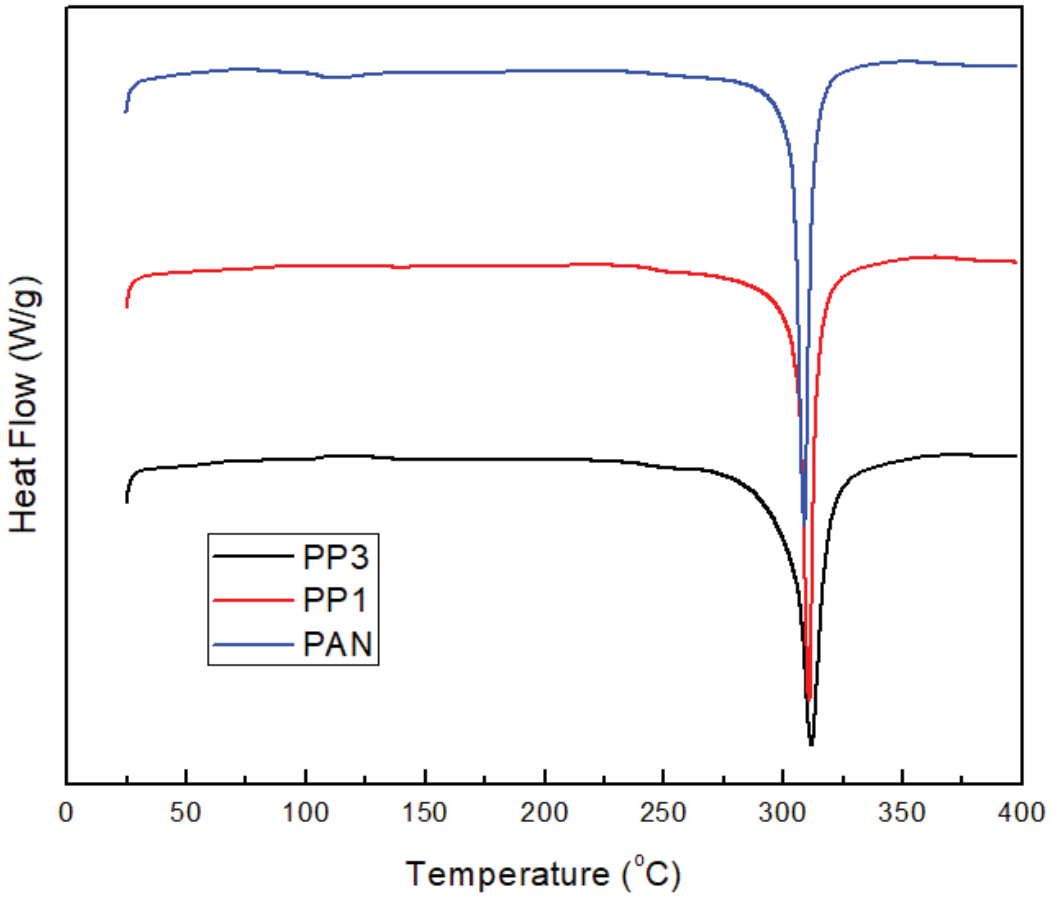

Figure 5.10 DSC graphs of electrospun PAN/PPy nanofibers containing different amount of PPy.

PPy has very poor mechanical properties. Therefore, in the present study, PAN was used as the host polymer for PPy to improve the mechanical properties of the PPy. Tensile tests were performed to measure the mechanical properties of PAN/PPy nanofibers to determine the optimum PPy amount for nanofiber synthesis. Table 5.3 shows the tensile properties of the PAN/PPy nanofibers containing 10 wt% and 25 wt% PPy. Mechanical tests of sample containing 50 wt% PPy was not performed because of bead formation. In the case of 10 wt % PPy (PP1), strain value of nanofibers was significantly higher than 25 wt% PPy amount (PP3) due to the brittle property of PPy. However, tensile strength (calculated by dividing the load at break by the original minimum crosssectional area) of nanofibers were not affected by PPy amount. Average diameter of nanofibers decreased from 268 nm to 153nm with increasing PPy amount from 10 wt% to 25 wt%. Besides, when CNTs were added into PAN/PPy solution

containing 25 wt% PPy, solution could not be electrospun and fibers formation did not occur. Therefore, optimum PPy content was determined as 10 wt% for this study.

Table 5.3 Average diameter and tensile properties of PAN/PPy nanofibers containing 10 and 25 wt% PPy.

Sample	Average Diameter (nm)	Tensile strain (%)	Tensile strength (Mpa)
PP1	268	23.33	9.34
PP3	153	1.41	9.89

5.2.2 Aligned and Random PAN/PPy Bicomponent Nanofibers

PAN/PPy nanofibers were examined for osteogenic differentiation of mesenchymal stem cells as scaffolds. SEM image of aligned PAN/PPy nanofibers (PP2) are given in Fig. 5.11. Aligned nanofibers were collected by a rotating collector with the rotation speed of 1000 rpm. As illustrated in SEM image, alignment of PAN/PPy nanofibers was achieved and more organized nanofibers were obtained.

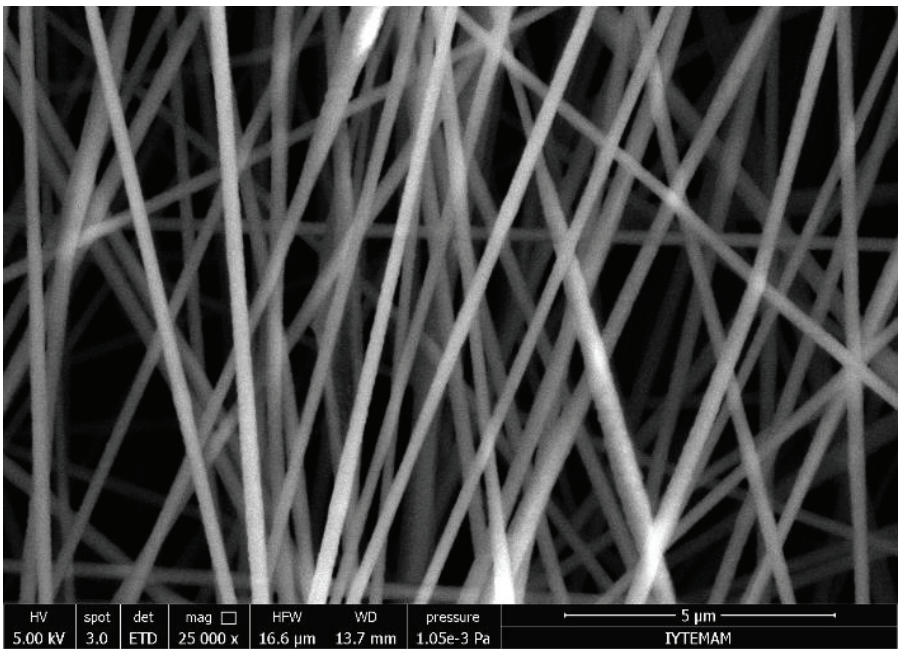

Figure 5.11 SEM images of aligned nanofibers PP2 at 5 µm scale.

The result of mechanic test of the PAN/PPy nanofibers are given in Table 5.4. PAN improved the brittle property of PPy and the optimum PPy content was determined as 10 wt%. Aligned (PP2) and random (PP1) PAN/PPy nanofibers containing 10 wt% PPy are compared in Table 5.4. Alignment of nanofibers improved significantly tensile strength of nanofibers, tensile strength of nanofibers increased from 9.34 MPa to 36.77 MPa after alignment. However, tensile strain of nanofibers decreased about 4 fold after alignment process. The average diameter of PP1 was 268 nm, whereas that of PP2 was 225 nm.

Contact angle values for random and aligned nanofibers are shown in Table 5.4. Results showed that alignment of nanofibers did not influence contact angle value. Both random and aligned PAN/PPy nanofibers gave contact angle of about 32^{o}. Pure PPy is a hydrophobic polymer, however, contact angle results indicated the hydrophilic property of PAN/PPy nanofibers, hydrophilicity of nanofiber scaffolds further affects the cell attachment on nanofiber surfaces.

Table 5.4 Average diameter, tensile properties and contact angles of random and aligned PAN/PPy nanofibers containing 10 wt% PPy.

Sample	Average Diameter (nm)	Tensile strain (%)	Tensile strength (Mpa)	Contact Angle (^{o})
PP1	268	23.33	9.34	32.817
PP2	225	5.15	36.77	32.005

Polarized FT-IR spectra of the random and aligned PAN/PPy nanofibers are displayed in Fig. 5.12. The peaks at 1270 cm^{-1} and 1654 cm^{-1} are induced by C-N and C=N streching, respectively. The peaks observed at 1454 cm^{-1} and 2237 cm^{-1} were the characteristics vibrations peaks of PAN (Li et al. 2008). FT-IR results confirmed the PPy existence in PAN solution. Black and red lines show the polarized FT-IR spectra of random nanofibers. For random nanofibers, positions and peak intensities of parallel and perpendicularly polarized FT-IR spectra were the same. There was no specific molecular orientation in this sample. However, the polarized FT-IR spectra of aligned PAN/PPy nanofibers showed anisotropy. When the IR beam was polarized parallel to the fiber axis

(green line), higher absorption was observed. The intensities and peaks positions were changed for parallel and perpendicular directions. This indicated that the polymer chain in the fiber was streched and aligned in the fiber axis during electrospinning process (Nobeshima et al. 2016).

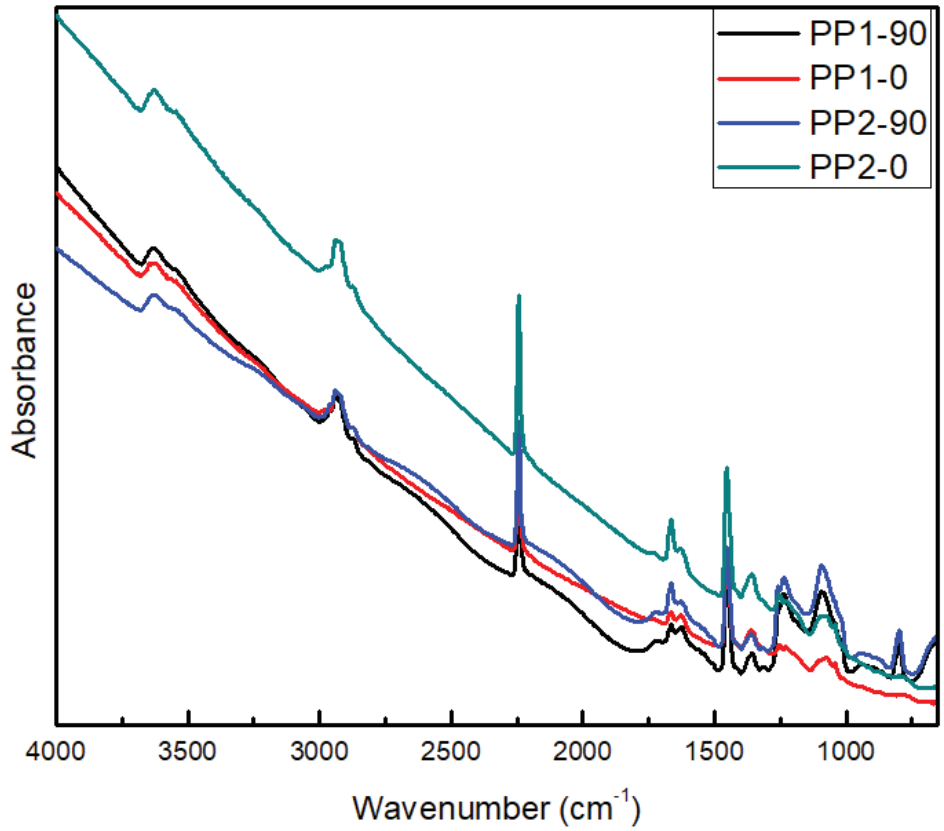

Figure 5.12 Polarized FT-IR spectra (parallel (0°) and perpendicular (90°) polarized IR spectra of PP1 and PP2.

5.2.3 Electrospun PAN/PPy Nanofibers Containing Different Amount of CNTs

When we embedded CNTs into the PAN/PPy solution containing 25 wt% PPy, this solution could not be electrospun. SEM pictures of these samples showed that (Fig. 5.13) when 1 wt% CNTs was added some nanofibers electrospun, however these nanofibers contained lots of beads and irregularities. For 5 wt% CNT content, almost no fiber were observed (Fig. 5.13.b), electrospinning resulted only in the formation of discrete beads. PPy has low solubility and high electrical conductivity. CNTs addition

makes PAN/PPy solution more conductive. Therefore, formation of electrospun nanofibers becomes more difficult for high PPy and CNT contents.

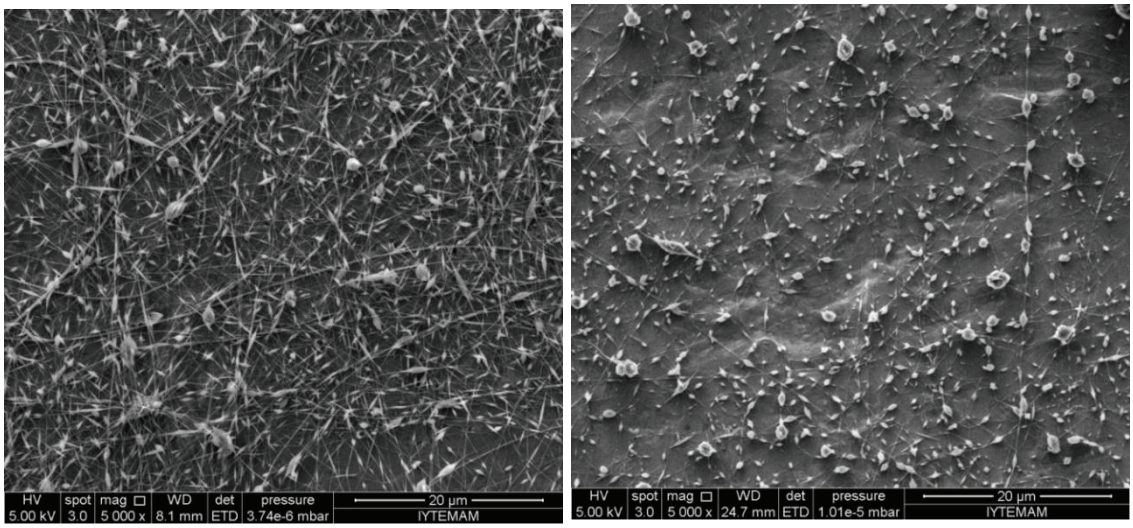

(a) (b)

Figure 5.13 SEM micrographs of CNT embedded electrospun PAN/PPy nanofibers containing 25 wt% PPy (a) PPC1 (b) PPC2.

To obtain PAN/PPy electrospun nanofibers with CNTs, PPy amount was decreased to 10 wt%. Fig. 5.14 displays the SEM micrographs of the nanofibers for different content of CNT. Electrospun nanofibers showed a smooth surface for 1 wt% content of CNT (PPC3), however increasing CNT content prevented a continuous spinning, so with increasing amount of CNT, number of bead increased dramatically. For 4 wt% CNT content (PPC6), obtained nanofibers contained lots of beads and disordered sites on their surface.

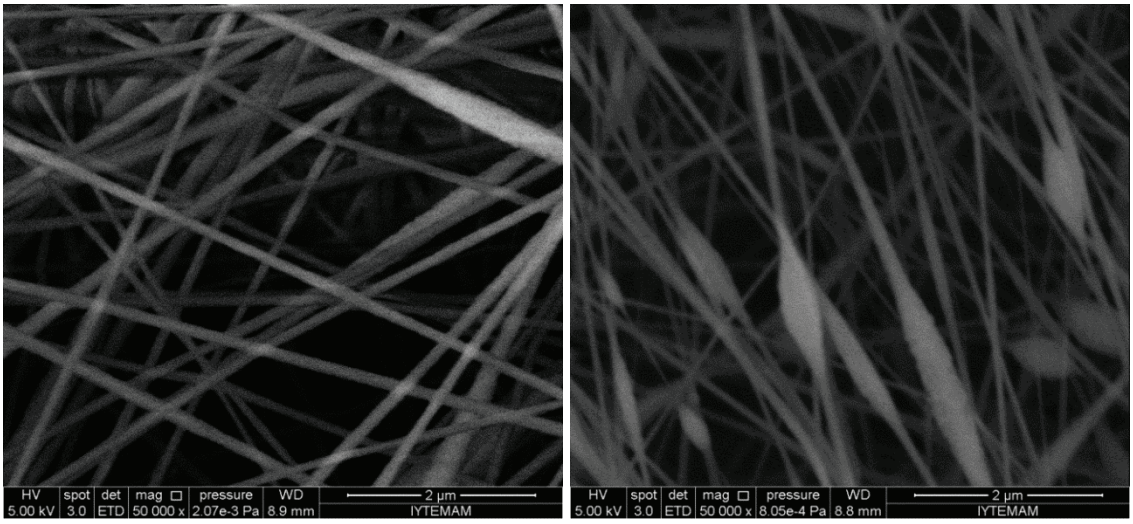

(a) (b)

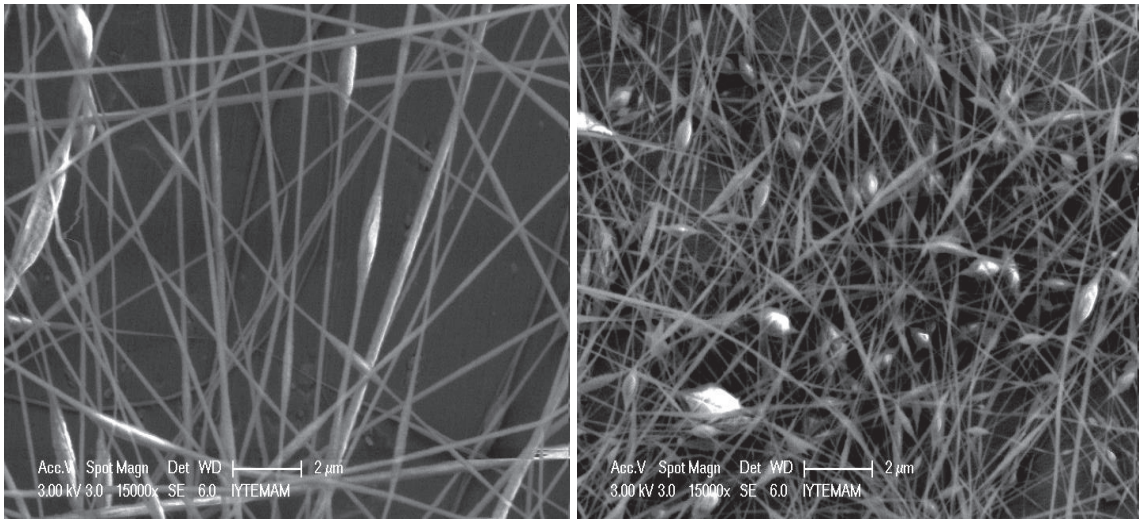

(c) (d)

Figure 5.14 SEM micrographs of CNT embedded electrospun PAN/PPy nanofibers containing 10 wt% PPy and (a) PPC3 (b) PPC4 (c) PPC5 (d) PPC6 at 2µm scale.

These findings suggested that with the increase of CNT content, CNTs agglomerated and these agglomerated sites caused disoredered sites and beads on the nanofibers. TEM images indicated that there were two reason of these disordered nanofibers. The first reason was CNT agglomeration as observed from Fig. 5.15.a. In order to dissolve CNTs homogenously, PAN/PPy solutions containing CNTs were kept in ultrasonic bath for 24 h. However, during electrospinning process a lot of CNT clustered and a bead formation occured. The second reason of disorders was due to CNTs

not beeing embedded into the PAN/PPy nanofibers shown in Fig. 5.15.b. Some CNTs stayed out of the nanofiber under high electrical field during nanofiber formation process.

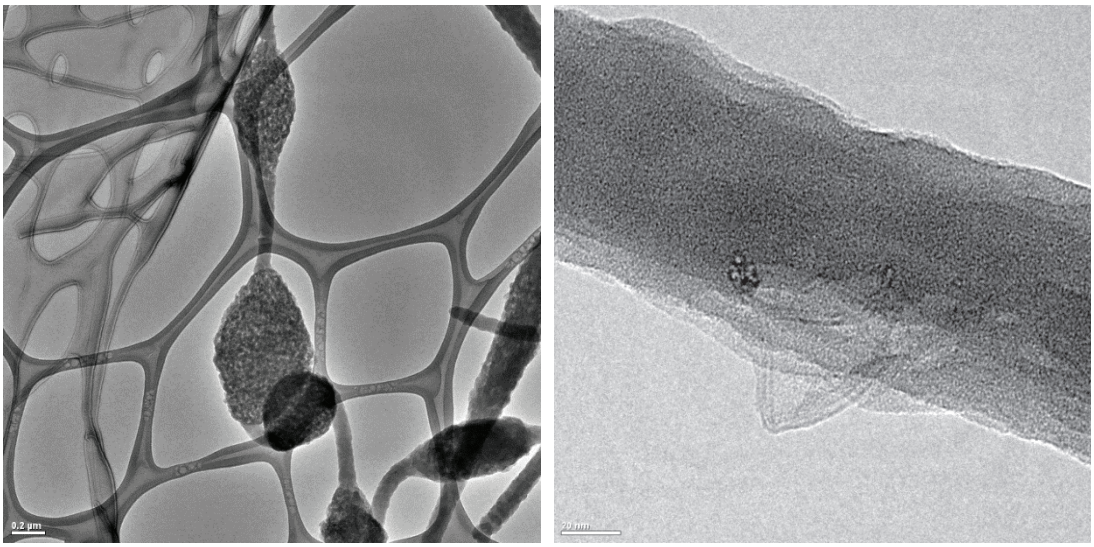

(a) (b)

Figure 5.15 TEM images of beads on nanofibers caused by (a) CNT agglomeration (b) not embedded CNTs.

Fig. 5.16 displays TGA thermograms of PAN/PPy nanofibers containing 10 wt% PPy and different amount of CNTs. A dramatic weigth loss observed between 300-500 °C in air was due to decomposition of PAN/PPy nanofibers. Without CNTs, nanofibers decomposed a bit lower temperature. The combustion of CNTs occured after 500 ºC (Fig. 5.1). CNTs enhaced the thermal stability of nanofibers.

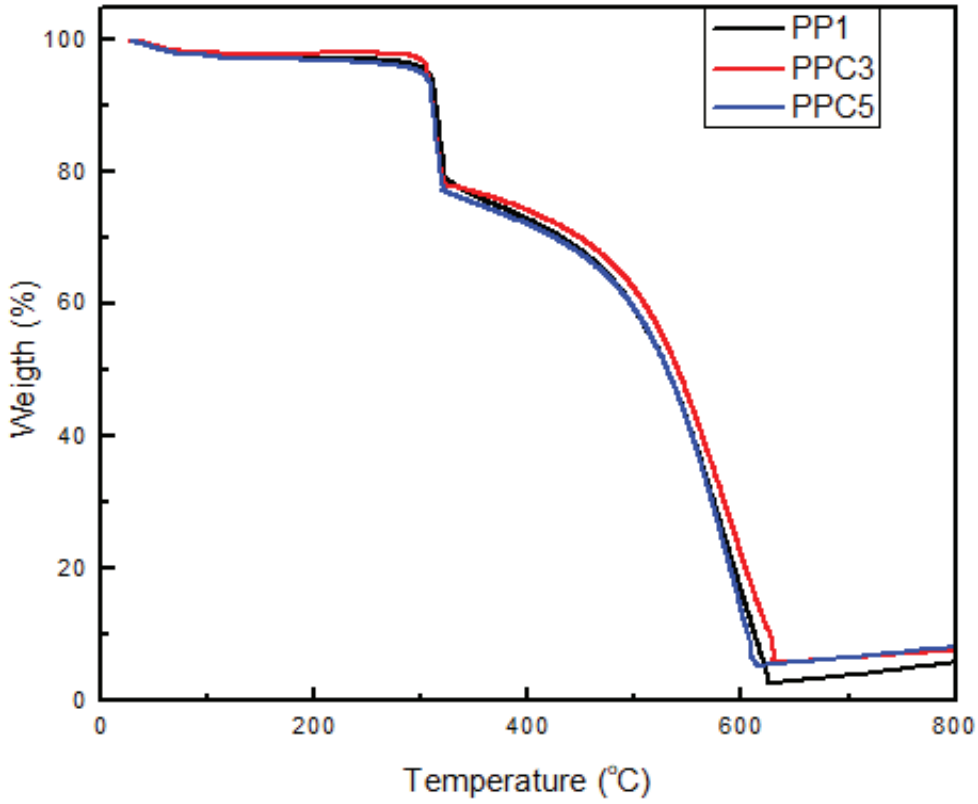

Figure 5.16 TGA thermograms of CNT embedded electrospun PAN/PPy nanofibers.

To sum up, 10 wt % and 25 wt% PPy contents of total polymer weight were examined and the results indicated that 25 wt% PPy with CNTs could not be electrospun when CNT was embedded into the polymer. For 10 wt% PPy content electrospinning was possible for 1, 2, 3 and 4 wt% CNT amounts. However, with increasing CNT incorporation, number of beads on nanofiber surface increased, disordered nanofibers were observed. Therefore, functional CNTs were also studied in order to enhance CNT dispersion in PAN/PPy nanofibers and to obtain smooth and ordered nanofibers with less number of beads on their surfaces.

Figure 5.17 shows SEM micrographs of PAN/PPy nanofibers containing as-grown and functional CNTs. PAN/PPy electrospun nanofibers containing 10 wt% PPy were highly ordered and no beads were observed on nanofibers (Fig. 5.6.a). When 1 wt% CNT was embedded beads and some disordered part were formed on the surface of nanofibers. CNT addition affected the conductivity of solution and the spinnability decreased and agglomerated CNT parts caused some disordered parts on the nanofibers. 1 and 4 wt% CNT ratios were examined. When 1 wt% functionalized CNTs were

embedded, density of nanofibers increased and observed bead numbers decreased (Fig. 5.17.b). For 4 wt% CNT content also the same properties were enhanced with functional CNT usage (Fig. 5.17.d). Besides, for 4 wt% CNT compared to 1 wt%, the improvement of the nanotube quality could be observed better. When 4 wt% as-grown CNT was embedded to the nanofibers almost whole surface of nanofibers covered with beads and when functional CNTs were used a significant difference occured. There were still some beads, however, much fewer than the sample containing as-grown CNTs.

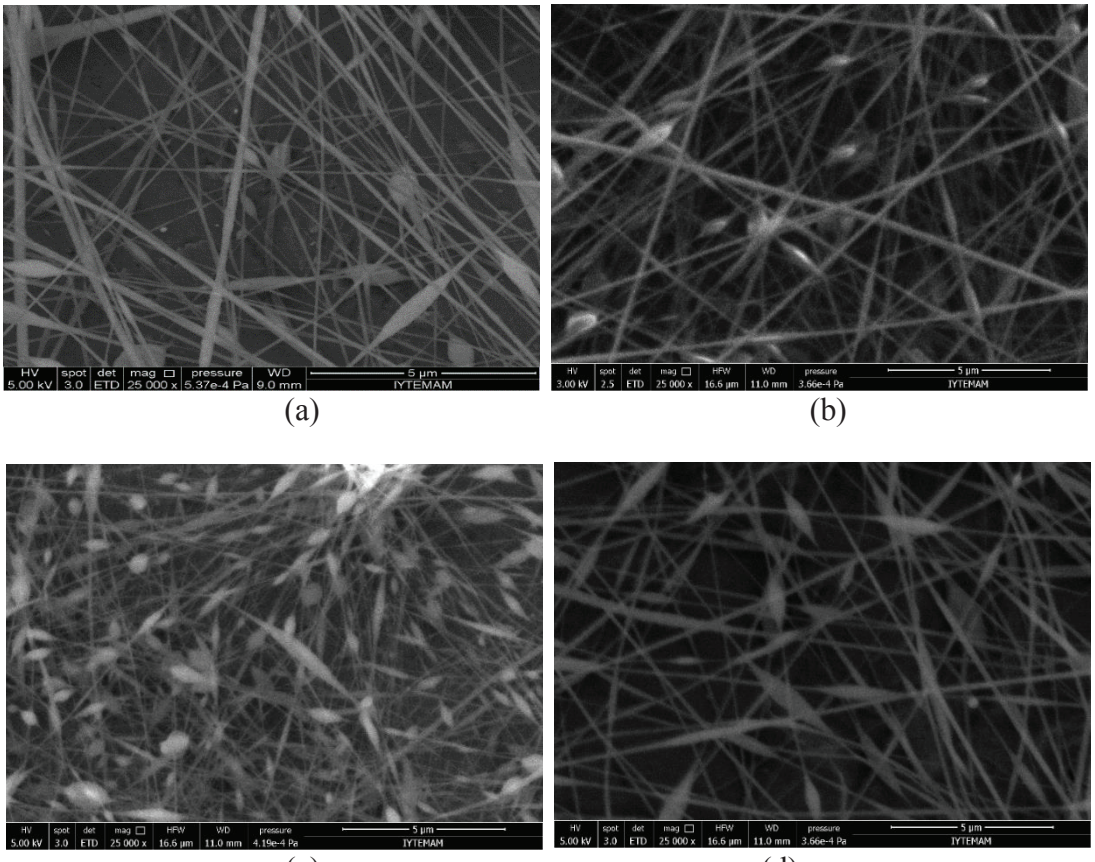

Figure 5.17 SEM micrographs of PAN/PPy/CNT electrospun nanofibers incorporated with 1 wt% and 4 wt% as-grown and functional CNTs, (a) PPC3 (b) PPC7 (c) PPC6 (d) PPC8.

Raman spectra of the PAN/PPy/CNT electrospun nanofibers containing 1 wt% CNT is displayed in Fig. 5.18. D peak and G peak were observed at about 1300 cm^{-1} and 1590

cm^{-1}, respectively. Nitrile group (-CN) peak was observed at 2240 cm^{-1}. I_D/I_G ratio was significantly low when as-grown CNTs were utilized because of the highly graphitized

CNTs. I_D/I_G increased with the addition of functional CNTs. Graphitization decreased with functionalized CNT addition because of broken bonds after acid treatment.

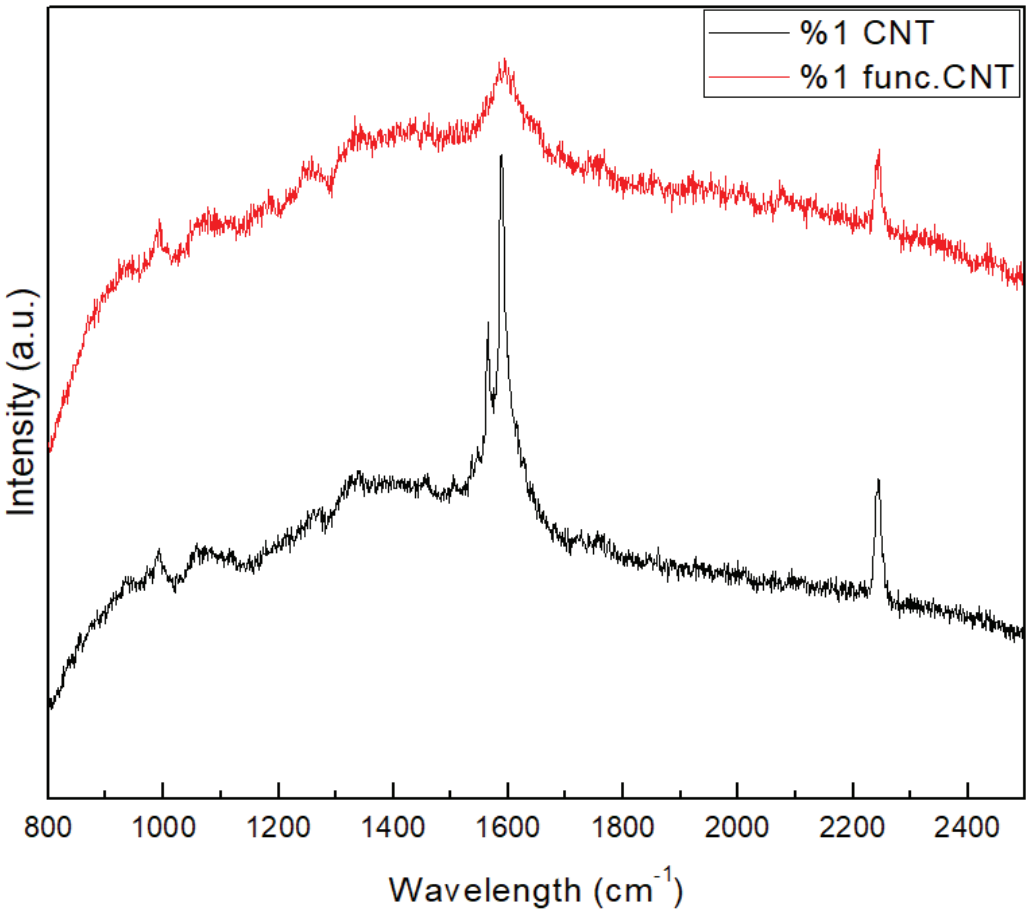

Figure 5.18 Raman spectra of PAN/PPy/CNT nanofibers containing 1 wt% as-grown and functionalized CNTs.

Raman spectra of the PAN/PPy/CNT electrospun nanofibers containing 4 wt% CNT is displayed in Fig. 5.19. For 4 wt% CNT content only D peak and G peak were observed, with the increasing amount of CNTs nitrile group peak disappeared. For 4 wt% CNT content also I_D/I_G value was higher for the sample containing functional CNTs compared to sample containing as-grown CNTs because of the broken bonds in functionalized CNTs.

I_D/I_G ratios were higher for 4 wt% CNT content compared to 1 wt% CNT because of CNT agglomeration and disordered parts on the nanofibers. These Raman data and SEM micrographs were in agreement; increasing CNT content caused disordered

nanofibers, so graphitization decreased with increasing CNT content in PAN/PPy nanofibers.

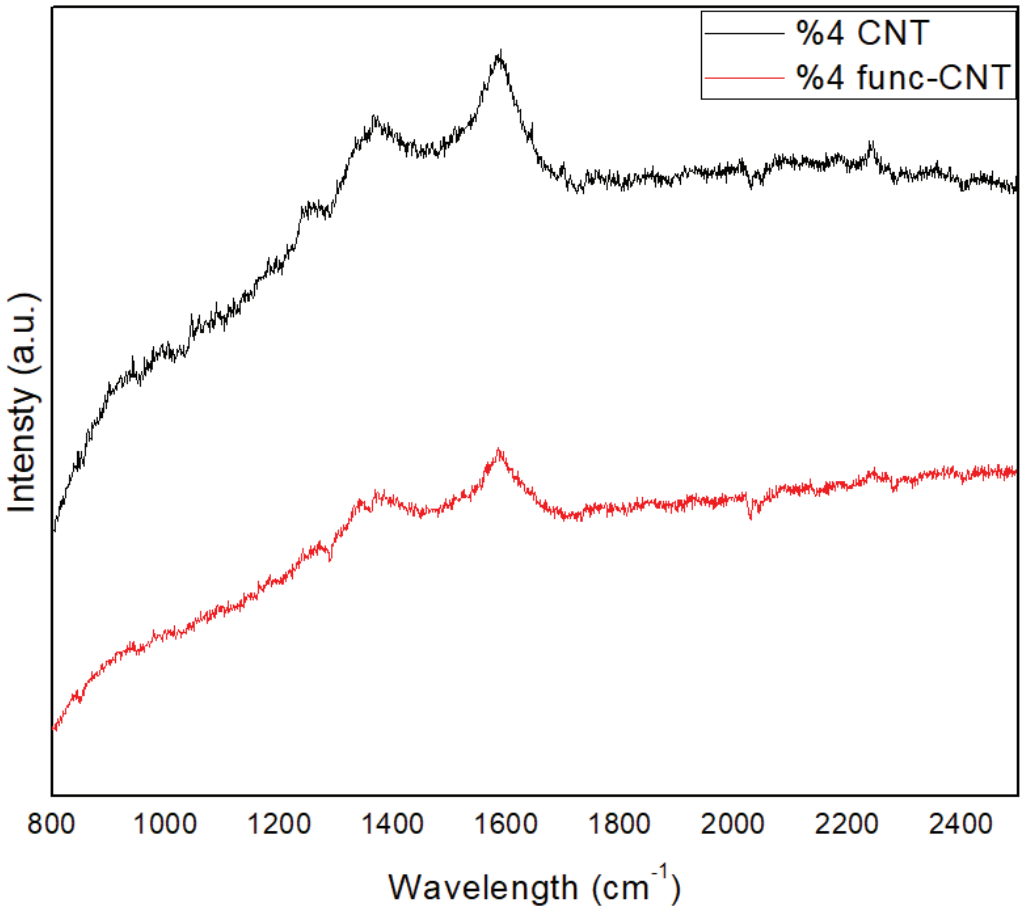

Figure 5.19 Raman spectra of PAN/PPy/CNT nanofibers containing 4 wt% as-grown and functionalized CNTs.

TEM analysis showed concentric tubular structure of CNTs in nanofibers as shown in Fig. 5.20. CNTs were aligned along the direction of nanofibers during electrospinning process under high electrical field. In addition, it was appearent from TEM images that CNTs were MWCNTs and wall number was generally 3 or 4.

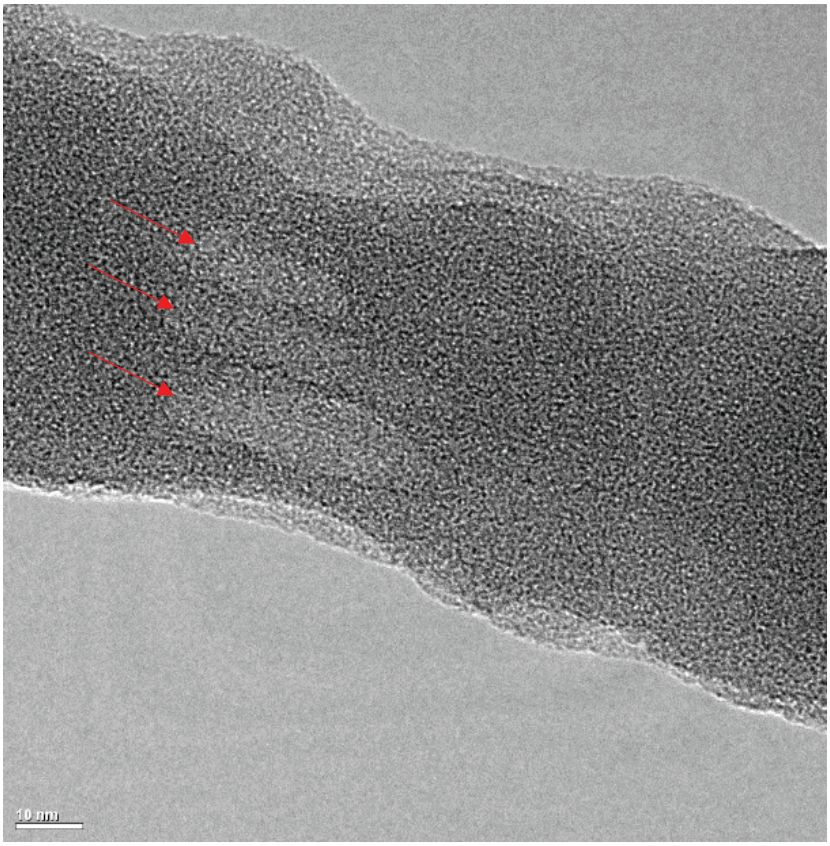

Figure 5.20 TEM images of PAN/PPy nanofibers containing 10 wt% PPy 1 wt% of functionalized CNT (PPC7).

Fig. 5.21 shows the FT-IR spectra of CNT embedded PAN/PPy nanofibers. Peaks observed at 1454 cm^{-1} and 2354 cm^{-1} are the characterisitc peaks of PAN and the peaks at 1270 cm^{-1} and 1654 cm^{-1} are induced by C-N and C=N streching, respectively. The peak at 1454 cm^{-1} and 1068 cm^{-1} corresponded to the C=C and C-H. This data confirmed the PPy existence in PAN (Ju et al. 2008). Addition of as-grown CNTs did not change the FT-IR spectrum of PAN/PPy nanofibers due to the symmetrycal structure of as-grown CNTs. However, sample including functionalized CNTs showed a broad peak at about 3400 cm^{-1} which is a characteristic of the O-H streching of hydroxylic group. Peaks between 2800-3500 cm^{-1} were characteristic peaks of C-H and O-H bonds which could be related to carboxylic and hydroxylic groups (Osorio et al. 2008).

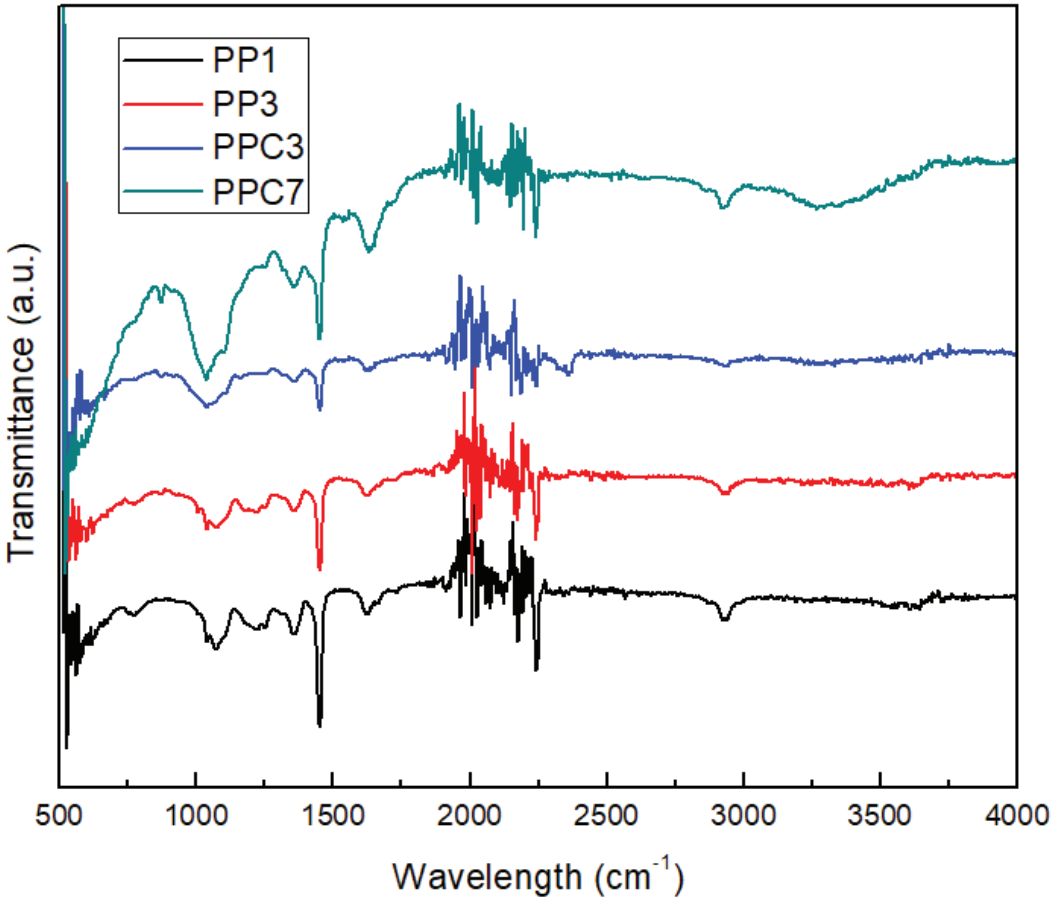

Figure 5.21 FT-IR spectra of PAN/PPy and CNT embedded PAN/PPy nanofibers.

In order to investigate electroactivity of PAN/PPy nanofibers CV method was utilized. For CV measurements, the nanofibers were coated on graphite electrode and used as the working electrode. Nanofibers with different PPy amounts, PP1 and PP3 showed two oxidation and one reduction peak approximately at the same positions as observed in Fig. 5.22. Oxidation peaks were observed at 0.2 and 0.7 V and reduction peak was observed at 0.4 V. Nanofibers including 10 wt% PPy (both CNT embedded and not embedded) showed the first oxidation wave at approximately 0.2V. The CV results indicated that the highest output current was provided by PAN/PPy nanofibers containing 25 wt% PPy. The conductivity of nanofibers improved by increasing PPy amount from 10 to 25 wt%. Addition of CNTs also increased the conductivity of the nanofibers. This increases in conductivity was provided by the electrically conductive nature of CNTs and PPy. CV results of the fibers suggested that this material was electroactive and can be used as an electrochemical actuator in acidic solutions.

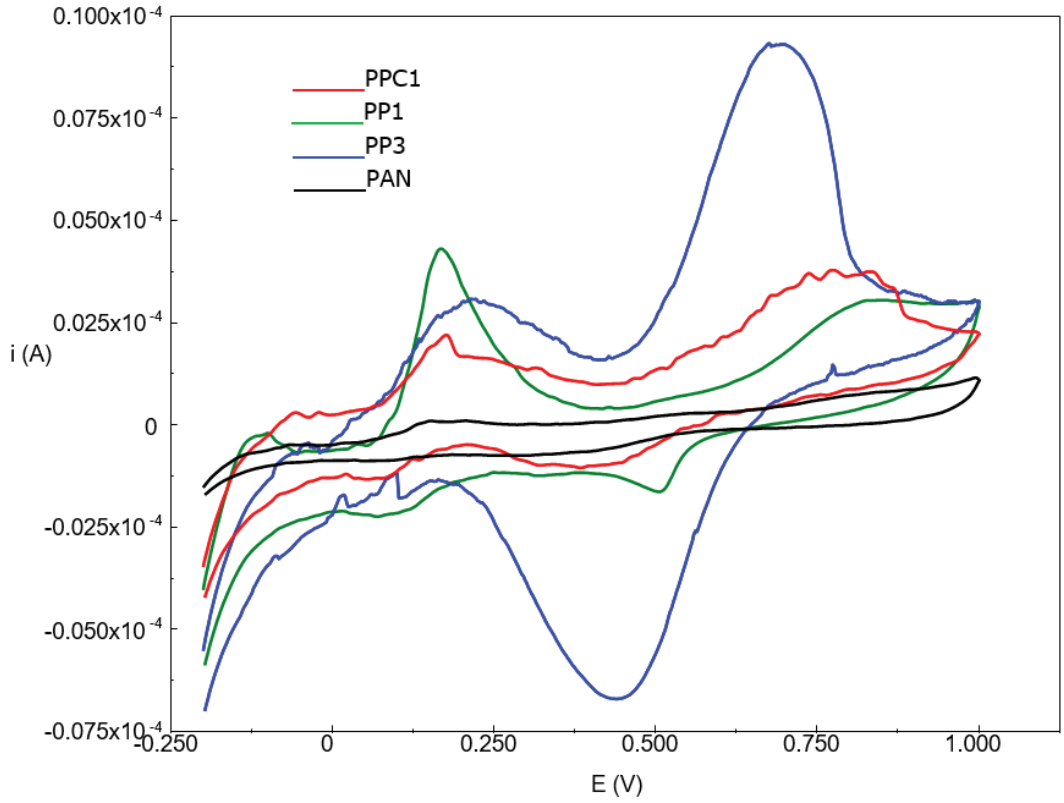

Fig. 5.22 Cyclic voltammograms of PAN/PPy nanofibers with different PPy and CNT contents in 0.1 M HCl solution.

Electrochemical impedance measurements were performed for the PAN/PPy nanofibers containing different PPy and CNT amounts. The change in impedance curve for electrodes covered with electrospun PAN/PPy nanofibers are given in Fig. 5.23. The electrochemical impedance data give information about the nature of electrochemical process occurring at the electrode/electrolyte interface. The Nyquist graphs of nanofibers were given in the frequency range of 0.01 Hz to 100 kHz. A significant difference in the impedance spectra was observed when the PPy amount changed. Nyquist plots of PAN/PPy nanofibers exhibited semicircles. The diameter of the semicircle represents the charge-transfer resistance of PAN/PPy nanofibers (Giray et al. 2013) and diameter of semicircles increased with PPy amount and CNT addition.

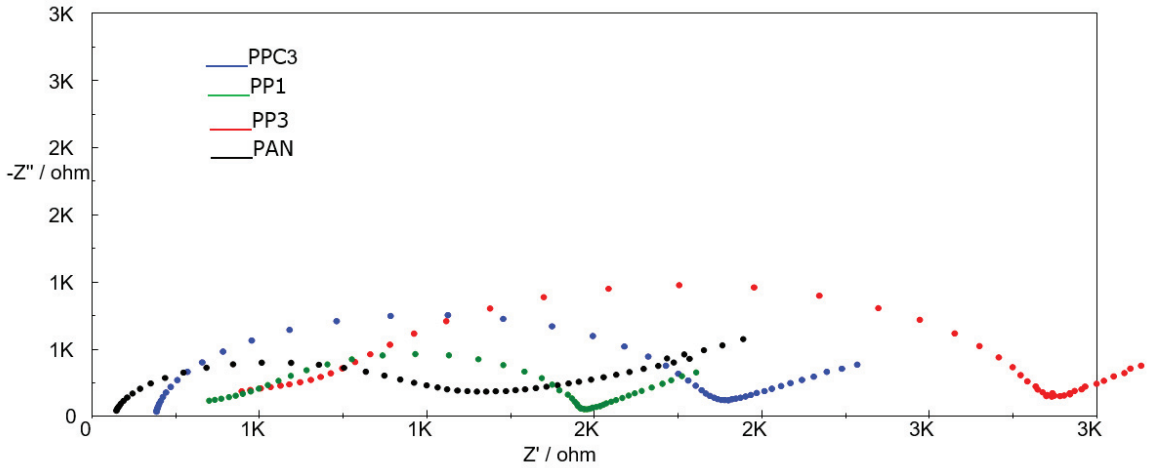

Fig. 5.23 Electrochemical impedance plots of PAN/PPy nanofibers with different PPy and CNT contents.

Resistance value of nanofibers calculated from Nyquist plots decreased with increasing PPy amounts as given in Table 5.5. While PAN nanofibers showed a 2603 ohm impedance value, the impedance were 1688 and 1066 ohm for PPy ratios of 10 and 25 respectively. The highest PPy content showed the highest electrical conductivity. CNT addition also decreased the resistance value from 1688 to 1481 ohm. It was consistent with cyclic voltammetry results which showed that increasing PPy and CNT addition decreased resistance and improved electrical properties of nanofibers.

Hydrophilicity of nanofiber scaffolds further affects the cell attachment on nanofiber surfaces. PPy is a hydrophobic material. However, as a co-polymer PAN improved the hydrophobic property of PAN/PPy nanofibers and electrospun PAN/PPy nanofibers indicated a hydrophilic property in water contact angle measurements, as shown in Table 5.6. However, with increasing PPy amount of PPy from 10 to 25, contact angle increased about 7°. CNT is also hydrophobic material and when 1 wt% CNT was embedded into PAN/PPy nanofibers containing 10 wt% PPy, the contact angle increased significantly, by 21°. Therefore, PAN/PPy/CNT nanofibers were hydrophobic compared to PAN/PPy nanofibers.

Table 5.5 Impedance values of PAN/PPy nanofibers with different PPy and CNT contents.

Sample	PAN	PP1	PP3	PPC3
Impedance (ohm)	2603	1688	1066	1481

Table 5.6 Contact angle values of PAN/ PPy nanofibers with different composition.

Nanofibers	Average Diameter (nm)	Contact Angle (^{o})
10 wt% PPy	268.0	32.8
25 wt% PPy	161.4	39.4
10 wt %PPy+1 wt% CNT	128.3	53.3

5.3 CNT Embedded PAN/PPy Nanofibers as Keratinocytes Scaffold

Morphology of keratinocytes (HaCaT) and their interaction with PAN/PPy nanofibrous scaffold were observed for 7 days by SEM. Representative images of keratinocytes grown on PAN/PPy scaffold containing 10 wt% PPy are shown in Fig. 5.24 For 1 day of culture, keratinocytes were observed to attach on PAN/PPy scaffolds. Cells were able to proliferate on these scaffolds as observed by an increase in the amount of cells on 3rd and 7th days of culture. These results suggested that keratinocytes were able to adhere and proliferate on PAN/PPy scaffolds.

Images of fluorescence microscopy for control keratinocytes and cells grown on PAN/PPy nanofibers containing 10 wt% PPy (PP1) are illustrated in Fig. 5.25 It was observed that after 1 day, skin cells spread on the coverslip surface and attached to the fibers. With increasing culturing time, the number of cells increased and cell groups were observed among fibers after 3 days and these groups became very crowded at the end of 7 days of culturing. Cells seeded on glass surface spread and covered the whole coverslip

surface, whereas those seeded on fibrous scaffold attached to the fibers and formed groups on the surface of fibers.

The data indicated that with increasing PPy content, diameter of fibers were reduced. Fig. 5.26 shows SEM pictures of cells seeded on nanofibers containing 25 wt% PPy (PP3). The cells attached and spread on the fibers. The cell morphology was similar to cells seeded on scaffold containing lower PPy content which had lower diameters. Thus, it was suggested that diameter of fibers did not influence the cell attachment and proliferation.

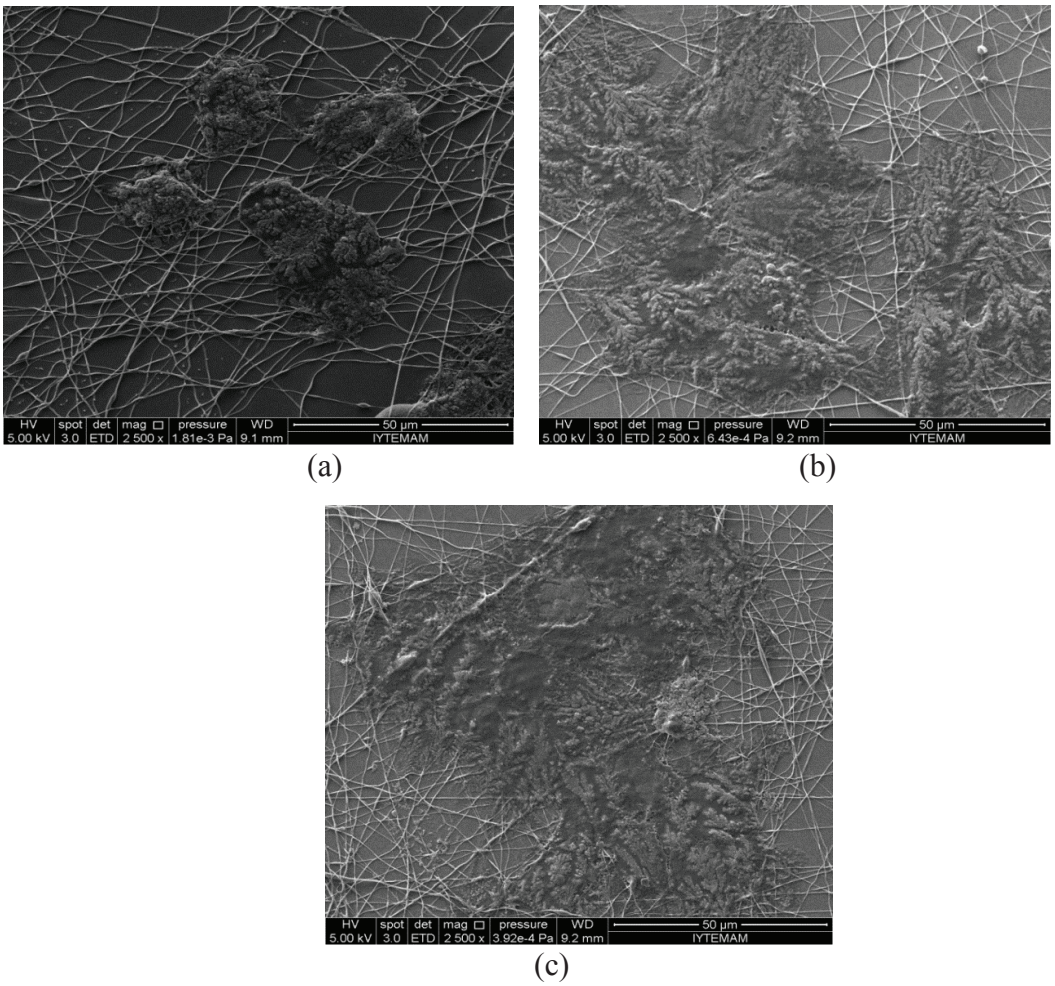

(a) (b)

(c)

Figure 5.24 SEM images of skin cells seeded on electrospun PAN/PPy nanofibers (10 wt% PPy) after a) 1 day, b) 3 days, and c) 7 days of culture, scale bars 50 µm.

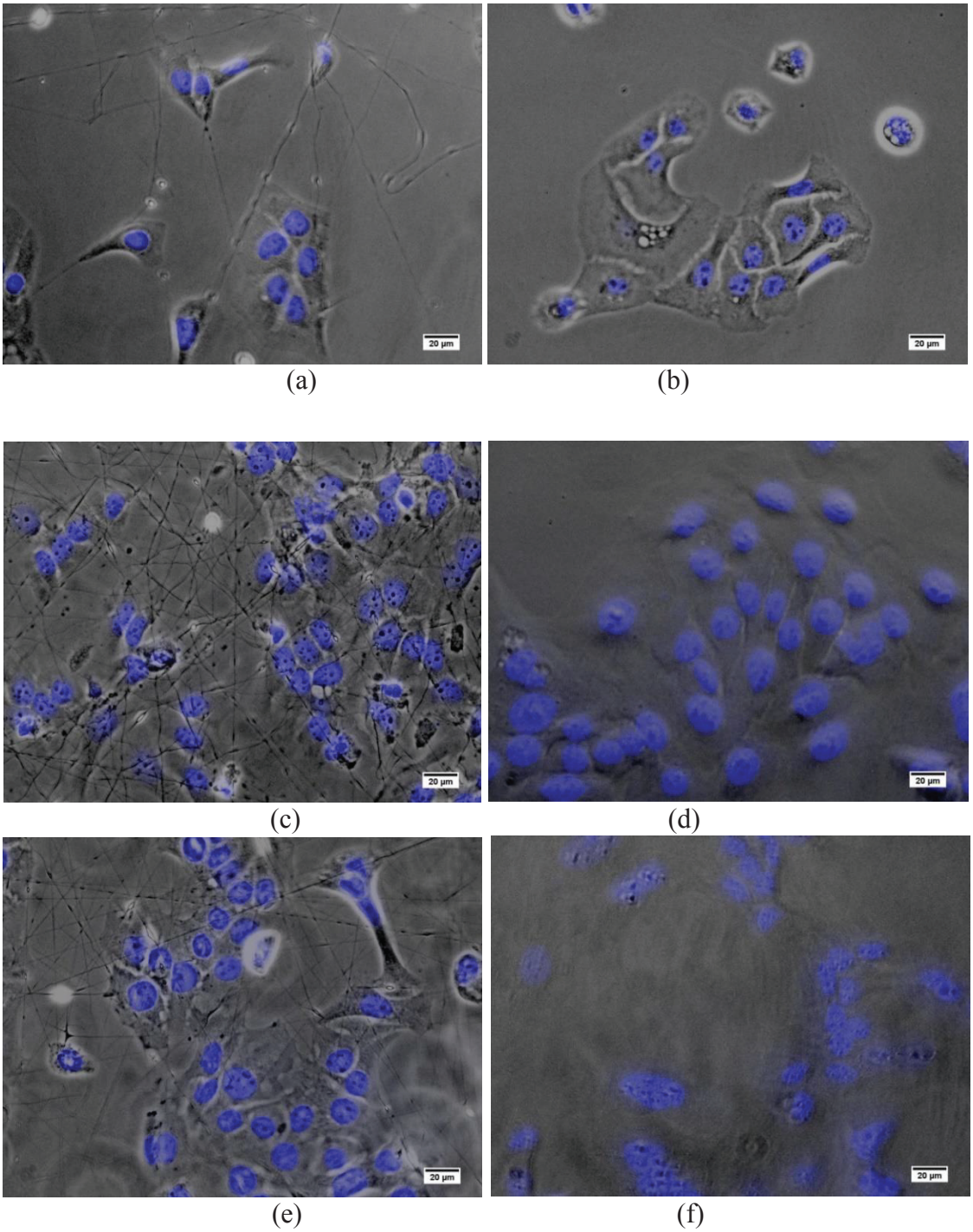

(a) (b)

(c) (d)

(e) (f)

Figure 5.25 Fluorescence microscopy images of skin cells seeded on PP1 nanofibers after a) 1 day, c) 3 days, e) 7 days of culture and their glass control after b) 1 day d) 3 days f) 7 days of culture, scale bars 20 µm.

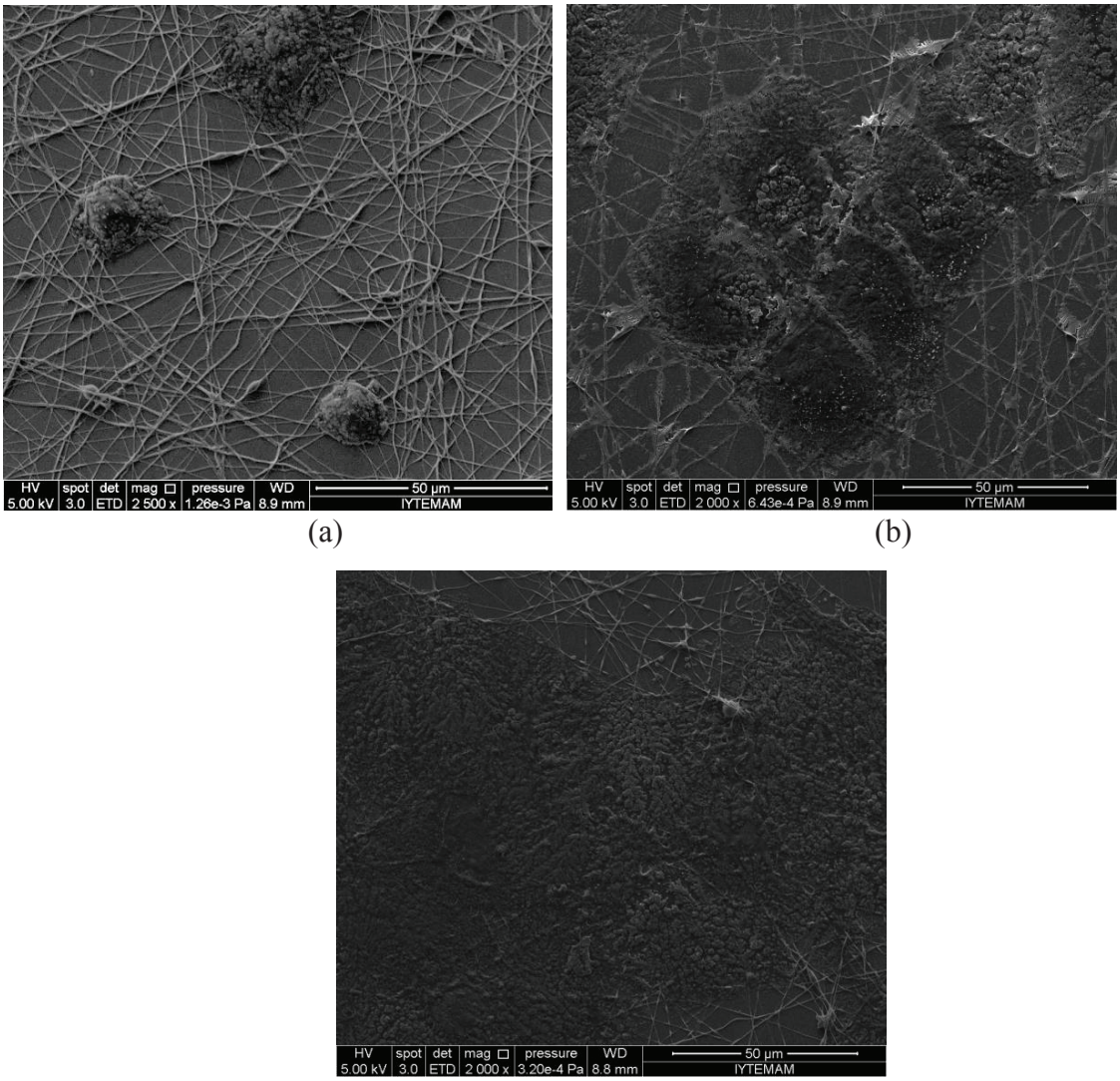

(a) (b)

(c)

Figure 5.26 SEM images of electrospun nanofibers PP3 after keeping in cell culture for a) 1 day, b) 3 days, c) 7 days, scale bars 50 µm.

Fig. 5.27 illustrates how seeded and proliferated cells adhered and spread onto coverslip surface and attached to the fibers containing 25 wt% PPy (PP3) after 1, 3 and 7 days of plating. PAN/PPy nanofibrous scaffold was found to be a three dimensional cellular matrix. It was clearly observed from Fig. 27.c, there was a significant difference in shape of cells after 7 days of culture. Nucleus of cells compared to control keratinocytes, were very small. Their shapes were not circular after 7 days of culture. This indicated that nanofibrous scaffold caused a morphological change.

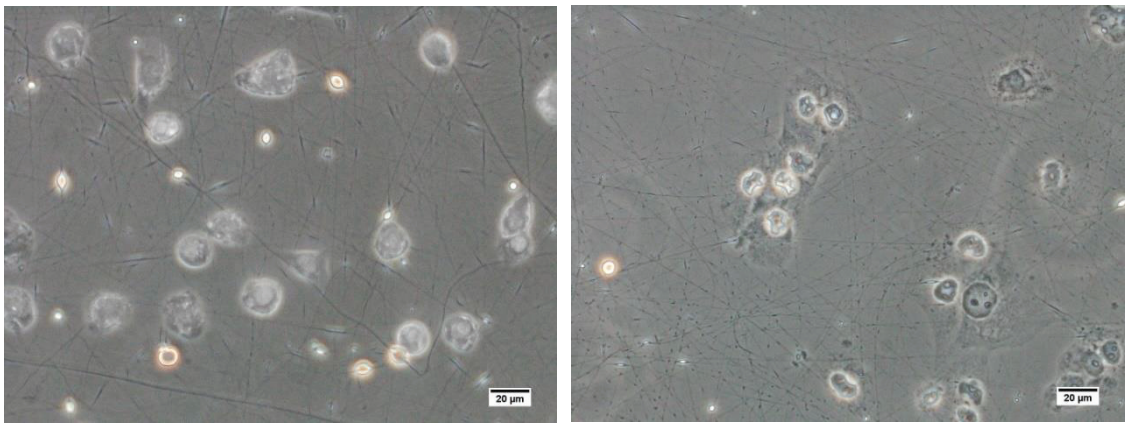

(a) (b)

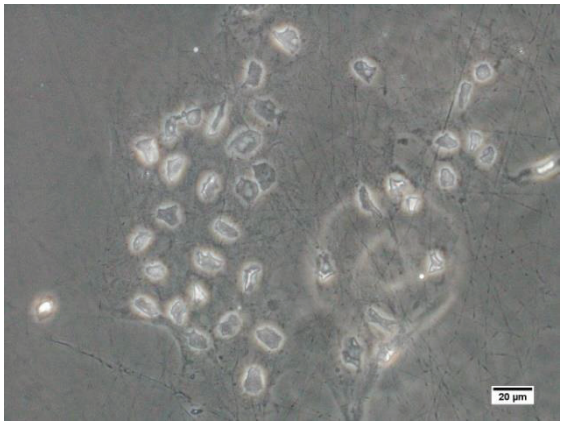

(c)

Figure 5.27 Phase-contrast microscopy images of skin cells seeded on PP3 after a) 1 day, b) 3 days, c) 7 days of culture, scale bars 20 µm.

CNTs can be used in scaffolds for tissue engineering (Kim et al. 2015). In order to test effects of CNTs on keratinocyte proliferation, 1 wt% CNT was added into the PAN/PPy nanofiber containing 10 wt% PPy (PPC3). The cell density was monitored from day 1 to day 7. SEM images of keratinocytes grown on nanofibers containing CNTs demonstrated morphology of nanofibers and cells in detail in Fig. 5.28. Cells attached to the nanofibers and while some parts of cells placed on the surface of nanofibers, some parts placed under the nanofibers. At the same time after 1 day of culture some cells were observed to remain among fibers. Beads and disordered parts of nanofibers were also observed clearly from these SEM pictures.

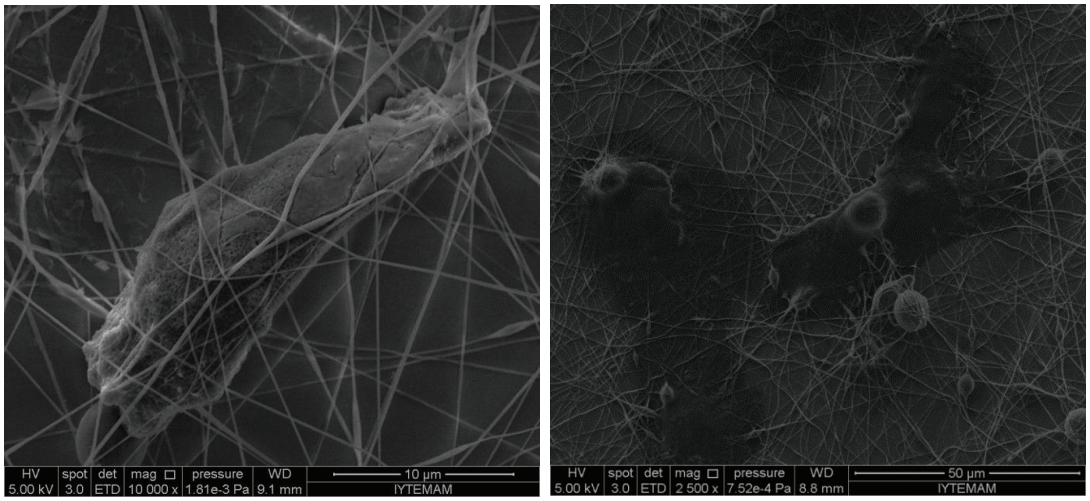

(a) (b)

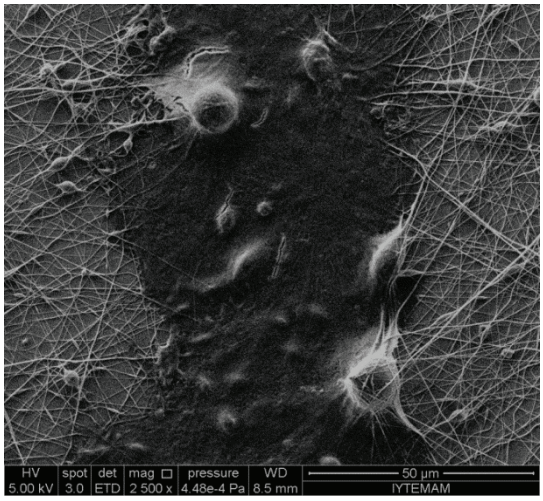

(c)

Figure 5.28 SEM images of electrospun nanofibers containing 10 wt% PPy and 1 wt% CNT after keeping in cell culture for a) 1 day, b) 3 days, c) 7 days. Scale bars 50 µm.

Fluorescence images of keratinocytes seeded on PPC3 nanofibers are given in Fig. 5.29. Cells adapted to the new environment and attached to the nanofibers containing CNTs as observed from fluorescence microscopy image at the 1st day of culture, and continued to proliferate until day 7. PPC3 electrospun nanofibers were also found to be biocompatible. After 7 days of culture cells on glass reached the confluency, there was no more place for cells to grow whereas cells on nanofibers were still continuing to proliferate among nanofibers.

The viability of keratinocytes on these nanofibers were examined by MTT method. Fig. 5.30 displays MTT assay of the keratinocytes on PAN/PPy nanofibers. At the end of first day there was no significant difference in cell proliferation on all of three

scaffolds. However proliferation on PP3 was higher than the other two scaffolds after 3 days of culture. At the end of seven days, it was observed that PP3 scaffold showed a large increase in proliferation compared to other scaffolds. Besides, keratinocytes proliferation on scaffold containing PPC3 also showed good increase compared to PP1. The lowest viability of cells were observed on nanofibrous scaffold PP1. Cells showed a tenfold increase during their 7 days on glass coverslip. A similar increase was observed for keratinocytes that were growing on PPC3. This suggested that even though fibers affected the morphology, accumulation and the structuring of cells, they did not interfere with proliferation or show any cytotoxicity.

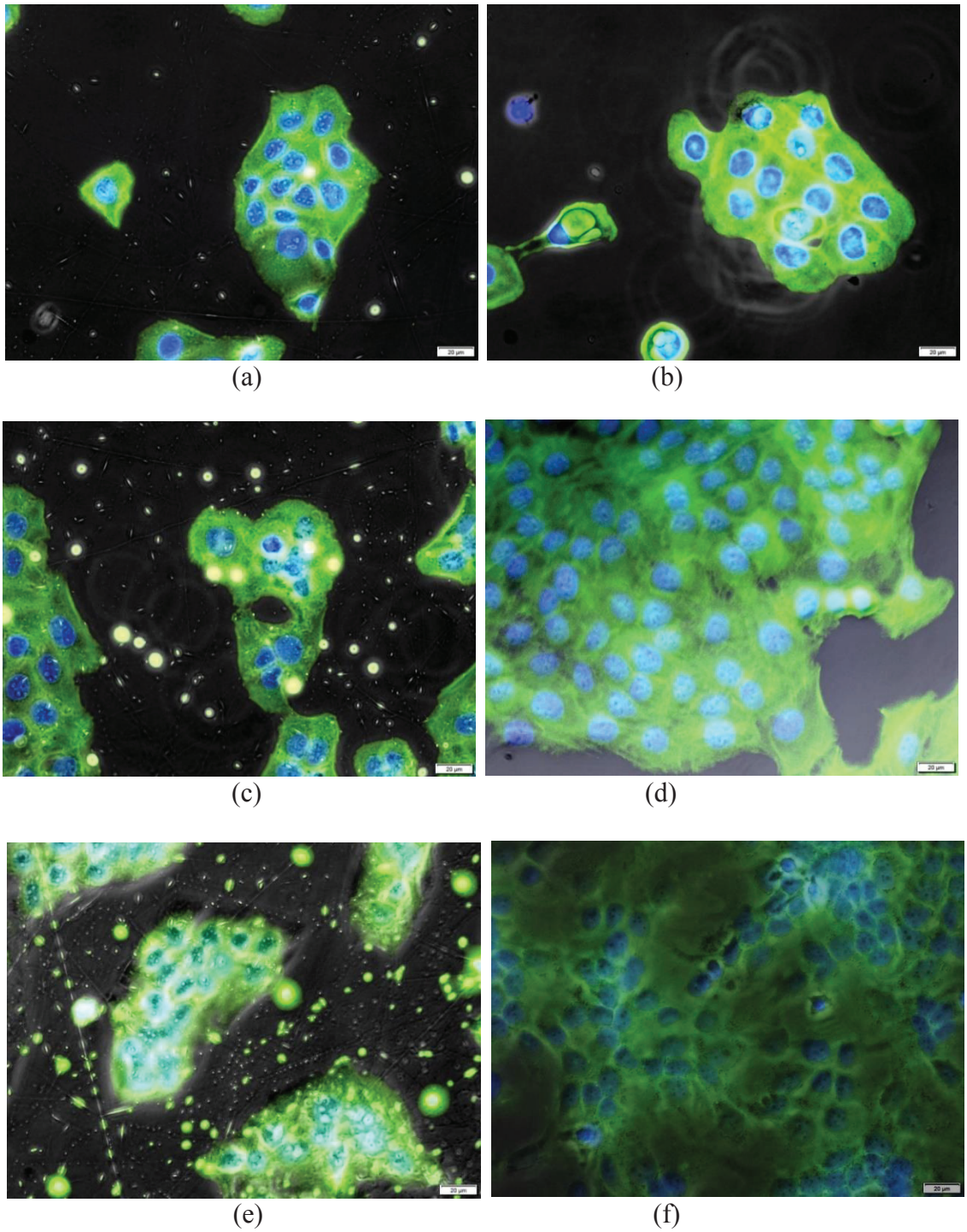

Figure 5.29 Fluorescence microscopy images of keratinocytes seeded on PPC3 electrospun nanofibers after a) 1 day, c) 3 days, e) 7 days of culture and their glass control after b) 1 day, d) 3 days, f) 7 days of culture, scale bars 20 µm.

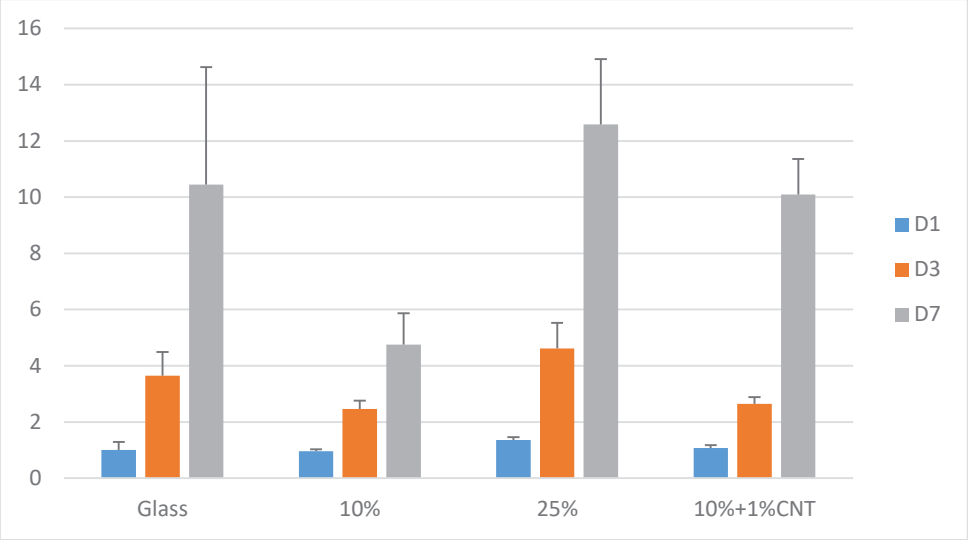

Figure 5.30 MTT assay of keratinocytes seeded on PAN/PPy nanofibers containing 10 wt% PPy (PP1), 25 wt% PPy (PP3) and 10 wt% PPy and 1 wt% CNT (PPC3) nanofibers after 1, 3 and 7 days of culture.

5.4 Random and Aligned CNT Embedded PAN/PPy Nanofibers for Osteogenic Differentiation of Mesenchymal Stem Cells

Scaffold mechanical properties and cell-cell interaction are two significant parameters that regulate osteogenic differentiation of mesenchymal stem cells (Mao, Shin, and Mooney 2016). The effect of nanofiber alignment on osteogenic differentiation of mesenchymal stem cells was studied. Seeded cell number was 5000 cells and culture time was 21 days. Random and aligned PAN/PPy nanofibers were investigated for osteogenic differentiation of mesenchymal stem cells.

Morphology of cells were analysed by SEM. Mesenchymal stem cells images (Fig. 5.31) display that cells were adhered well on random PAN/PPy nanofibers. They had a rough topography. Cells formed intimate contact with multiple fibers. Proliferation also was provided by these randomly oriented nanofibrous scaffold. Especially after 21 days of culture cells covered whole surface of nanofibers. The cells on random nanofibers showed a tendency of creating groups and getting together on the nanofibrous scaffold. When mesenchymal stem cells were induced to differentiate in osteogenic medium, circular cell groups were observed. These cells had a porous surface morphology. After 21 days in osteogenic medium, effective bone mineralization was clearly observed on random PAN/PPy nanofibers. These results suggested that the random PAN/PPy fibers

are suitable for the cellular attachment, proliferation, and osteogenic differentiation of mesenchymal cells.

SEM analysis shown in figure 5.32 depicts both the cellular morphology and the orientation of the aligned PAN/PPy nanofibers. The cells appeared to align and elongate in the major fiber direction. Whereas, a curvature was observed in the direction of cell growth when randomly aligned nanofibers (PP1) were used. The elongated morphology of cells was clearly observed in SEM images. Cells had a more organized structure on aligned nanofibers compared to cells grown on randomly oriented nanofibers. Alignment of nanofibers allowed to obtain an anisotropic cellular structure. With increasing culturing time, cells proliferated and the anisotropic cell growth became more evident. In osteogenic medium, cells proliferated along the direction of nanofibers as well.

SEM images illustrated randomly distributed cells on glass as shown in Fig. 5.33. When glass control surfaces were used as scaffolds without nanofibers, mesenchymal stem cells attached and spread on the two dimensional glass surface in growth medium but they did not differentiate. Especially in Fig. 5.33.e the morphology of a mesenchymal stem cell was clearly observed. However, with increasing culturing time, cells seeded in osteogenic medium differentiated and after 21 days of culture minarilization occured.

In order to understand the behavior of PAN/PPy nanofibers in growth and osteogenic induction, both random (PP1) and aligned (PP2) nanofibers were put into the growth and osteogenic mediums and cells were not seeded. They remained in the mediums for 21 days. SEM images of nanofibers indicated that after 21 days, the morphology of fibers did not change (Fig. 5.34).

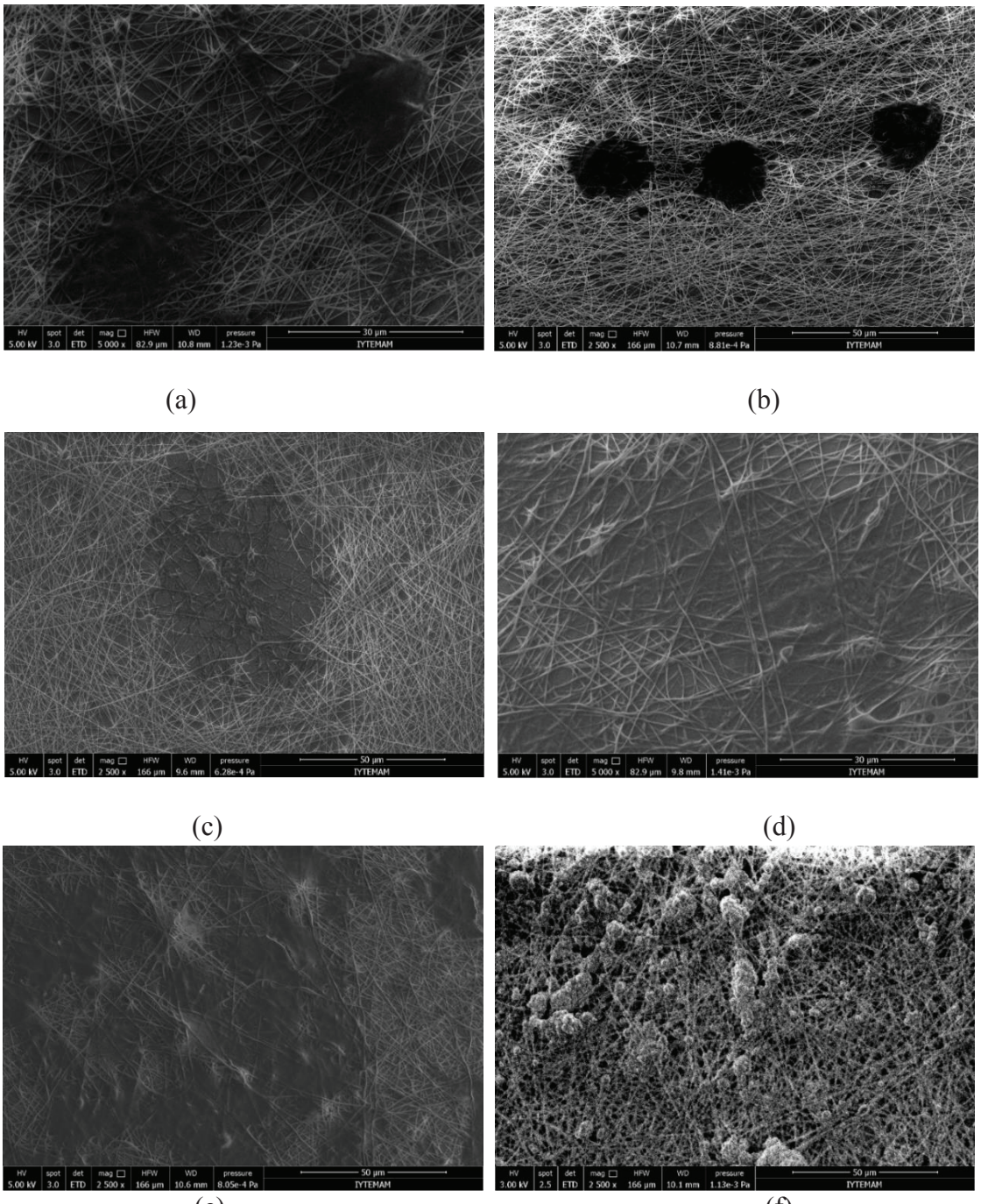

Figure 5.31 SEM images of mesenchymal stem cells after culturing in growth medium (a) 7, (c)14, (e) 21 days, after culturing in osteogenic medium for (b) 7, (d) 14, (f) 21 days on PP1.

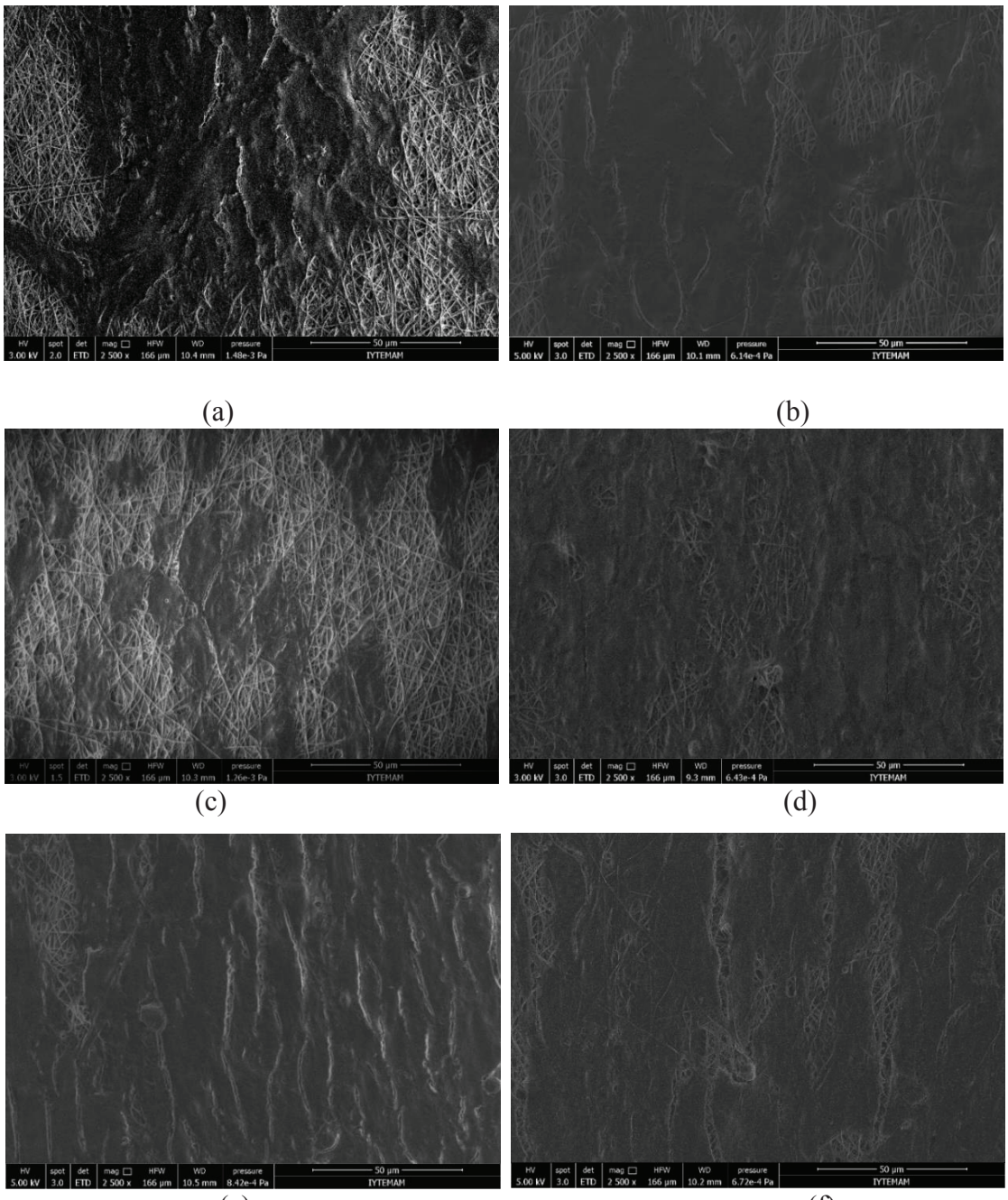

Figure 5.32 SEM images of mesenchymal stem cells after culturing in growth medium (a) 7, (c)14, (e) 21 days, after cultiring in osteogenic medium for (b) 7, (d) 14, (f) 21 days on aligned nanofibers (1000 rpm).

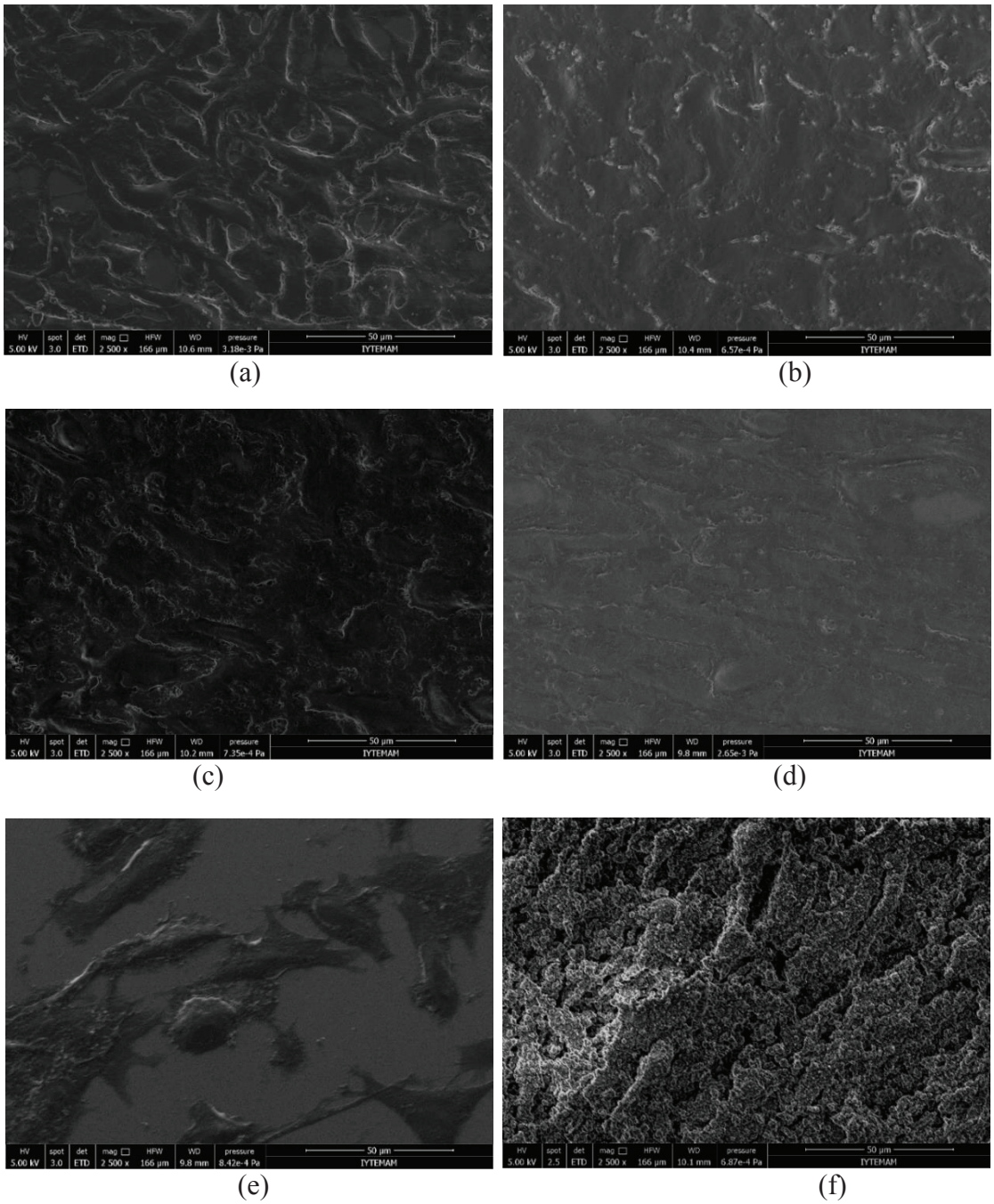

Figure 5.33 SEM images of mesenchymal stem cells after culturing in growth medium (a) 7, (c)14, (e) 21 days, after cultiring in osteogenic medium for (b) 7, (d) 14, (f) 21 days on glass control coverslips.

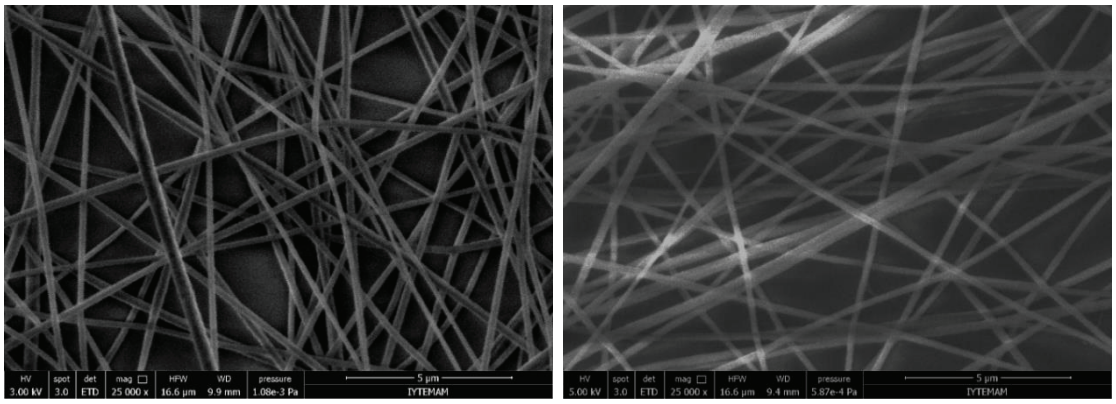

(a) (b)

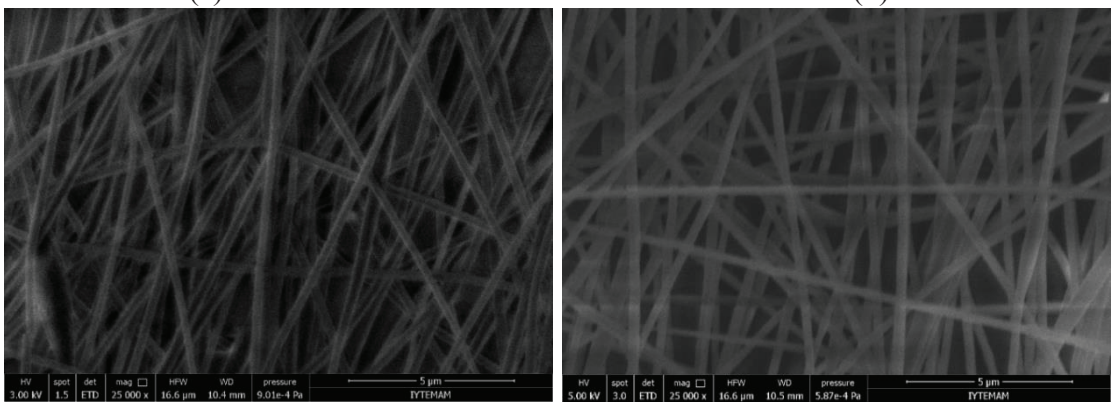

(c) (d)

Figure 5.34 SEM images of PP1 kept in (a) growth (b) osteogenic medium, and PP2 kept in (c) growth, (d) osteogenic medium after 21 days.

MTT-assay showed that PAN/PPy nanofibers were non-toxic for osteoblasts and could be utilized as scaffold for osteogenic differentiation of mesenchymal cells and proliferation rate of osteoblasts was a bit higher for nanofibrous scaffold compared to glass coverslips. Cell culture time was 21 days. MTT assay was used to evaluate the cell viability and proliferation rate of random and aligned PAN/PPy nanofibers. Fig. 5.35 displays MTT assay of the mesenchymal stem cells seeded on glass control surface and PP1 nanofibers. Under growth conditions (gc), cell proliferation increased during 21 days for both PP1 and glass control surface. However, under osteogenic conditions (oc) cell proliferation increased till 14 days and then decreased a little bit for both PP1 and glass control surface.

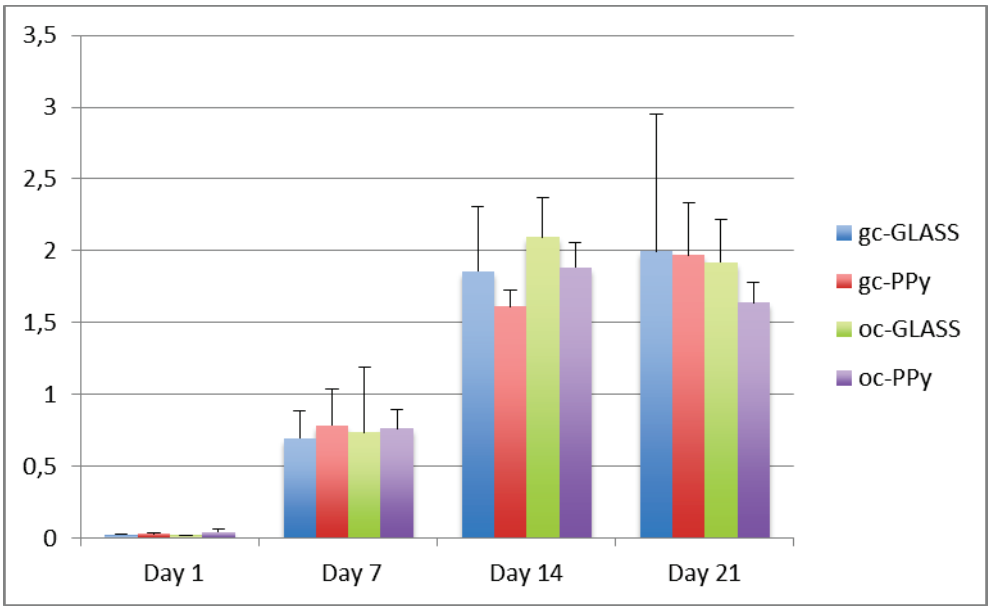

Figure 5.35 MTT assay of mesenchymal stem cells (gc) and osteoblasts (oc) seeded on glass coverslips and random PAN/PPy nanofibers after 1,7, 14 and 21 days of culture.

Aligned PAN/PPy (PP2) nanofibers also supported osteogenic differentiation of mesenchymal stem cells and cell proliferation as given from Fig. 5.36. Under oc for both PP2 and glass surface, proliferation rate increased regularly with time. Aligned nanofibers also showed a regular increase in proliferation rate during 21 days. However, for glass surface under gc it was observed a sharp increase at 14th day and then at 21st day proliferation was almost the same as 14th day. At the end of 21 days, for both gc and oc PP2 nanofibers showed higher proliferation than glass control surface. Besides, compared to random nanofibers, aligned nanofibers promoted higher viability under both gc and oc.

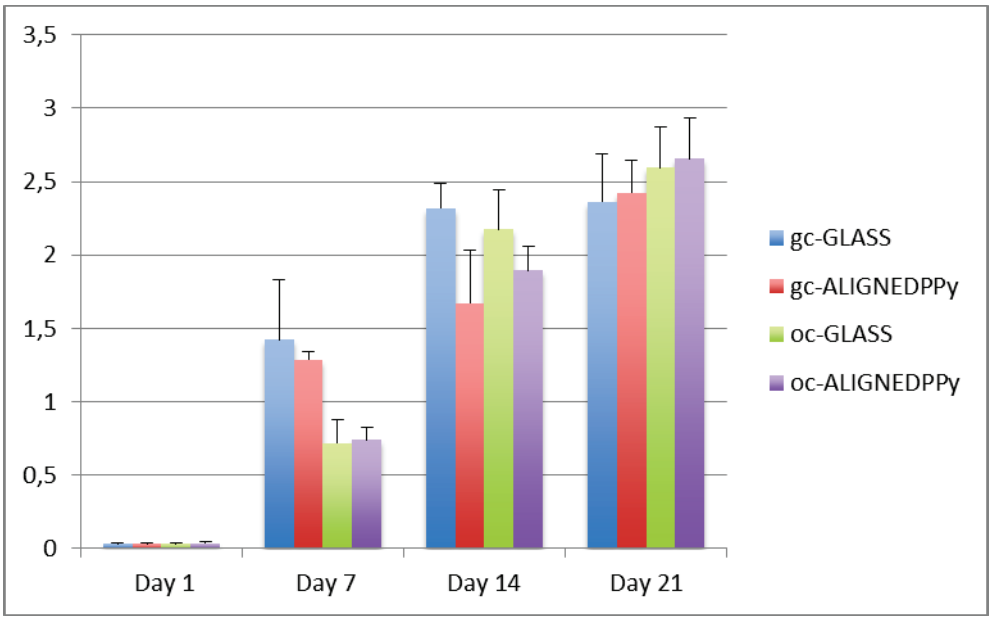

Figure 5.36 MTT assay of mesenchymal stem cells (gc) and osteoblasts (oc) seeded on glass coverslips and aligned PAN/PPy nanofibers after 1,7, 14 and 21 days of culture.

The mineral deposition on PAN/PPy electrospun nanofibrous scaffolds was confirmed using Alizarin Red staining after the 21 days of incubation period. Alizarin red results showed the bioactivity of the PAN/PPy scaffolds, see Fig. 5.37. Mineralization assay with alizarin red dye indicated that mesenchymal stem cells osteogenesis took place with osteogenic induction. Red parts in the figure 5.35.b, 5.35.d, 5.35.f showed calcifications in mesenchymal stem cells under osteogenic differentiation. However, nodules were not observed in cells grown on control samples remained under growth conditions. Alizarin red dye on aligned nanofibers (PP2) proved that osteogenesis on these nanofibers occurred on the alignment direction while a random red dying observed on PP1 (Fig. 37.b) and glass (Fig. 37.f).

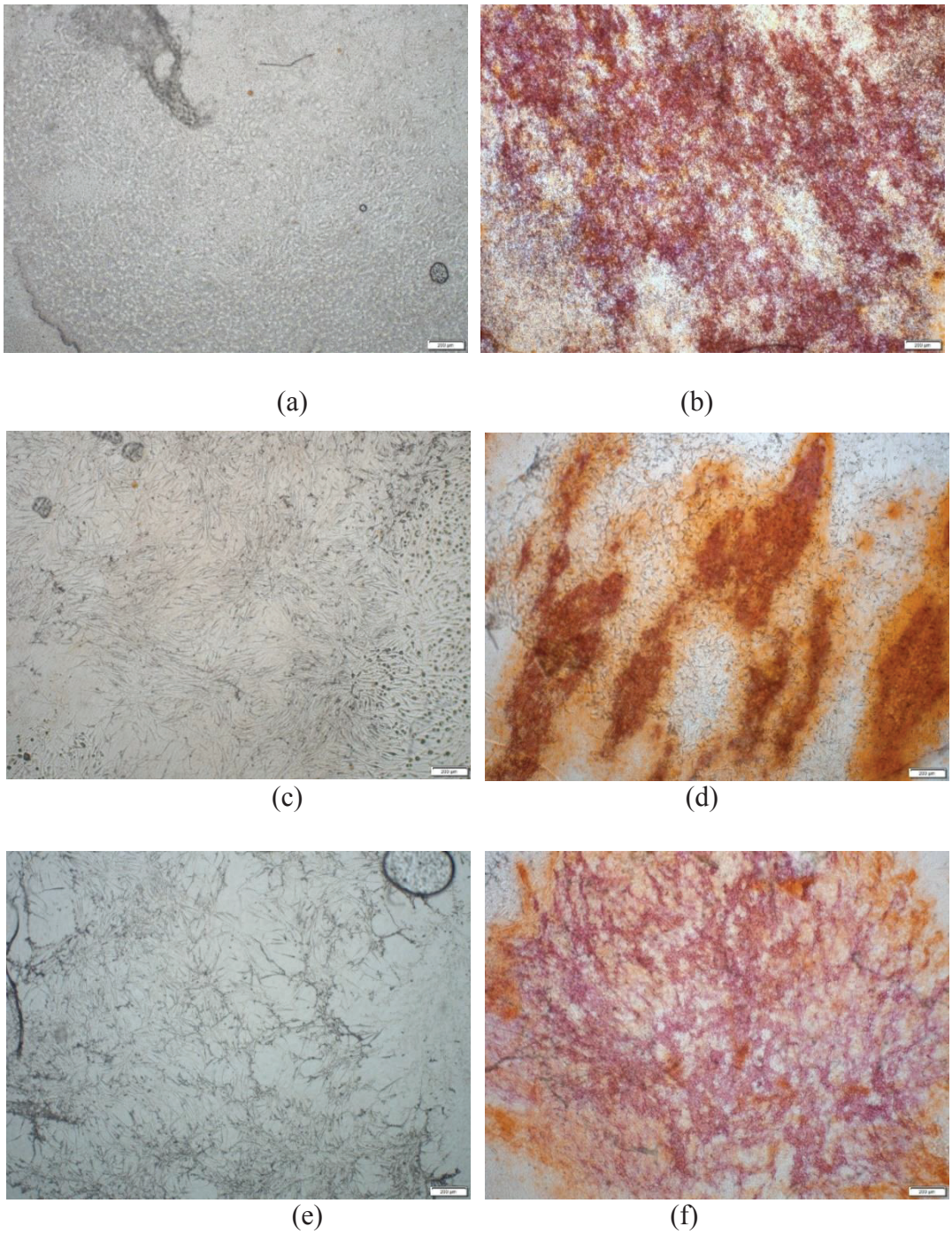

Figure 5.37 Alizarin red staining on (a) PP1, (c) PP2, (e) glass control at growth conditions, (b) PP1, (d) PP2, (f) glass control at osteogenic conditions.

CHAPTER 6

CONCLUSIONS

Electrospun PAN/PPy bicomponent beadless nanofibers with 10 and 25 wt% PPy amounts were obtained at the solution temperature of 60 ^{o}C. PAN improved the surface regularity of PAN/PPy nanofibers and therefore increasing PPy content caused irregularities on fiber surfaces. Solution viscosities decreased and conductivity increased with increasing PPy amounts and it provided thinner diameter of nanofibers. The average diameter of electrospun nanofibers were 197 nm and 112 nm for 10 wt% and 25 wt% PPy amount, respectively. PPy content influenced significantly tensile strain of nanofibers due to brittle property of PPy. Strain value of nanofibers containing 10 wt% PPy content was 23.33% while nanofibers containing 25 wt% PPy was 1.41%. However, tensile strength of nanofibers were not affected by PPy content. PAN/PPy nanofibers contact angle tests showed that nanofibers were hydrophilic and increasing PPy content decreased the contact angle of sample.

PAN/PPy aligned nanofibers were prepared using a rotating collector at 1000 rpm rotation speed. Alignment of nanofibers enhanced significantly tensile strength of nanofibers, tensile strength of nanofibers increased from 9.34 MPa to 36.77 MPa after alignment. However, tensile strain of nanofibers decreased from 23.33% to 5.15% after alignment process.

When CNTs were added into PAN/PPy solution containing 25 wt% PPy, solution could not be electrospun and fibers formation did not occur due to the high electrical conductivity of solution. Optimum PPy content was determined as 10 wt% for CNT incorporated PAN/PPy nanofiber synthesis. CNT addition caused bead formation on the surface of nanofibers. When CNT content was increased to 4 wt% lots of beads and disordered sites formed on nanofibers while a smooth fiber surface was observed for 1 wt% CNT content. High CNT content prevented a continuous spinning because of agglomeration of CNTs.

In order to enhance dispersion of CNTs and to obtain smooth and ordered nanofibers, functional CNTs had been studied. With the fuctionalization of CNTs, density of nanofibers increased and observed bead numbers decreased. For high CNT content (4

wt%) the improvement in nanofiber quality after functional CNT usage was observed better. After functionalization the bead problem could not be solved completely, however significant improvement on nanofibers surface roughness occurred. TEM results indicated that functional CNTs were aligned along the direction of nanofibers during electrospinning process under high electrical field and with the increase of CNT content, CNTs agglomerated and these agglomerated sites caused the formation of beads on the nanofibers. CNTs utilized in this study were MWCNTs containing generally 3 or 4 walls. CV and EIS results showed that addition of CNTs and increasing PPy content provided higher electrical condutivity and PAN/PPy and CNT embedded PAN/PPy nanofibers were electroactive and can be used as an electrochemical actuator in acidic solutions.

PAN/PPy and PAN/PPy/CNT nanofibers biocompatibility were investigated by utilizing them as keratinocyte scaffold. It was found that the diameter of nanofibers did not influence the cellular morphology. However, growing among nanofibers affected the morphology of cells. We indicated that CNTs did not affect the biocompatibility of PAN/PPy nanofibers and adhesion and proliferation of keratinocytes occurred on PAN/PPy/CNT scaffold. Biocompatible PAN/PPy and PAN/PPy/CNT nanofibrous scaffolds were synthesized for keratinocytes growth and it was found that these synthetic scaffolds could provide an appropriate growth surface for these cells.

We investigated random and aligned PAN/PPy nanofibers as scaffold for osteogenic differentiation of mesenchymal stem cells. These electrospun nanofibers were found to be biocompatible for osteoblast growth and were supported differentiation of mesenchymal stem cells. Cell attachment and proliferation were observed for both mesenchymal stem cells and osteoblasts. The cells on random nanofibers showed a tendency of creating groups and getting together on the randomly oriented nanofibrous scaffold whereas the cells appeared to align and elongate in the major fiber direction when they were seeded on aligned nanofibers. Alignment of nanofibers allowed to obtain an anisotropic cellular structure. MTT-assay indicated that PAN/PPy nanofibers were non-toxic and alizarin red assay showed that mesenchymal stem cells osteogenesis taken place with osteogenic induction on these nanofibers.

REFERENCES

Abdal-hay, Abdalla, Abdel Salam Hamdy, and Khalil Abdelrazek Khalil. 2015. "Fabrication of durable high performance hybrid nanofiber scaffolds for bone tissue regeneration using a novel, simple in situ deposition approach of polyvinyl alcohol on electrospun nylon 6 nanofibers." *Materials Letters* 147:25-28.

Arash, B, Q Wang, and VK Varadan. 2014. "Mechanical properties of carbon nanotube/polymer composites." *Scientific reports* 4.

Aviss, KJ, JE Gough, and S Downes. 2010. "Aligned electrospun polymer fibres for skeletal muscle regeneration." *Eur Cell Mater* 19:193-204.

Awuzie, CI. 2017. "Conducting Polymers." *Materials Today: Proceedings* 4 (4):5721-5726.

Aytac, Zeynep, Huseyin Sener Sen, Engin Durgun, and Tamer Uyar. 2015. "Sulfisoxazole/cyclodextrin inclusion complex incorporated in electrospun hydroxypropyl cellulose nanofibers as drug delivery system." *Colloids and Surfaces B: Biointerfaces* 128:331-338.

Baddour, Carole E, and Cedric Briens. 2005. "Carbon nanotube synthesis: a review." *International journal of chemical reactor engineering* 3 (1).

Bai, Hua, Lu Zhao, Canhui Lu, Chun Li, and Gaoquan Shi. 2009. "Composite nanofibers of conducting polymers and hydrophobic insulating polymers: preparation and sensing applications." *Polymer* 50 (14):3292-3301.

Baughman, RH. 1996. "Conducting polymer artificial muscles." *Synthetic metals* 78 (3):339-353.

Baumgarten, Peter K. 1971. "Electrostatic spinning of acrylic microfibers." *Journal of colloid and interface science* 36 (1):71-79.

Bay, Lasse, Keld West, Peter Sommer-Larsen, Steen Skaarup, and Mohammed Benslimane. 2003. "A conducting polymer artificial muscle with 12% linear strain." *Advanced Materials* 15 (4):310-313.

Bhardwaj, Nandana, and Subhas C Kundu. 2010. "Electrospinning: a fascinating fiber fabrication technique." *Biotechnology advances* 28 (3):325-347.

Bhattarai, Shanta Raj, Narayan Bhattarai, Ho Keun Yi, Pyong Han Hwang, Dong Il Cha, and Hak Yong Kim. 2004. "Novel biodegradable electrospun membrane: scaffold for tissue engineering." *Biomaterials* 25 (13):2595-2602.

Bredas, Jean Luc, and G Bryan Street. 1985. "Polarons, bipolarons, and solitons in conducting polymers." *Accounts of Chemical Research* 18 (10):309-315.

Buchko, Christopher J, Loui C Chen, Yu Shen, and David C Martin. 1999. "Processing and microstructural characterization of porous biocompatible protein polymer thin films." *Polymer* 40 (26):7397-7407.

Burroughes, JH, DDC Bradley, AR Brown, RN Marks, K Mackay, RH Friend, PL Burns, and AB Holmes. 1990. "Light-emitting diodes based on conjugated polymers." *nature* 347 (6293):539-541.

Cao, Yong, Paul Smith, and Alan J Heeger. 1993. "Counter-ion induced processibility of conducting polyaniline." *Synthetic Metals* 57 (1):3514-3519.

Casper, Cheryl L, Jean S Stephens, Nancy G Tassi, D Bruce Chase, and John F Rabolt. 2004. "Controlling surface morphology of electrospun polystyrene fibers: effect of humidity and molecular weight in the electrospinning process." *Macromolecules* 37 (2):573-578.

Chen, H, RK Truckenmuller, CA van Blitterswijk, and L Moroni. 2013. "Fabrication of nanofibrous scaffolds for tissue engineering applications." *Nanomaterials in tissue engineering: Fabrication and applications. Series in Biomaterials (56). USA: Woodhead Publishing*:158-182.

Chen, I-Han, Cheng-Chien Wang, and Chuh-Yung Chen. 2010. "Fabrication and structural characterization of polyacrylonitrile and carbon nanofibers containing plasma-modified carbon nanotubes by electrospinning." *The Journal of Physical Chemistry C* 114 (32):13532-13539.

Chiang, CK, CR Fincher Jr, YW Park, AJ Heeger, H Shirakawa, EJ Louis, SC Gau, and Alan G MacDiarmid. 1977. "Electrical conductivity in doped polyacetylene." *Physical Review Letters* 39 (17):1098-1101.

Choe, Kiyoung, and Kwang J Kim. 2006. "Polyacrylonitrile linear actuators: Chemomechanical and electro-chemomechanical properties." *Sensors and Actuators A: Physical* 126 (1):165-172.

Chronakis, Ioannis S, Sven Grapenson, and Alexandra Jakob. 2006. "Conductive polypyrrole nanofibers via electrospinning: electrical and morphological properties." *Polymer* 47 (5):1597-1603.

Courty, S, J Mine, AR Tajbakhsh, and EM Terentjev. 2003. "Nematic elastomers with aligned carbon nanotubes: New electromechanical actuators." *EPL (Europhysics Letters)* 64 (5):654.

Deitzel, JM, W Kosik, SH McKnight, NC Beck Tan, JM DeSimone, and S Crette. 2002. "Electrospinning of polymer nanofibers with specific surface chemistry." *Polymer* 43 (3):1025-1029.

Deitzel, Joseph M, James Kleinmeyer, DEA Harris, and NC Beck Tan. 2001. "The effect of processing variables on the morphology of electrospun nanofibers and textiles." *Polymer* 42 (1):261-272.

Deshmukh, SP, and K Li. 1998. "Effect of ethanol composition in water coagulation bath on morphology of PVDF hollow fibre membranes." *Journal of Membrane Science* 150 (1):75-85.

Doshi, Jayesh, and Darrell H Reneker. 1993. "Electrospinning process and applications of electrospun fibers." Industry Applications Society Annual Meeting, 1993., Conference Record of the 1993 IEEE.

Dosunmu, OO, George G Chase, W Kataphinan, and DH Reneker. 2006. "Electrospinning of polymer nanofibres from multiple jets on a porous tubular surface." *Nanotechnology* 17 (4):1123.

Dufour, B, P Rannou, D Djurado, M Bee, and A Pron. 2003. "Doping-induced stretchability of metallic poly (aniline)." *Synthetic metals* 135:323-324.

Dufour, B, P Rannou, D Djurado, M Zagorska, I Kulszewicz-Bajer, and A Pron. 2003. "The role of chain and dopant engineering in the preparation of processible conducting polymers with desired properties." *Synthetic metals* 135:63-68.

Dyke, Christopher A, and James M Tour. 2004. "Covalent functionalization of single-walled carbon nanotubes for materials applications." *The Journal of Physical Chemistry A* 108 (51):11151-11159.

Eichhorn, Stephen J, and William W Sampson. 2005. "Statistical geometry of pores and statistics of porous nanofibrous assemblies." *Journal of the royal society Interface* 2 (4):309-318.

Fan, Hong Song, Xian Tao Wen, Yan Fei Tan, R Wang, HD Cao, and Xing Dong Zhang. 2005. "Compare of electrospinning PLA and PLA/β-TCP scaffold in vitro." Materials Science Forum.

Fang, Jian, HaiTao Niu, Tong Lin, and XunGai Wang. 2008. "Applications of electrospun nanofibers." *Chinese science bulletin* 53 (15):2265-2286.

Fidelus, JD, E Wiesel, FH Gojny, K Schulte, and HD Wagner. 2005. "Thermo-mechanical properties of randomly oriented carbon/epoxy nanocomposites." *Composites Part A: Applied Science and Manufacturing* 36 (11):1555-1561.

Flemming, RG, CJ Murphy, GA Abrams, SL Goodman, and PF Nealey. 1999. "Effects of synthetic micro-and nano-structured surfaces on cell behavior." *Biomaterials* 20 (6):573-588.

Fofonoff, Timothy Andrew. 2008. "Fabrication and Use of Conducting Polymer Linear Actuators." PhD, Mechanical engineering, MIT.

Foulds, Nicola C, and Christopher R Lowe. 1986. "Enzyme entrapment in electrically conducting polymers. Immobilisation of glucose oxidase in polypyrrole and its application in amperometric glucose sensors." *Journal of the Chemical Society, Faraday Transactions 1: Physical Chemistry in Condensed Phases* 82 (4):1259-1264.

Fujihara, K, M Kotaki, and S Ramakrishna. 2005. "Guided bone regeneration membrane made of polycaprolactone/calcium carbonate composite nano-fibers." *Biomaterials* 26 (19):4139-4147.

Gibas, Iwona, and Helena Janik. 2010. "Synthetic polymer hydrogels for biomedical applications."

Gilmore, Kerry J, Magdalena Kita, Yao Han, Amy Gelmi, Michael J Higgins, Simon E Moulton, Graeme M Clark, Robert Kapsa, and Gordon G Wallace. 2009. "Skeletal muscle cell proliferation and differentiation on polypyrrole substrates doped with extracellular matrix components." *Biomaterials* 30 (29):5292-5304.

Giray, Digdem, Timucin Balkan, Birgit Dietzel, and A Sezai Sarac. 2013. "Electrochemical impedance study on nanofibers of poly (m-anthranilic acid)/polyacrylonitrile blends." *European Polymer Journal* 49 (9):2645-2653.

Goldberg, Michael, Robert Langer, and Xinqiao Jia. 2007. "Nanostructured materials for applications in drug delivery and tissue engineering." *Journal of Biomaterials Science, Polymer Edition* 18 (3):241-268.

Guimard, Nathalie K, Natalia Gomez, and Christine E Schmidt. 2007. "Conducting polymers in biomedical engineering." *Progress in polymer science* 32 (8):876-921.

Guo, Jiasong, Huanxing Su, Yuanshan Zeng, Yu-Xiang Liang, Wai Man Wong, Rutledge G Ellis-Behnke, Kwok-Fai So, and Wutian Wu. 2007. "Reknitting the injured spinal cord by self-assembling peptide nanofiber scaffold." *Nanomedicine: Nanotechnology, Biology and Medicine* 3 (4):311-321.

Guo, Wenhan, Chao Liu, Xuemei Sun, Zhibin Yang, Hamid G Kia, and Huisheng Peng. 2012. "Aligned carbon nanotube/polymer composite fibers with improved mechanical strength and electrical conductivity." *Journal of Materials Chemistry* 22 (3):903-908.

Gurunathan, Kaushik, A Vadivel Murugan, Rajendiran Marimuthu, UP Mulik, and DP Amalnerkar. 1999. "Electrochemically synthesised conducting polymeric materials for applications towards technology in electronics, optoelectronics and energy storage devices." *Materials Chemistry and Physics* 61 (3):173-191.

Haghi, AK, and M Akbari. 2007. "Trends in electrospinning of natural nanofibers." *physica status solidi (a)* 204 (6):1830-1834.

Han, Gaoyi, and Gaoquan Shi. 2006. "Electrochemical actuator based on single-layer polypyrrole film." *Sensors and Actuators B: Chemical* 113 (1):259-264.

Hara, Susumu, Tetsuji Zama, Wataru Takashima, and Keiichi Kaneto. 2004a. "Gel-like polypyrrole based artificial muscles with extremely large strain." *Polymer journal* 36 (11):933-936.

Hara, Susumu, Tetsuji Zama, Wataru Takashima, and Keiichi Kaneto. 2004b. "TFSI-doped polypyrrole actuator with 26% strain." *Journal of Materials Chemistry* 14 (10):1516-1517.

Hata, Kenji, Don N Futaba, Kohei Mizuno, Tatsunori Namai, Motoo Yumura, and Sumio Iijima. 2004. "Water-assisted highly efficient synthesis of impurity-free single-walled carbon nanotubes." *Science* 306 (5700):1362-1364.

Hayati, I, AI Bailey, and Th F Tadros. 1987. "Investigations into the mechanisms of electrohydrodynamic spraying of liquids: I. Effect of electric field and the environment on pendant drops and factors affecting the formation of stable jets and atomization." *Journal of Colloid and Interface Science* 117 (1):205-221.

Herod, Timothy E, and Joseph B Schlenoff. 1993. "Doping-induced strain in polyaniline: stretchoelectrochemistry." *Chemistry of materials* 5 (7):951-955.

Holzwarth, Jeremy M, and Peter X Ma. 2011. "3D nanofibrous scaffolds for tissue engineering." *Journal of Materials Chemistry* 21 (28):10243-10251.

Huang, Zheng-Ming, Y-Z Zhang, M Kotaki, and S Ramakrishna. 2003. "A review on polymer nanofibers by electrospinning and their applications in nanocomposites." *Composites science and technology* 63 (15):2223-2253.

Ismail, Yahya A, Jose G Martínez, Ahmad S Al Harrasi, Seon J Kim, and Toribio F Otero. 2011. "Sensing characteristics of a conducting polymer/hydrogel hybrid microfiber artificial muscle." *Sensors and Actuators B: Chemical* 160 (1):1180-1190.

Ismail, Yahya A, Su Ryon Shin, Kwang Min Shin, Seong Gil Yoon, Kiwon Shon, Sun I Kim, and Seon Jeong Kim. 2008. "Electrochemical actuation in chitosan/polyaniline microfibers for artificial muscles fabricated using an in situ polymerization." *Sensors and Actuators B: Chemical* 129 (2):834-840.

Jaiswal, AK, H Chhabra, VP Soni, and JR Bellare. 2013. "Enhanced mechanical strength and biocompatibility of electrospun polycaprolactone-gelatin scaffold with surface deposited nano-hydroxyapatite." *Materials Science and Engineering: C* 33 (4):2376-2385.

Jansen, JC, M Macchione, and E Drioli. 2005. "High flux asymmetric gas separation membranes of modified poly (ether ether ketone) prepared by the dry phase inversion technique." *Journal of membrane science* 255 (1):167-180.

Ji, Liwen, Andrew J Medford, and Xiangwu Zhang. 2009a. "Electrospun polyacrylonitrile/zinc chloride composite nanofibers and their response to hydrogen sulfide." *Polymer* 50 (2):605-612.

Ji, Liwen, Andrew J Medford, and Xiangwu Zhang. 2009b. "Fabrication of carbon fibers with nanoporous morphologies from electrospun polyacrylonitrile/poly (L-lactide) blends." *Journal of Polymer Science Part B: Polymer Physics* 47 (5):493-503.

Ji, Liwen, Yingfang Yao, Ozan Toprakci, Zhan Lin, Yinzheng Liang, Quan Shi, Andrew J Medford, Christopher R Millns, and Xiangwu Zhang. 2010. "Fabrication of carbon nanofiber-driven electrodes from electrospun polyacrylonitrile/polypyrrole bicomponents for high-performance rechargeable lithium-ion batteries." *Journal of Power Sources* 195 (7):2050-2056.

Jia, Zhijie, Zhengyuan Wang, Cailu Xu, Ji Liang, Bingqing Wei, Dehai Wu, and Shaowen Zhu. 1999. "Study on poly (methyl methacrylate)/carbon nanotube composites." *Materials Science and Engineering: A* 271 (1):395-400.

Jorio, A, R Saito, JH Hafner, CM Lieber, dM Hunter, T McClure, G Dresselhaus, and MS Dresselhaus. 2001. "Structural (n, m) determination of isolated single-wall carbon nanotubes by resonant Raman scattering." *Physical Review Letters* 86 (6):1118.

Ju, Young-Wan, Gyoung-Rin Choi, Hong-Ryun Jung, and Wan-Jin Lee. 2008. "Electrochemical properties of electrospun PAN/MWCNT carbon nanofibers electrodes coated with polypyrrole." *Electrochimica Acta* 53 (19):5796-5803.

Ju, Young Min, Jin San Choi, Anthony Atala, James J Yoo, and Sang Jin Lee. 2010. "Bilayered scaffold for engineering cellularized blood vessels." *Biomaterials* 31 (15):4313-4321.

Kai, Dan, Molamma P Prabhakaran, Guorui Jin, and Seeram Ramakrishna. 2011. "Polypyrrole-contained electrospun conductive nanofibrous membranes for cardiac tissue engineering." *Journal of Biomedical Materials Research Part A* 99 (3):376-385.

Kennedy, Kelsey M, Archana Bhaw-Luximon, and Dhanjay Jhurry. 2016. "Cell-matrix mechanical interaction in electrospun polymeric scaffolds for tissue engineering: Implications for scaffold design and performance." *Acta biomaterialia*.

Ketpang, Kriangsak, and Jun Seo Park. 2010. "Electrospinning PVDF/PPy/MWCNTs conducting composites." *Synthetic Metals* 160 (15):1603-1608.

Ki, Chang Seok, Doo Hyun Baek, Kyung Don Gang, Ki Hoon Lee, In Chul Um, and Young Hwan Park. 2005. "Characterization of gelatin nanofiber prepared from gelatin–formic acid solution." *Polymer* 46 (14):5094-5102.

Kim, Chan, Young Il Jeong, Bui Thi Nhu Ngoc, Kap Seung Yang, Masahito Kojima, Yoong Ahm Kim, Morinobu Endo, and Jae-Wook Lee. 2007. "Synthesis and characterization of porous carbon nanofibers with hollow cores through the thermal treatment of electrospun copolymeric nanofiber webs." *Small* 3 (1):91-95.

Kim, Taeyoung, Indumathi Sridharan, Bofan Zhu, Joseph Orgel, and Rong Wang. 2015. "Effect of CNT on collagen fiber structure, stiffness assembly kinetics and stem cell differentiation." *Materials Science and Engineering: C* 49:281-289.

Ladd, Mitchell R, Tanner K Hill, James J Yoo, and Sang Jin Lee. 2011. "Electrospun nanofibers in tissue engineering." In *Nanofibers-Production, Properties and Functional Applications*. InTech.

Le, Thanh-Hai, Yukyung Kim, and Hyeonseok Yoon. 2017. "Electrical and electrochemical properties of conducting polymers." *Polymers* 9 (4):150.

Lee, Jae Y, Chris A Bashur, Aaron S Goldstein, and Christine E Schmidt. 2009. "Polypyrrole-coated electrospun PLGA nanofibers for neural tissue applications." *Biomaterials* 30 (26):4325-4335.

Li, Chunyu, Erik T Thostenson, and Tsu-Wei Chou. 2008. "Sensors and actuators based on carbon nanotubes and their composites: a review." *Composites Science and Technology* 68 (6):1227-1249.

Li, Xianfeng, Xiufeng Hao, Hubei Yu, and Hui Na. 2008. "Fabrication of Polyacrylonitrile/polypyrrole (PAN/Ppy) composite nanofibres and nanospheres with core–shell structures by electrospinning." *Materials Letters* 62 (8):1155-1158.

Li, Yongfang. 2015. *Organic optoelectronic materials*. Vol. 91: Springer.

Liang, Dehai, Benjamin S Hsiao, and Benjamin Chu. 2007. "Functional electrospun nanofibrous scaffolds for biomedical applications." *Advanced drug delivery reviews* 59 (14):1392-1412.

Lin, Wei-Han, Jiashing Yu, Guoping Chen, and Wei-Bor Tsai. 2016. "Fabrication of multi-biofunctional gelatin-based electrospun fibrous scaffolds for enhancement of osteogenesis of mesenchymal stem cells." *Colloids and Surfaces B: Biointerfaces* 138:26-31.

Liu, Haifeng, Xili Ding, Gang Zhou, Ping Li, Xing Wei, and Yubo Fan. 2013. "Electrospinning of nanofibers for tissue engineering applications." *Journal of Nanomaterials* 2013:3.

Liu, Wenying, Stavros Thomopoulos, and Younan Xia. 2012. "Electrospun nanofibers for regenerative medicine." *Advanced healthcare materials* 1 (1):10-25.

Lodish, Harvey. 2008. *Molecular cell biology*: Macmillan.

Luu, YK, K Kim, BS Hsiao, B Chu, and M Hadjiargyrou. 2003. "Development of a nanostructured DNA delivery scaffold via electrospinning of PLGA and PLA–PEG block copolymers." *Journal of controlled release* 89 (2):341-353.

Ma, Peng-Cheng, Naveed A Siddiqui, Gad Marom, and Jang-Kyo Kim. 2010. "Dispersion and functionalization of carbon nanotubes for polymer-based nanocomposites: a review." *Composites Part A: Applied Science and Manufacturing* 41 (10):1345-1367.

Madden, John D, Ryan A Cush, Tanya S Kanigan, Colin J Brenan, and Ian W Hunter. 1999. "Encapsulated polypyrrole actuators." *Synthetic Metals* 105 (1):61-64.

Madden, John D, Derek Rinderknecht, Patrick A Anquetil, and Ian W Hunter. 2007. "Creep and cycle life in polypyrrole actuators." *Sensors and Actuators A: Physical* 133 (1):210-217.

Madden, John DW, Nathan A Vandesteeg, Patrick A Anquetil, Peter GA Madden, Arash Takshi, Rachel Z Pytel, Serge R Lafontaine, Paul A Wieringa, and Ian W Hunter. 2004. "Artificial muscle technology: physical principles and naval prospects." *Oceanic Engineering, IEEE Journal of* 29 (3):706-728.

Mao, Angelo S, Jae-Won Shin, and David J Mooney. 2016. "Effects of substrate stiffness and cell-cell contact on mesenchymal stem cell differentiation." *Biomaterials* 98:184-191.

Mazzoldi, A, A Della Santa, and D De Rossi. 2000. "Conducting polymer actuators: Properties and modeling." In *Polymer Sensors and Actuators*, 207-244. Springer.

Megelski, Silke, Jean S Stephens, D Bruce Chase, and John F Rabolt. 2002. "Micro-and nanostructured surface morphology on electrospun polymer fibers." *Macromolecules* 35 (22):8456-8466.

Mirfakhrai, Tissaphern, John DW Madden, and Ray H Baughman. 2007. "Polymer artificial muscles." *Materials today* 10 (4):30-38.

Miyagawa, Hiroaki, Amar K Mohanty, Lawrence T Drzal, and Manjusri Misra. 2004. "Nanocomposites from biobased epoxy and single-wall carbon nanotubes: synthesis, and mechanical and thermophysical properties evaluation." *Nanotechnology* 16 (1):118.

Mo, XM, CY Xu, Mea Kotaki, and S Ramakrishna. 2004. "Electrospun P (LLA-CL) nanofiber: a biomimetic extracellular matrix for smooth muscle cell and endothelial cell proliferation." *Biomaterials* 25 (10):1883-1890.

Mottaghitalab, Vahid, Binbin Xi, Geoffrey M Spinks, and Gordon G Wallace. 2006. "Polyaniline fibres containing single walled carbon nanotubes: enhanced performance artificial muscles." *Synthetic metals* 156 (11):796-803.

Nagarajan, Sakthivel, Habib Belaid, Céline Pochat-Bohatier, Catherine Teyssier, Igor Iatsunskyi, Emerson Coy, Sébastien Balme, David Cornu, Philippe Miele, and Narayana S Kalkura. 2017. "Design of Boron Nitride/Gelatin Electrospun Nanofibers for Bone Tissue Engineering." *ACS Applied Materials & Interfaces* 9 (39):33695-33706.

Nair, Sujith, Sudarshan Natarajan, and Seong H Kim. 2005. "Fabrication of electrically conducting polypyrrole-poly (ethylene oxide) composite nanofibers." *Macromolecular rapid communications* 26 (20):1599-1603.

Nerurkar, Nandan L, Dawn M Elliott, and Robert L Mauck. 2007. "Mechanics of oriented electrospun nanofibrous scaffolds for annulus fibrosus tissue engineering." *Journal of orthopaedic research* 25 (8):1018-1028.

Nobeshima, Taiki, Heisuke Sakai, Yuya Ishii, Sei Uemura, and Manabu Yoshida. 2016. "Polarized FT-IR Study of Uniaxially Aligned Electrospun Poly (DL-Lactic Acid) Fiber Films." *Journal of Photopolymer Science and Technology* 29 (2):353-356.

Noh, Hyung Kil, Sung Won Lee, Jin-Man Kim, Ju-Eun Oh, Kyung-Hwa Kim, Chong-Pyoung Chung, Soon-Chul Choi, Won Ho Park, and Byung-Moo Min. 2006. "Electrospinning of chitin nanofibers: degradation behavior and cellular response to normal human keratinocytes and fibroblasts." *Biomaterials* 27 (21):3934-3944.

Nur-E-Kamal, Alam, Ijaz Ahmed, Jabeen Kamal, Melvin Schindler, and Sally Meiners. 2005. "Three dimensional nanofibrillar surfaces induce activation of Rac." *Biochemical and biophysical research communications* 331 (2):428-434.

Oliveira, Michele F, Diego Suarez, Júlio Cézar Barbosa Rocha, Alvaro Vianna Novaes de Carvalho Teixeira, Maria E Cortés, Frederico B De Sousa, and Rubén D Sinisterra. 2015. "Electrospun nanofibers of polyCD/PMAA polymers and their potential application as drug delivery system." *Materials Science and Engineering: C*.

Ong, Yit Thai, Abdul Latif Ahmad, Sharif Hussein Sharif Zein, and Soon Huat Tan. 2010. "A review on carbon nanotubes in an environmental protection and green engineering perspective." *Brazilian Journal of Chemical Engineering* 27 (2):227-242.

Osorio, AG, ICL Silveira, VL Bueno, and CP Bergmann. 2008. "H 2 SO 4/HNO 3/HCl—functionalization and its effect on dispersion of carbon nanotubes in aqueous media." *Applied Surface Science* 255 (5):2485-2489.

Park, Ok-Kyung, Sungho Lee, Han-Ik Joh, Jun Kyung Kim, Phil-Hyun Kang, Joog Hee Lee, and Bon-Cheol Ku. 2012. "Effect of functional groups of carbon nanotubes on the cyclization mechanism of polyacrylonitrile (PAN)." *Polymer*.

Patel, Deven Chandrakant. 2012. "Preparation and characterization of electrospun poly (D, L-Lactide-co-Glycolide) scaffolds for vascular tissue engineering and the advancement of an in vitro blood brain barrier model."

Pelipenko, J, P Kocbek, B Govedarica, R Rošic, S Baumgartner, and J Kristl. 2013. "The topography of electrospun nanofibers and its impact on the growth and mobility of keratinocytes." *European Journal of Pharmaceutics and Biopharmaceutics* 84 (2):401-411.

Pham, Quynh P, Upma Sharma, and Antonios G Mikos. 2006. "Electrospinning of polymeric nanofibers for tissue engineering applications: a review." *Tissue engineering* 12 (5):1197-1211.

Philp, Douglas, and J Fraser Stoddart. 1996. "Self-assembly in natural and unnatural systems." *Angewandte Chemie International Edition* 35 (11):1154-1196.

Popov, Valentin N. 2004. "Carbon nanotubes: properties and application." *Materials Science and Engineering: R: Reports* 43 (3):61-102.

Potrč, Tanja, Saša Baumgartner, Robert Roškar, Odon Planinšek, Zoran Lavrič, Julijana Kristl, and Petra Kocbek. 2015. "Electrospun polycaprolactone nanofibers as a potential oromucosal delivery system for poorly water-soluble drugs." *European Journal of Pharmaceutical Sciences* 75:101-113.

Prabaharan, M, R Jayakumar, and SV Nair. 2011. "Electrospun nanofibrous scaffolds-current status and prospects in drug delivery." In *Biomedical applications of polymeric nanofibers*, 241-262. Springer.

Prestwich, Glenn D. 2007. "Simplifying the extracellular matrix for 3-D cell culture and tissue engineering: A pragmatic approach." *Journal of cellular biochemistry* 101 (6):1370-1383.

Qi, Hongfei, Zhihong Ye, Hailong Ren, Nana Chen, Qingyan Zeng, Xianglong Wu, and Tingli Lu. 2016. "Bioactivity assessment of PLLA/PCL/HAP electrospun nanofibrous scaffolds for bone tissue engineering." *Life sciences* 148:139-144.

Rajoria, Himanshu, and Nader Jalili. 2005. "Passive vibration damping enhancement using carbon nanotube-epoxy reinforced composites." *Composites Science and Technology* 65 (14):2079-2093.

Ramakrishna, Seeram. 2005. *An introduction to electrospinning and nanofibers*: World Scientific.

Reneker, Darrell H, and Iksoo Chun. 1996. "Nanometre diameter fibres of polymer, produced by electrospinning." *Nanotechnology* 7 (3):216.

Sandler, J, MSP Shaffer, T Prasse, W Bauhofer, K Schulte, and AH Windle. 1999. "Development of a dispersion process for carbon nanotubes in an epoxy matrix and the resulting electrical properties." *Polymer* 40 (21):5967-5971.

Sangsanoh, Pakakrong, Orawan Suwantong, Artphop Neamnark, Poonlarp Cheepsunthorn, Prasit Pavasant, and Pitt Supaphol. 2010. "In vitro biocompatibility of electrospun and solvent-cast chitosan substrata towards Schwann, osteoblast, keratinocyte and fibroblast cells." *European Polymer Journal* 46 (3):428-440.

Sargeant, Timothy D, Mustafa O Guler, Scott M Oppenheimer, Alvaro Mata, Robert L Satcher, David C Dunand, and Samuel I Stupp. 2008. "Hybrid bone implants: self-assembly of peptide amphiphile nanofibers within porous titanium." *Biomaterials* 29 (2):161-171.

Schmidt, Christine E, Venkatram R Shastri, Joseph P Vacanti, and Robert Langer. 1997. "Stimulation of neurite outgrowth using an electrically conducting polymer." *Proceedings of the National Academy of Sciences* 94 (17):8948-8953.

Seo, Imsun, Myoungho Pyo, and Gyoujin Cho. 2002. "Micrometer to nanometer patterns of polypyrrole thin films via microphase separation and molecular mask." *Langmuir* 18 (20):7253-7257.

Shah, Ramille N, Nirav A Shah, Marc M Del Rosario Lim, Caleb Hsieh, Gordon Nuber, and Samuel I Stupp. 2010. "Supramolecular design of self-assembling nanofibers for cartilage regeneration." *Proceedings of the National Academy of Sciences* 107 (8):3293-3298.

Shao, Shijun, Shaobing Zhou, Long Li, Jinrong Li, Chao Luo, Jianxin Wang, Xiaohong Li, and Jie Weng. 2011. "Osteoblast function on electrically conductive electrospun PLA/MWCNTs nanofibers." *Biomaterials* 32 (11):2821-2833.

Shao, Weili, Jianxin He, Feng Sang, Qian Wang, Li Chen, Shizhong Cui, and Bin Ding. 2016. "Enhanced bone formation in electrospun poly (l-lactic-co-glycolic acid)–tussah silk fibroin ultrafine nanofiber scaffolds incorporated with graphene oxide." *Materials Science and Engineering: C* 62:823-834.

Sheridan, Robert L, Jeffrey R Morgan, Jennifer L Cusick, Lisa M Petras, Martha M Lydon, and Ronald G Tompkins. 2001. "Initial experience with a composite autologous skin substitute." *Burns* 27 (5):421-424.

Sill, Travis J, and Horst A von Recum. 2008. "Electrospinning: applications in drug delivery and tissue engineering." *Biomaterials* 29 (13):1989-2006.

Skotheim, Terje A. 1997. *Handbook of conducting polymers*: CRC press.

Smela, Elisabeth, and Nikolaj Gadegaard. 1999. "Surprising volume change in PPy (DBS): an atomic force microscopy study." *Advanced Materials* 11 (11):953-957.

Smela, Elisabeth, and Nikolaj Gadegaard. 2001. "Volume change in polypyrrole studied by atomic force microscopy." *The Journal of Physical Chemistry B* 105 (39):9395-9405.

Smela, Elisabeth, Wen Lu, and Benjamin R Mattes. 2005. "Polyaniline Actuators: Part 1. PANI (AMPS) in HCl." *Synthetic metals* 151 (1):25-42.

Smela, Elisabeth, and Benjamin R Mattes. 2005. "Polyaniline actuators: Part 2. PANI (AMPS) in methanesulfonic acid." *Synthetic metals* 151 (1):43-48.

Smith, Laura A, Xiaohua Liu, and Peter X Ma. 2008. "Tissue engineering with nano-fibrous scaffolds." *Soft Matter* 4 (11):2144-2149.

Son, Won Keun, Ji Ho Youk, Taek Seung Lee, and Won Ho Park. 2004. "Preparation of antimicrobial ultrafine cellulose acetate fibers with silver nanoparticles." *Macromolecular rapid communications* 25 (18):1632-1637.

Spinks, Geoffrey M, Vahid Mottaghitalab, Mehrdad Bahrami-Samani, Philip G Whitten, and Gordon G Wallace. 2006. "Carbon-Nanotube-Reinforced Polyaniline Fibers for High-Strength Artificial Muscles." *Advanced Materials* 18 (5):637-640.

Spinks, Geoffrey M, Su Ryon Shin, Gordon G Wallace, Philip G Whitten, In Young Kim, Sun I Kim, and Seon Jeong Kim. 2007. "A novel “dual mode” actuation in chitosan/polyaniline/carbon nanotube fibers." *Sensors and Actuators B: Chemical* 121 (2):616-621.

Spinks, Geoffrey M, and Van-Tan Truong. 2005. "Work-per-cycle analysis for electromechanical actuators." *Sensors and Actuators A: Physical* 119 (2):455-461.

Subbiah, Thandavamoorthy, GS Bhat, RW Tock, S Parameswaran, and SS Ramkumar. 2005. "Electrospinning of nanofibers." *Journal of Applied Polymer Science* 96 (2):557-569.

Tahhan, May, Van-Tan Truong, Geoffrey M Spinks, and Gordon G Wallace. 2003. "Carbon nanotube and polyaniline composite actuators*." *Smart Materials and Structures* 12 (4):626.

Tavakkol, Elham, Hossein Tavanai, Amir Abdolmaleki, and Mohammad Morshed. 2017. "Production of conductive electrospun polypyrrole/poly (vinyl pyrrolidone) nanofibers." *Synthetic Metals* 231:95-106.

Thavasi, V, G Singh, and S Ramakrishna. 2008. "Electrospun nanofibers in energy and environmental applications." *Energy & Environmental Science* 1 (2):205-221.

Thostenson, Erik T, Prashant G Karandikar, and Tsu-Wei Chou. 2005. "Fabrication and characterization of reaction bonded silicon carbide/carbon nanotube composites." *Journal of Physics D: Applied Physics* 38 (21):3962.

Umana, Mirtha, and Jess Waller. 1986. "Protein-modified electrodes. The glucose oxidase/polypyrrole system." *Analytical Chemistry* 58 (14):2979-2983.

Wang, Bo, Qing Cai, Shen Zhang, Xiaoping Yang, and Xuliang Deng. 2011. "The effect of poly (L-lactic acid) nanofiber orientation on osteogenic responses of human osteoblast-like MG63 cells." *Journal of the mechanical behavior of biomedical materials* 4 (4):600-609.

Wang, Xia, Deng-Guang Yu, Xiao-Yan Li, SW Annie Bligh, and Gareth R Williams. 2015. "Electrospun medicated shellac nanofibers for colon-targeted drug delivery." *International journal of pharmaceutics* 490 (1):384-390.

Wang, Xin, Philip D Bradford, Wei Liu, Haibo Zhao, Yoku Inoue, Jon-Paul Maria, Qingwen Li, Fuh-Gwo Yuan, and Yuntian Zhu. 2011. "Mechanical and electrical property improvement in CNT/Nylon composites through drawing and stretching." *Composites Science and Technology* 71 (14):1677-1683.

Wong, Joyce Y, Robert Langer, and Donald E Ingber. 1994. "Electrically conducting polymers can noninvasively control the shape and growth of mammalian cells." *Proceedings of the National Academy of Sciences* 91 (8):3201-3204.

Woo, Kyung Mi, Victor J Chen, and Peter X Ma. 2003. "Nano-fibrous scaffolding architecture selectively enhances protein adsorption contributing to cell attachment." *Journal of biomedical materials research Part A* 67 (2):531-537.

Wu, Huijun, Jintu Fan, Chih-Chang Chu, and Jun Wu. 2010. "Electrospinning of small diameter 3-D nanofibrous tubular scaffolds with controllable nanofiber orientations for vascular grafts." *Journal of Materials Science: Materials in Medicine* 21 (12):3207-3215.

Xie, Xiao-Lin, Yiu-Wing Mai, and Xing-Ping Zhou. 2005. "Dispersion and alignment of carbon nanotubes in polymer matrix: a review." *Materials Science and Engineering: R: Reports* 49 (4):89-112.

Xu, CY, R Inai, M Kotaki, and S Ramakrishna. 2004. "Aligned biodegradable nanofibrous structure: a potential scaffold for blood vessel engineering." *Biomaterials* 25 (5):877-886.

Yang, Shoufeng, Kah-Fai Leong, Zhaohui Du, and Chee-Kai Chua. 2001. "The design of scaffolds for use in tissue engineering. Part I. Traditional factors." *Tissue engineering* 7 (6):679-689.

Yardimci, Atike Ince, Metin Tanoglu, and Yusuf Selamet. 2013. "Development of electrically conductive and anisotropic gel-coat systems using CNTs." *Progress in Organic Coatings* 76 (6):963-965.

Yardimci, Atike Ince, Selahattin Yılmaz, and Yusuf Selamet. 2015. "The effects of catalyst pretreatment, growth atmosphere and temperature on carbon nanotube synthesis using Co–Mo/MgO catalyst." *Diamond and Related Materials* 60:81-86.

Yeow, ML, Yutie Liu, and K Li. 2005. "Preparation of porous PVDF hollow fibre membrane via a phase inversion method using lithium perchlorate (LiClO 4) as an additive." *Journal of membrane science* 258 (1):16-22.

Yu, Gang, Jun Gao, Jan C Hummelen, Fred Wudl, and Alan J Heeger. 1995. "Polymer photovoltiac cells: Enhanced efficiencies via a network of internal donor-acceptor heterojunctions." *Science* 270 (5243):1789.

Yuan, Xiaoyan, Yuanyuan Zhang, Cunhai Dong, and Jing Sheng. 2004. "Morphology of ultrafine polysulfone fibers prepared by electrospinning." *Polymer International* 53 (11):1704-1710.

Zhang, Chunxue, Xiaoyan Yuan, Lili Wu, Yue Han, and Jing Sheng. 2005. "Study on morphology of electrospun poly (vinyl alcohol) mats." *European polymer journal* 41 (3):423-432.

Zhang, Shihai, Nanyan Zhang, Cheng Huang, Kailiang Ren, and QM Zhang. 2005. "Microstructure and Electromechanical Properties of Carbon Nanotube/Poly (vinylidene fluoride—trifluoroethylene—chlorofluoroethylene) Composites." *Advanced Materials* 17 (15):1897-1901.

Zhang, Zhanpeng, Jiang Hu, and Peter X Ma. 2012. "Nanofiber-based delivery of bioactive agents and stem cells to bone sites." *Advanced drug delivery reviews* 64 (12):1129-1141.

Zheng, Jianfen, Aihua He, Junxing Li, Jian Xu, and Charles C Han. 2006. "Studies on the controlled morphology and wettability of polystyrene surfaces by electrospinning or electrospraying." *Polymer* 47 (20):7095-7102.

Zheng, Wen, Joselito M Razal, Philip G Whitten, Raquel Ovalle-Robles, Gordon G Wallace, Ray H Baughman, and Geoffrey M Spinks. 2011. "Artificial muscles based on polypyrrole/carbon nanotube laminates." *Advanced materials* 23 (26):2966-2970.

Zhong, Jian, Huan Zhang, Juan Yan, and Xiao Gong. 2015. "Effect of nanofiber orientation of electrospun nanofibrous scaffolds on cell growth and elastin expression of muscle cells." *Colloids and Surfaces B: Biointerfaces* 136:772-778.

Zhou, YX, PX Wu, ZY Cheng, J Ingram, and S Jeelani. 2008. "Improvement in electrical, thermal and mechanical properties of epoxy by filling carbon nanotube." *Express polymer letters* 2 (1):40-48.

Zhu, Jiang, JongDae Kim, Haiqing Peng, John L Margrave, Valery N Khabashesku, and Enrique V Barrera. 2003. "Improving the dispersion and integration of single-walled carbon nanotubes in epoxy composites through functionalization." *Nano letters* 3 (8):1107-1113.

ATİKE İNCE YARDIMCI

Date and Place of Birth: 10.03.1984/ France
Institution: Izmir Institute of Technology
Mobile Phone: 00 90 533 336 76 71
E-mail: atikeince@iyte.edu.tr

EDUCATION

Philosophy of Doctorate, 2017
Izmir Institute of Technology
Material Science and Engineering
Department

Master of Science, 2010
Izmir Institute of Technology
Physics Department

Bachelor of Science, 2007
Balikesir University
Major: Physics Education

RESEARCH EXPERIENCE

Chemical Vapor Deposition
Electrospinning
Scanning Electron Microscopy
Raman Spectroscopy
Profilometer
Thermal Oxidation
Photolithography

TEACHING EXPERIENCE

General Physics Lab-1
General Physics Lab-2
Modern Physics Lab.
Electronic circuit Lab.

PUBLICATIONS (ARTICLES)

Atike Ince Yardimci, Metin Tanoglu, Yusuf Selamet, 'Development of electrically conductive and anisotropic gel-coat systems using CNTs', Progress in Organic Coatings, 76 (2013) 963– 965.

Atike Ince Yardimci, Selahattin Yilmaz, Yusuf Selamet, 'The effects of catalyst pretreatment, growth atmosphere and temperature on carbon nanotube synthesis using Co–Mo/MgO catalyst', Diamond and Related Materials, 60 (2015) 81–86.

Atike Ince Yardimci, Hande Aypek, Ozgur Ozturk, Selahattin Yilmaz, Engin Ozcivici, Gulistan Mese and Yusuf Selamet, 'Properties and Biocompatibility of CNT Incorporated Polyacrilonitrile/Polypyrrole Nanofibers' (Submitted to J. Bioactive and Compatible Polymers).

Atike Ince Yardimci, Metin Tanoglu, Selahattin Yılmaz, and Yusuf Selamet, 'Preparation of CNT Embedded PAN/PPy Nanofibers Synthesized by Electrospinning Method' (to be prepared in 2018).

Atike Ince Yardimci, Öznur Başkan Selahattin Yilmaz, Engin Ozcivici, Gulistan Mese and Yusuf Selamet, 'Osteogenic Differentiation of Mesenchymal Stem Cells on Random and Aligned PAN/PPy Nanofibrous Scaffolds' (to be prepared in 2018).